

**REPUBLIC OF TURKEY
ERCIYES UNIVERSITY
GRADUATE SCHOOL OF NATURAL AND APPLIED SCIENCE
DEPARTMENT OF CHEMISTRY
(Physical Chemistry)**

**SYNTHESIS AND CHARACTERIZATION OF SOME
CARBON/LAYERED DOUBLE HYDROXIDE FOR
SUPERCAPACITOR APPLICATIONS**

**Prepared By
MUSTAFA RAQEEB MOHAMMED**

**Supervisor
Prof. Dr. Şaban PATAT**

MSc. Thesis

**Kayseri – Turkey
January 2018**

**REPUBLIC OF TURKEY
ERCIYES UNIVERSITY
GRADUATE SCHOOL OF NATURAL AND APPLIED SCIENCES
DEPARTMENT OF CHEMISTRY**

**SYNTHESIS AND CHARACTERIZATION OF SOME
CARBON/LAYERED DOUBLE HYDROXIDE FOR
SUPERCAPACITOR APPLICATIONS**

MSc. Thesis

**Prepared by
MUSTAFA RAQEEB MOHAMMED**

**Supervisor
Prof. Dr. Şaban PATAT**

**Thesis Was Supported by Scientific Research Projects Unit of Erciyes
University, the Project FYL-2017-7619**

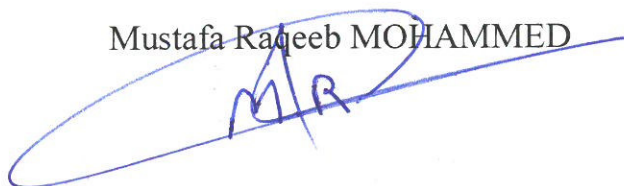
**January 2018
KAYSERİ**

COMPLIANCE WITH SCIENTIFIC ETHICS

I hereby declare that all information in this document has been obtained and presented in accordance with academic rules and ethical conduct. I also declare that, as required by these rules and conduct, I have fully cited and referenced all material and results that are not original to this work.

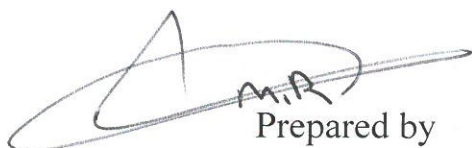
Prepared by

Mustafa Raqeeb MOHAMMED



COMPLIANCE WITH GUIDELINES

The MSc Thesis entitled **“Synthesis and Characterization of some Carbon/layered Double Hydroxide for Supercapacitor Applications”** has been prepared in accordance with Thesis Proposal and Writing Guidelines of Graduate School of Natural and Applied Sciences of Erciyes University



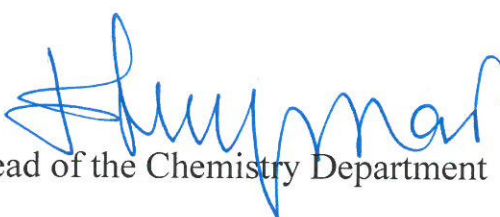
Prepared by

Mustafa Raqeeb MOHAMMED



Supervisor

Prof. Dr. Şaban PATAT



Head of the Chemistry Department

Prof. Dr. Emin SARIPINAR

ACCEPTANCE AND APPROVAL PAGE

This study entitled **“Synthesis and Characterization of Some Carbon/Layered Double Hydroxide for Supercapacitor Applications”** has been prepared by **Mustafa Raqeeb MOHAMMED** under the supervision of Prof. Dr. Şaban PATAT was accepted by the jury as a MSc. thesis in Department of Chemistry, Graduate School of Natural and Applied Science, Erciyes University

02/01/2018

JURY:

Supervisor: Prof. Dr. Şaban PATAT

Member: Prof. Dr. Talat ÖZPOZAN

Member: Associate Prof Dr. Hakan USTA

That the acceptance of this thesis has been approved by the decision of the Institute's Board of Directors with the date 02./01./2018 and 2018/01/02 decision number.


02.01.2018...

Prof. Dr. Mehmet AKKURT

Director of the Institute

ACKNOWLEDGEMENTS

I would like to express my special thank to my advisor, Prof Dr Şaban PATAT, for his understanding, guidance, and wisdom

It was a great opportunity for me to complete my MSc. study and work in Erciyes University Nanotechnology Research Center (Ernam)

I also would like to express my appreciation to the Ministry of Higher Education and Scientific Research of Republic of Iraq for financial support during period my studies.

I want to express my greatest gratitude to my dear wife, and my sons, for their encouragement, patience and also I would like to special thanks my parents and my friends for their encouragement.

Last but not least I would like to thanks Süleyman Yıldız and all my classmates. Words cannot describe my feeling toward them

Thanks for everything.

MUSTAFA RAQEEB MOHAMMED

January 2018

SYNTHESIS AND CHARACTERIZATION OF SOME CARBON/LAYERED DOUBLE HYDROXIDE FOR SUPERCAPACITOR APPLICATIONS

Prepared by Mustafa RAQEEB MOHAMMED

Erciyes University, Graduate School of Natural and Applied Sciences MSc. Thesis,
January 2018

Supervisor: Prof Dr Şaban PATAT

ABSTRACT

In this work, nickel-manganese oxides/hydroxide/carbonate@activated carbon (AC), NiMn layered double hydroxide@activated carbon and cobalt-manganese oxide/hydroxide/carbonate@activated carbon composite electrode materials for supercapacitor have been synthesized by a hydrothermal method from the solution of metals salts and urea after the thermal hydrolysis of urea. Physical properties, morphology, and specific surface area of the composites were characterized by X-Ray powder diffraction (XRD), scanning electron microscopy (SEM) equipped with energy-dispersive spectroscopy (EDX), DC conductivity and nitrogen absorption/desorption measurements. SEM images confirmed the NiMn layered double hydroxide, Mn_3O_4 , MnCO_3 , NiCO_3 , $\text{Ni}(\text{OH})_2$, Co_3O_4 , $\text{Co}(\text{OH})_2$ and CoCO_3 dispersed on the external surface of activated carbon particles.

The electrochemical performance of the composites was investigated by cyclic voltammetry and galvanostatic charge/discharge measurements. The electrochemical investigation shows that AC//AC@NiMn(1:1) and AC//AC@CoMn(1:1) asymmetric supercapacitors (ASC) exhibit high energy and power densities, good rate capability and excellent cycling stability, which can be attributed to the synergetic effects between the conductivity of the activated carbon and the redox properties of the metal oxide/hydroxide/carbonate. The AC//AC@NiMn(1:1) ASC operating at 1.2 V delivers a high energy density of 5.5 Wh/kg^{-1} at a power density of 1000 W/kg^{-1} and excellent cycling stability with 96% retention of initial capacitance after 5000 cycles. The AC//AC@CoMn(1:1) ASC operating at 1.2 V delivers a high energy density of 4.9 Wh/kg^{-1} at a power density of 1000 W/kg^{-1} and excellent cycling stability with 97% retention of initial capacitance after 5000 cycles.

This work shows that nickel-manganese oxides/hydroxide/carbonate@activated carbon, NiMn layered double hydroxide@activated carbon and cobalt-manganese oxide/hydroxide/carbonate@activated carbon composite electrode materials were found to be promising electrode materials for the supercapacitor working at high current density.

Keywords: layered double hydroxide (LDH), activated carbon, and electrochemical capacitor

**Süper Kapasitörlerde Kullanılan Bazı Karbon/Tabakalı Çift Hidroksit
Kompozitlerin Sentezi ve Karakterizasyonu**

Mustafa RAQEEB MOHAMMED

Erciyes Üniversitesi, Fen Bilimleri Enstitüsü Yüksek Lisans Tezi

Ocak 2018

Danışman: Prof Dr Şaban PATAT

ÖZET

Bu çalışmada, elektrokimyasal kapasitörlerde kullanılan nikel-mangan oksit/hidroksit/karbonat@aktif karbon (AC), NiMn tabakalı çift hidroksit@aktif karbon ve kobalt-mangan oksit/hidroksit/karbonat@aktif karbon kompozit elektrot maddeleri; metal tuzları ve üre içeren çözeltilerden hidrotermal yöntem ile hazırlandı. Sentezlenen kompozitlerin fiziksel özellikleri, morfolojisi ve spesifik yüzey alanı X-ışınları toz kırınımı (XRD), taramalı elektron mikroskobu (SEM), enerji dağılımlı spektroskopi (EDX), DC iletkenliği ve azot adsorpsiyon/desorpsiyon ölçümleri ile tanımlandı. SEM görüntüleri; NiMn tabakalı çift hidroksit, Mn_3O_4 , $MnCO_3$, $NiCO_3$, $Ni(OH)_2$, Co_3O_4 , $Co(OH)_2$ ve $CoCO_3$ taneciklerinin aktif karbon taneciklerinin yüzeyine dağıldığını gösterdi.

Kompozitlerin elektrokimyasal performansı dönüşümlü voltametri ve galvanostatik şarj/deşarj ölçümleri ile araştırıldı. Elektrokimyasal araştırma ile AC//AC@NiMn(1:1) ve AC//AC@CoMn(1:1) asimetrik süperkapasitörlerin (ASC) aktif karbonun iletkenliği ve metal oksit/hidroksit/karbonat kompozitlerinin redoks özelliği arasındaki sinerjik etki nedeniyle yüksek enerji ve güç yoğunluğu, yüksek akım ve yüksek döngü performansına sahip olduğu bulunmuştur. 0-1.2V voltaj aralığında çalışan AC//AC@NiMn(1:1) ASC kapasitörünün 1000W/kg güç yoğunluğunda 5.5 Wh/kg enerji yoğunluğuna sahip olduğu ve 5000 döngü sonrası başlangıç kapasitesinin %96 kadarını koruduğu bulunmuştur. Aynı şekilde 0-1.2V voltaj aralığında çalışan AC//AC@CoMn(1:1) ASC kapasitörünün 1000W/kg⁻¹ güç yoğunluğunda 4.9 Wh/kg⁻¹ enerji yoğunluğuna sahip olduğu ve 5000 döngü sonrası başlangıç kapasitesinin %97 kadarını koruduğu bulunmuştur.

Bu alıřmada nikel-mangan oksit/hidroksit/karbonat@AC, NiMn tabakalı ift hidroksit@AC ve kobalt-mangan oksit/hidroksit/karbonat kompozitlerin yksek akım sper kapasitr uygulamalarında mit verici elektrot maddeleri olduėu bulunmuřtur.

Anahtar Kelime: tabkalı ift hidroksit, aktif karbon ve elektrokimyasal kapasitr.

TABLE OF CONTENTS

COMPLIANCE WITH SCIENTIFIC ETHICS	i
COMPLIANCE WITH GUIDELINES	ii
ACCEPTANCE AND APPROVAL PAGE	iii
JURY:	iii
Acknowledgements.....	iv
ÖZET	vi
ABSTRACT	v
CONTENTS	viii
LIST OF ABBREVIATIONS	xi
LIST OF TABLES	xii
LIST OF FIGURES	xiii

CHAPTER 1

INTRODUCTION	1
--------------------	---

CHAPTER 2

SUPERCAPACITORS	6
2.1.Introduction	6
2.2 Applications of Supercapacitors.....	11
2.2.1 Industrial Applications:	11
2.2.2 Transportation	12
2.2.3 Consumer Electronics	13
2.2.4 Energy Harvesting	14
2.2.5 Grid Storage	15

2.2.6 Aircraft:.....	15
2.2.7 Medical:	16
2.2.8 Military:.....	16
2.3 Supercapacitor's Storage Mechanism.....	16
2.3.1 Electric Double Layered Capacitors (EDLCs).....	18
2.3.2 Pseudocapacitors.....	22
2.3.3 Hybrid Capacitors.....	25
2.4 Design of Supercapacitors	26
2.4.1 Electrolytes for Supercapacitors.....	26
2.4.2 Separator	28
2.4.3 Current Collectors	28
2.4.4 Additives.....	28
2.5 Performance Evaluation of Supercapacitors	29
CHAPTER 3	30
MATERIALS AND METHOD	30
3.1 Material Preparation	30
3.1.1 Synthesis of Activated Carbon/Nickel Manganese Hydroxide Carbonates Composites [AC@NiMn(n:m)] and Nickel Manganese Hydroxide Carbonates [NiMn(n:m)].....	30
3.1.2 Synthesis of Activated Carbon/Cobalt-Manganese Carbonates Hydroxide Hydrates Composites [AC@CoMn (n:m) (CO ₃) _x (OH) _y .zH ₂ O] and Cobalt- Manganese Carbonates Hydroxide Hydrates[CoMn (n:m) (CO ₃) _x (OH) _y .zH ₂ O] ...	31
3.2 Structural Characterization	33
3.2.1 X-Ray Powder Diffraction	33
3.2.2 Scanning Electron Microscope Measurements	33
3.2.3 Conductivity Measurement.....	33
3.2.4 N ₂ Adsorption/Desorption Measurement	34
3.2.4.1 Adsorption Isotherms.....	34

3.3 Electrochemical Characterization	36
---	-----------

CHAPTER 4

RESULTS AND DISCUSSIONS

4.1 Activated Carbon/Nickel Manganese Hydroxide Carbonates [AC@NiMn(n:m)] and Nickel Manganese Hydroxide Carbonates [NiMn(n:m)] Composites	39
4.1.1 X-Ray Powder Diffraction	39
4.1.2 N₂ Adsorption/Desorption Isotherms	46
4.1.3 Scanning Electron Microscope (SEM)	48
4.1.4 Electrochemical Characterization	50
4.2 Activated Carbon/Cobalt-Manganese Carbonates Hydroxide Hydrates Composites [AC@CoMn (n:m) (CO₃)_x(OH)_y.zH₂O] and Cobalt-Manganese Carbonates Hydroxide Hydrates[CoMn (n:m) (CO₃)_x(OH)_y.zH₂O].....	62
4.2.1 X-Ray Powder Diffraction (XRD)	62
4.2.2 N₂ Adsorption/Desorption Isotherms	67
4.2.3 Scanning Electron Microscope (SEM)	69
4.2.4 Electrochemical Characterization	71
CHAPTER 5	80
CONCLUSIONS	80
REFERENCES	81
CURRICULUM VITAE.....	83

List of Abbreviations, Symbols and Nomenclature

AC	Activated Carbon
ASC	Asymmitric supertcapacitor
SC	symmitric supertcapacitor
SMES	superconducting magnetic energy storage
C	Capacitance
C _s	Specific Capacitance
CV	Cyclic Voltammetry
GCD	Galvanostatic Charge-Discharge
EDLC	Electrical double layer capacitors
SEM	Scanning electron microscope
XRD	X-ray diffraction
EDS	Energy dispersive spectroscopy
BET	Brunauer-Emmett-Teller
d	Distance
EC	Electrochemical Capacitor
F	Farad
I	Current
m	Mass
Δt	Total Discharging Time
T	Thickness
ΔV	Voltage Drop, Potential Difference
V _s	Scan Rate
ε ₀	the vacuum permittivity constant
ε _r	the relative permittivity of dielectric
FC	Faradic capacitors
μ	Micro
Ω	Ohm
E	Energy
P	Power
Q	Charge
Δt	Time interval
ΔV	Voltage interval
SSA	specific surface area
UPS	uninterruptible power supplies
AMR	automated meter readin
LIC	Li-ion capacitor
ESR	equivalent series resistance
EIS	electrochemical impedance spectroscopic
IUPAC	International Union of Pure and Applied Chemistry
EDX	Energy dispersive X-ray spectroscopy

LIST OF FIGURES

Fig 1.1. Ragone plot for commercially available energy storage systems.....	2
Figure 1.2 Characteristics of energy storage devices. Adapted from Maxwell white paper.	4
Fig 2.1 Schematic diagram of charge storage in conventional capacitors: a)dielectric capacitor b)electrolytic capacitor	7
Fig 2.2 Schematic diagram showing voltage distribution and equivalent circuit of a)conventional (dielectric or film) capacitor charged, and b) supercapacitor (electric double layer capacitor, EDLC) charged.....	10
Figure 2.3 Applications of supercapacitors in transportation a)hybrid city-transit bus, b)engine starting module, c)electric trams, Mannheim, Germany and d)supercapacitor buses, Shanghai, China.	13
Figure 2.4 Applications of supercapacitors in consumer electronics a)mobile phone device b)camera flash, c)cordless screwdriver, and d)toys.....	14
Figure 2.5 Typical applications of supercapacitors for energy harvesting a)World's first energy-generating revolving door, Netherlands, b)a mechanically powered flashlight, c)wireless power modules, and d)a stand-alone power source for a street light.....	15
Fig 2.6 Classification of supercapacitors	17
Fig 2.7 EDL models, a)Helmholtz model, b)Gouy-Chapman model, and c)Stern model	19
Fig. 2.8 Charged and discharged states of EDLC	20
Fig. 2.9 a)cyclic voltammetry and b)galvanostatic charge/discharge plots for EDLC cell	21
Fig. 2.10 Illustration of the charge storage in pseudocapacitor	24
Fig 2.11 a)cyclic voltammetry and b)constant current charge/discharge curves for pseudocapacitors.....	25
Fig 2.12 Key performance metrics, test methods and major factors for.....	29
the evaluation of SCs	29
Figure 3.1 Linear scanning voltammetry curve.....	34
Fig 3.2 The IUPAC classification of adsorption isotherms	36

Fig 4.1 XRD pattern for NiMn(1:0) composite.....	41
Fig 4.2 XRD pattern for NiMn(0:1) composite.....	41
Fig 4.3 XRD pattern for NiMn(1:1) composite.....	42
Fig 4.4 XRD pattern for AC@NiMn(0:1) composite.....	42
Fig 4.5 XRD pattern for AC@NiMn(1:0) composite.....	43
Fig 4.6 XRD pattern for AC@NiMn(1:1) composite.....	43
Fig 4.7 XRD pattern for AC@NiMn(1:2) composite.....	44
Fig 4.8 XRD pattern for AC@NiMn(1:3) composite.....	44
Fig 4.9 XRD pattern for AC@NiMn(2:1) composite.....	45
Fig 4.10 XRD pattern for AC@NiMn(3:1) composite.....	46
Fig 4.11 Nitrogen adsorption/desorption isotherms of a) NiMn(1:0) b) NiMn(0:1) c) NiMn(1:1) d) AC@NiMn(1:0) e) AC@NiMn(0:1) f) AC and g) AC@NiMn(1:1).....	47
Fig 4.12 Nitrogen adsorption/desorption isotherms of a) AC@NiMn(1:2) b) AC@ NiMn (1:3) c) AC@NiMn (2:1) and d) AC@NiMn (3:1) composites.....	48
Fig 4.13 SEM images for a) NiMn(0:1) b) NiMn(1:0) c) NiMn(1:1) d) AC@NiMn(1:0) e) AC@NiMn(0:1) and f) AC	49
Fig 4.14 SEM images for a) AC@NiMn(1:1) b) AC@NiMn(1:2) c) AC@NiMn(1:3) d) AC@NiMn (2:1) and e) AC@NiMn (3:1)	50
Fig 4.15 Electrochemical performance of AC//AC symmetric capacitor using 6M KOH solution a) cyclic voltammogram at 0.01V/s b) constant current charge/discharge voltage profiles c) effect of the constant current density on the capacitance d) galvanostatic charge/discharge curves after cycling measurements e) cycle life and f) the energy density versus power density values.	53
Fig 4.16 Electrochemical performance of NiMn(1:1)//NiMn(1:1) symmetric capacitor using 6M KOH solution a) cyclic voltammogram at 0.01V/s b) constant current charge/discharge voltage profiles c) effect of the constant current density on the capacitance d) galvanostatic charge/discharge curves after cycling measurements e) cycle life and f) the energy density versus power density values.	54
Fig 4.17 Electrochemical performance of AC@NiMn(1:1)//AC@NiMn(1:1) symmetric capacitor using 6M KOH solution a) cyclic voltammogram at	

- 0.01 V/s **b)** constant current charge/discharge voltage profiles **c)** effect of the constant current density on the capacitance **d)** galvanostatic charge/discharge curves after cycling measurements **e)** cycle life and **f)** the energy density versus power density values. 55
- Fig 4.18** Electrochemical performance of AC@NiMn(1:2)//AC@NiMn(1:2) symmetric capacitor using 6M KOH solution **a)** cyclic voltammogram at 0.01 V/s **b)** constant current charge/discharge voltage profiles **c)** effect of the constant current density on the capacitance **d)** galvanostatic charge/discharge curves after cycling measurements **e)** cycle life and **f)** the energy density versus power density values 56
- Fig 4.19** Electrochemical performance of AC@NiMn(1:3)//AC@NiMn(1:3) symmetric capacitor using 6M KOH solution **a)** cyclic voltammogram at 0.01 V/s **b)** constant current charge/discharge voltage profiles **c)** effect of the constant current density on the capacitance **d)** galvanostatic charge/discharge curves after cycling measurements **e)** cycle life and **f)** the energy density versus power density values 57
- Fig 4.20** Electrochemical performance of AC@NiMn(2:1)//AC@NiMn(2:1) symmetric capacitor using 6M KOH solution **a)** cyclic voltammogram at 0.01 V/s **b)** constant current charge/discharge voltage profiles **c)** effect of the constant current density on the capacitance **d)** galvanostatic charge/discharge curves after cycling measurements **e)** cycle life and **f)** the energy density versus power density values 58
- Fig 4.21** Electrochemical performance of AC@NiMn(3:1)//AC@NiMn(3:1) symmetric capacitor using 6M KOH solution **a)** cyclic voltammogram at 0.01 V/s **b)** constant current charge/discharge voltage profiles **c)** effect of the constant current density on the capacitance **d)** galvanostatic charge/discharge curves after cycling measurements **e)** cycle life and **f)** the energy density versus power density values. 59
- Fig 4.22** Electrochemical performance of AC//AC@NiMn(1:1) asymmetric capacitor using 6M KOH solution **a)** cyclic voltammogram at 0.01 V/s **b)** constant current charge/discharge voltage profiles **c)** effect of the constant current density on the capacitance **d)** galvanostatic charge/discharge curves after cycling measurements **e)** cycle life and **f)** the energy density versus power density values. 60
- Fig 4.23** Comparison of electrochemical performance of the symmetric and asymmetric capacitors using 6M KOH solution **a)** effect of the current density on the capacitance **b)** cycle life **c)** the energy density versus power density. 61

Fig 4.24 XRD pattern for CoMn(1:0).....	63
Fig 4.25 XRD pattern for CoMn(0:1).....	63
Fig 4.26 XRD pattern for CoMn (1:1).....	64
Fig 4.27 XRD patterns for AC@CoMn(0:1)	64
Fig 4.28 XRD patterns for AC@CoMn(1:0)	65
Fig 4.29 XRD patterns for AC@CoMn (1:1)	65
Fig 4.30 XRD pattern for AC@CoMn (1:2).....	66
Figure 4.31 XRD pattern for AC@CoMn (1:3)	66
Figure 4.32 XRD pattern for AC@CoMn (2:1)	67
Fig 4.33 XRD pattern for AC@CoMn (3:1).....	67
Fig 4.34 Nitrogen adsorption/desorption isotherms of a) CoMn(1:0) b) AC@CoMn(1:0) c) CoMn(1:1) and d) AC	68
Fig 4.35 Nitrogen adsorption/desorption isotherms of a) AC@CoMn (1:2) b) AC@CoMn (1:3) c) AC@CoMn (2:1) and d) AC@CoMn(1:1) composites.....	69
Fig 4.36 SEM images of a) CoMn(1:0) b) CoMn(1:1) c) AC@CoMn(1:0) and d) AC@CoMn(1:1)	70
Fig 4.37 SEM image of a) AC@CoMn(1:2) b) AC@CoMn(1:3) c) AC@CoMn(2:1) and d) AC@CoMn(3:1).....	71
Fig 4.38 Electrochemical performance of CoMn(1:1)//CoMn(1:1) symmetric capacitor using 6M KOH solution a) cyclic voltammogram at 0.01V/s b) constant current charge/discharge curves c) effect of the constant current density on the capacitance d) galvanostatic charge/discharge curves after cycling measurements e) cycle life and f) the energy density versus power density values.	73
Fig 4.39 Electrochemical performance of AC@CoMn(1:1)//AC@CoMn(1:1) symmetric capacitor using 6M KOH solution a) cyclic voltammogram at 0.01V/s b) constant current charge/discharge curves c) effect of the constant current density on the capacitance d) galvanostatic charge/discharge curves after cycling measurements e) cycle life and f) the energy density versus power density values	74
Fig 4.40 Electrochemical performance of AC@CoMn(1:2)//AC@CoMn(1:2) symmetric capacitor using 6M KOH solution a) cyclic voltammogram at	

0.01V/s **b)** constant current charge/discharge curves **c)**effect of the constant current density on the capacitance **d)**galvanostatic charge/discharge curves after cycling measurements **e)**cycle life and **f)**the energy density versus power density values 75

Fig 4.41 Electrochemical performance of AC@CoMn(1:3)//AC@CoMn(1:3) symmetric capacitor using 6M KOH solution **a)**cyclic voltammogram at 0.01V/s **b)** constant current charge/discharge curves **c)**effect of the constant current density on the capacitance **d)**galvanostatic charge/discharge curves after cycling measurements **e)**cycle life and **f)**the energy density versus power density values 76

Fig 4.42 Electrochemical performance of AC@CoMn(2:1)//AC@CoMn(2:1) symmetric capacitor using 6M KOH solution **a)**cyclic voltammogram at 0.01V/s **b)** constant current charge/discharge curves **c)**effect of the constant current density on the capacitance **d)**galvanostatic charge/discharge curves after cycling measurements **e)**cycle life and **f)**the energy density versus power density values 77

Fig 4.43 Electrochemical performance of AC@CoMn(2:1)//AC@CoMn(1:1) asymmetric capacitor using 6M KOH solution **a)**cyclic voltammogram at 0.01V/s **b)**constant current charge/discharge curves **c)**effect of the constant current density on the capacitance **d)**galvanostatic charge/discharge curves after cycling measurements **e)**cycle life and **f)**the energy density versus power density values. 78

Fig 4.44 Comparison of electrochemical peformans of the symmetric and asymmetric capacitors using 6M KOH solution **a)**effect of the constant current density on the capacitance **b)**cycle life **c)**the energy density versus power density. 79

CHAPTER 1

INTRODUCTION

Fossil fuels such as oil, coal and natural gas supply over 85 % of the world's energy consumption. Global warming, environmental pollution, and the depletion of fossil fuels become great challenges for human being, so the use of clean and renewable energy such as solar, wind and waves becomes more and more important for sustainable long term development. The variation of renewable energy resources with time, duration and location limits their use and a wide range of applications. Large-scale energy storage and conversion systems are required for effective use of intermittent renewable energy resources (such as solar, wind and waves), electric vehicles and portable electronic devices. One of the most important applications of energy storage devices is to store the on-peak electricity and release it during the off-peak periods in a stable and reliable manner. A number of electrical energy storage technologies have been developed including pumped hydro, flywheel, compressed air, superconducting magnetic (SMES) and electrochemical energy storage and conversion systems. Among various energy conversion and storage systems, electrochemical energy storage and conversion systems are considered as the most promising technologies since they are technically and economically viable. They can be classified as fuel cells, batteries and supercapacitors according to their operating principles. Each type of device consists of two electrodes (cathode and anode) in an electrolyte, which is separated by a separator, where energy-transformation occur at the electrode/electrolyte interfaces. Batteries and fuel cells produce electrical energy from chemical energy via redox reactions at electrode surfaces, while a supercapacitor stores energy by storing charges on the surface of the electrodes or through the fast and reversible surface redox processes. A fuel cell is an open system where air and fuel are pumped to the electrode interfaces while battery is usually a closed system in which the energy storage materials are sealed into a container.

The performance of an energy storage system depends not only on the energy density but also power density. As shown in fig 1.1 (diagonal lines is discharge time of devices, $E=Pt$), supercapacitors fill the gaps between conventional capacitors and batteries (or fuel cells) in terms of energy and power densities. Supercapacitors can deliver much higher energy density than conventional capacitors while keeping the similar power densities and have much higher power densities and faster charge/discharge rates than batteries. Batteries have higher energy densities than supercapacitors. Although fuel cells can provide high energy densities, the low power densities and the use of precious metals catalysts limit their applications.

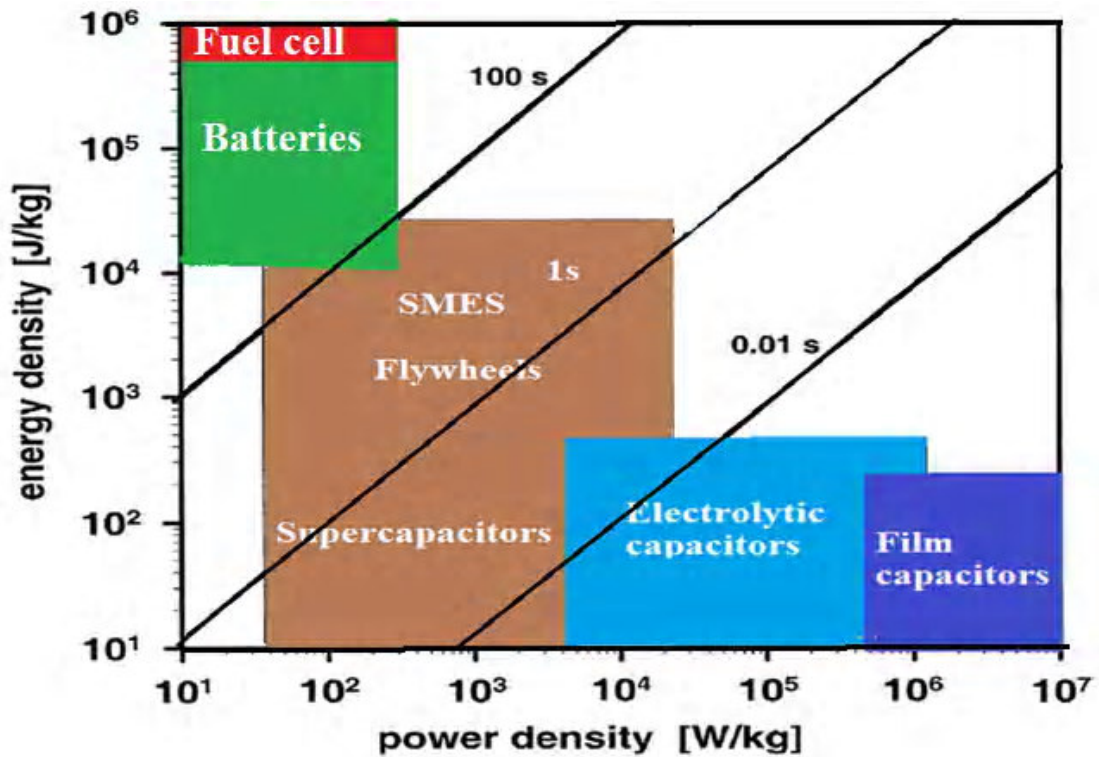


Fig 1.1. Ragone plot for commercially available energy storage systems.

Energy and power densities do not reflect other performance parameters such as safety, cycle life, and cost to evaluate the advantage and limitations of energy storage and conversion systems. Performance parameters of commonly available energy storage systems are shown in Fig 1.2 and table 1.1. As it can be seen in fig 1.2 and table 1.1, batteries alone can not provide the full solution for electricity storage due to low power density, limited cycle life, low charge/discharge rate and heat generation resulting in overheating, thermal runaway and even fire. Supercapacitors provide high power

density, fast charge/discharge rate, long cycle life and high safety compared to batteries. Performance of supercapacitors are suitable for those applications in which power bursts are needed, but high energy storage capacity is not required. They are playing an important role in electric vehicles and in high performance electronics. The combination of a supercapacitor with a battery or fuel cell can provide peak power to an electric vehicle for braking, hill climbing and accelerating. In addition, they can also meet the requirements for peak power and good performance of consumer electronics and digital devices to enhance the designs of circuits.

In contrast to batteries, supercapacitors might not provide sufficient energy/power densities or efficiencies to fuel low-emission hybrid cars and trucks. Therefore, the challenge for current supercapacitors is to improve the energy density without significantly losing the power density and the cycle life. One of the efficient way to increase the energy density is to develop hybrid electrochemical capacitors (so called asymmetric supercapacitors, ASC), which can also provide a wider operating potential window compared to symmetric supercapacitors. For an ASC, the active material used in one electrode is usually different from that used in the other electrode. For instance, a transition metal oxide/hydroxide can be used as the positive electrode, while activated carbon (AC) can used as the negative electrode in an ASC. Moreover, ASCs can make use of the different potential windows of the two electrodes to increase the maximum working voltage of the aqueous electrolyte in the cell system, which results in an improved specific capacitance and energy density.

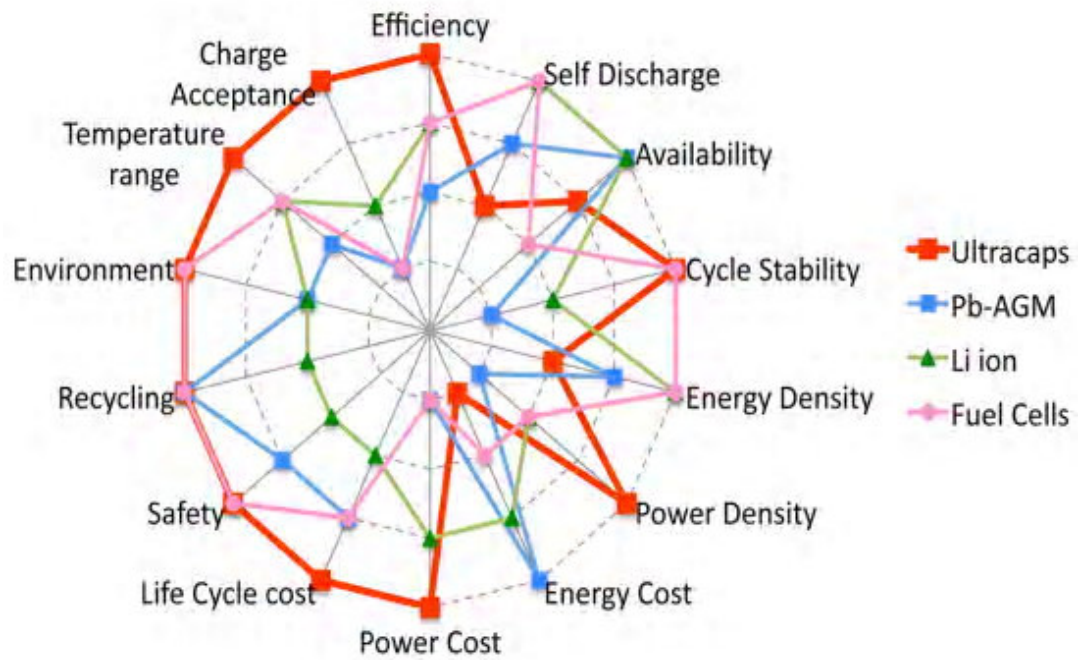


Figure 1.2 Characteristics of energy storage devices. Adapted from Maxwell white paper.

Table 1.1 Comparison of electrochemical energy deposition technologies

Characteristics	Capacitor	Supercapacitor	Battery
Specific energy (Wh/kg)	<0.1	1-10	10-250
Specific power (W/kg)	>>10.000	500-10.000	<1000
Discharge time	10^{-6} - 10^{-3}	s to min	0.3-3 h
Charge time	10^{-6} - 10^{-3}	s to min	1-5 h
Coulombic efficiency (%)	~ 100	85-98	70-85
Cycle life	~infinite	>500.000	~ 1000

Objectives

The main aim of this work is to synthesis and characterize the activated carbon@NiMn/oxide/hydroxide/carbonate and activated carbon@CoMn oxide/hydroxide/carbonate composites to improve the utilization of transition metal oxides as an electrode for supercapacitor applications. A hydrothermal method was used for preparing the composites. Their structure is identified by X-ray diffraction (XRD) and energy dispersive spectroscopy (EDS). The morphology is imaged by scanning electron microscopy (SEM). The BET surface area is calculated from N₂ adsorption/desorption isotherms. The DC conductivity is determined by linear scanning voltammetry measurement. The electrochemical properties of the composites were characterized by cyclic voltammetry and constant current charge/discharge measurements.

CHAPTER 2

SUPERCAPACITORS

2.1.Introduction

The conventional capacitor is made of two metal plates separated by a dielectric or ionic medium, which must be non-conductive to electrons, as shown in Figure 2.1. In the dielectric capacitors, the medium is a dielectric material (thin insulating layer), such as ceramic, glass and paper, in which the dipoles can be polarised to accumulate electric charge at the interface between the dielectric medium and the plate. In the electrolytic capacitors, the medium is a liquid or solid ionic conductor which is also called electrolyte and charge storage can be taken place by accumulation of positive ions at the interface between negative electrode and electrolyte and negative ions of an equal amount of charge at the interface between the positive electrode and the electrolyte.

An important feature of the electrolytic capacitor is that the ions are mobile in the electrolyte. Thus, when negative charge on the electrode side is increased, an equal amount of positive charge can accumulate on the electrolyte side. On the contrary, in the dielectric capacitor, the dipoles are non-mobile in the solid dielectric medium. Thus, the greater charge density can be obtained at the electrolyte/electrode interface than at the dielectric/electrode interface. As a result of this, the capacitance is in the mF range for the electrolytic capacitors, but in the μ F range for dielectric capacitors.

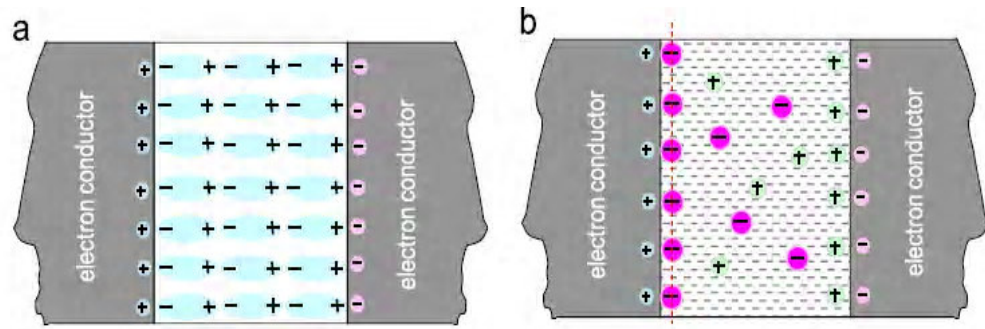


Fig 2.1 Schematic diagram of charge storage in conventional capacitors: **a)**dielectric capacitor **b)**electrolytic capacitor [1]

When a voltage is applied between the two plates, negative charges will be accumulated on one plate and positive charges on the other plate (fig 2.2a). The amount of charge (Q) in the capacitor is proportional to the applied potential (V). Their ratio Q/V is defined as the capacitance (C). The unit of capacitance is in farad (F), which is defined as coulomb per volt. The capacitance of each capacitor is constant. For a simple parallel capacitor, calculation of the capacitance can be made from the equation:

$$C = \frac{A \epsilon_0 \epsilon_r}{d} \quad 2.1$$

Where A is the surface area of the one plate, ϵ_0 is the vacuum permittivity constant with the value of $8.854 \times 10^{-12} \text{ F m}^{-1}$, ϵ_r is the relative permittivity of dielectric media, and d is the distance between the plates. For typical capacitors, the capacitance is normally lower than 10^{-2} F (1 nF/cm^2) due to the limited area ($A < 1 \text{ m}^2$), and large distance between the plates ($d \approx 1 \text{ }\mu\text{m}$). This capacitance value cannot meet the requirements in many fields such as microelectronics and hybrid heavy duty platforms.

In order to increase the amount of charge stored, one needs to minimize d and maximize A , a requirement that is met by a supercapacitor. Supercapacitor, also called as ultracapacitor or electrochemical capacitor, stores electrical energy at electrical double layers and/or by fast Faradaic processes and are governed by the same fundamental equations as conventional capacitors, but utilize higher surface area electrodes and thinner dielectrics to achieve greater capacitances. This leads to energy densities greater than those of conventional capacitors and power densities greater than those of batteries. This is why supercapacitors may become an attractive power solution for an increasing number of applications. As shown in Fig 2.2b, a supercapacitor is made of two

electrodes separated by an ion permeable separator to prevent short circuits between the electrodes and the cell is impregnated with a liquid electrolyte. When voltage is applied between positive and negative electrode in a supercapacitor, positive and negative ions within the electrolyte diffuse into the pores of the electrode of opposite charge, accumulate at the electrode/electrolyte interface and compensate for the electronic charge at the electrode surface, forming two charged layers (known as electric double layers, EDLs). The thickness d of the double layer is in the order of 5-10 Å for concentrated electrolytes, depending on the electrolyte concentration and the size of the ions. The double layer capacitance of each electrode can be estimated by considering it as a parallel-plate capacitor according to Eq. 2.1 and is about 5-25 $\mu\text{F}/\text{cm}^2$ for an carbon based electrode in concentrated electrolyte solution assuming a relative dielectric constant ϵ_r of 10 for water in the double layer. The capacitance of a single electrode, consisting of a high surface area carbon with 1000 m^2/g and a double layer capacitance of 20 $\mu\text{F}/\text{cm}^2$ is calculated to be 200 F/g.

Since the two electrodes of a supercapacitor form a series circuit of two individual capacitors C^+ and C^- , the reciprocal value ($1/C$) of the supercapacitor is equal to the sum of the reciprocal values of the negative electrode ($1/C^-$) and the positive electrode ($1/C^+$). Supercapacitors may have either symmetric or asymmetric electrodes. Symmetry implies that both electrodes have the same capacitance value, giving a capacitance of half the value of each single electrode (if $C^+ = C^-$, then $C = 0.5C^+ = 0.5C^-$). For asymmetric capacitors, the capacitance can be equal to that of the electrode with the smaller capacitance (if $C^+ \gg C^-$, then $C \approx C^-$).

$$C = \frac{Q}{V} \quad 2.2$$

$$\frac{1}{C} = \frac{1}{C^+} + \frac{1}{C^-} \quad 2.3$$

Where C is the capacitance (in Farad, F), Q is the amount of charge (in Coulombs, C) stored on each electrode/electrolyte interface, V is the voltage (in Volts, V) between two electrodes, C^+ is the capacitance of the positive electrode and C^- is the capacitance of the negative electrode. Current supercapacitor technology uses activated carbon as the electroactive material since it exhibits high conductivity and large surface area on order of 1000-2500 m^2/g , meaning that high capacitance values can be obtained in a small

space. For instance, comparing a capacitor and a supercapacitor of similar volume as shown in Figure 2.1, the dielectric capacitor stores only 0.003 F, whereas the supercapacitor stores >10,000 times more charge – about 50 F.

The specific capacitance of a supercapacitor cell (C_s , in F/g) is given by the function of specific capacitance (C_s^+ , C_s^-) and mass (m^+ , m^-) of positive and negative electrodes according to the following equation;

$$C_s = \frac{C}{m^+ + m^-} \quad 2.4$$

$$C_s = \frac{C^+ C^-}{(C^+ + C^-)(m^+ + m^-)} = \frac{C^+ C^-}{(C^+ + C^-)(m^+ + m^-)} \cdot \frac{m^+ m^-}{m^+ m^-} = \frac{\frac{C^+ C^-}{m^+ m^-}}{\frac{C^+ + C^-}{m^+ + m^-}} = \frac{C_s^+ C_s^-}{C_s^+ m^+ + C_s^- m^-} \cdot \frac{m^+ m^-}{m^+ + m^-} \quad 2.5$$

where C is the measured capacitance (in F) of the supercapacitor.

For symmetric supercapacitors with $m = m^+ = m^-$, $C_s^+ = C_s^- = C_e$ and $M = 2m$, the calculation of specific capacitance can be made by the following equation;

$$C_s = \frac{C}{m^+ + m^-} = \frac{C}{2m} = \frac{C}{M} = \frac{0.5C^+}{2m} = \frac{0.5C^-}{2m} = \frac{C^+}{4m} = \frac{C^-}{4m} = \frac{C^+}{2M} = \frac{C^-}{2M} = \frac{C_s^+}{4} = \frac{C_s^-}{4} = \frac{C_e}{4} \quad 2.6$$

where C_e is the specific capacitance of electrode in F/g⁻¹.

In the case of Asymmetric supercapacitors, the following equation should be satisfied for the charge balance ($q^+ = q^-$),

$$q^+ = q^- = C_s^+ V^+ m^+ = C_s^- V^- m^- \quad 2.7$$

where q^+ and V^+ is the charge (in C) and the voltage of the positive electrode, respectively; q^- and V^- is the charge (in C) and the voltage (in V) of the negative electrode, respectively.

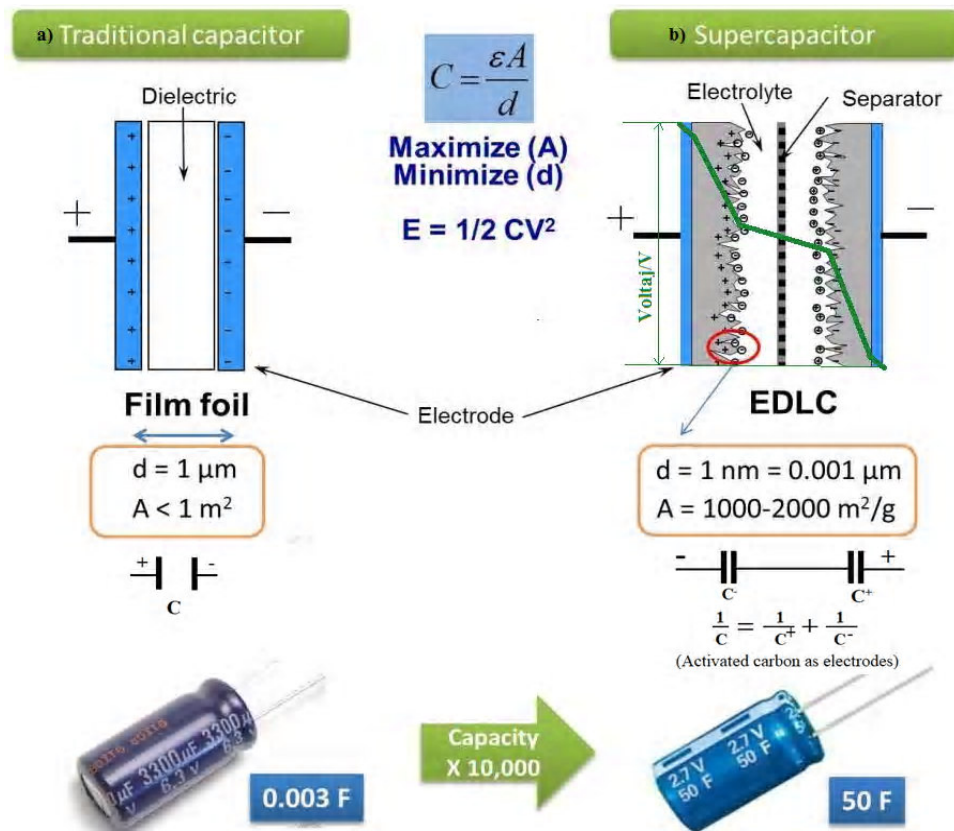


Fig 2.2 Schematic diagram showing voltage distribution and equivalent circuit of a) conventional (dielectric or film) capacitor charged, and b) supercapacitor (electric double layer capacitor, EDLC) charged.

The specific Energy (E_s) in Wh/kg and specific Power (P_s) in W/kg for a supercapacitor can be calculated as

$$E_s = \frac{1/2 CV^2}{3.6 \text{ 2m}} = \frac{1/2 CV^2}{M \text{ 3.6}} = \frac{1/2 C_s V^2}{3.6} \quad 2.8$$

$$P_s = \frac{E_s \text{ 3600}}{t} = \frac{IV \cdot 1000}{2M} = \frac{I_s V \cdot 1000}{2} \quad 2.9$$

Where I_s specific current, I/M (A/g). As indicated by the equation 2.8, in order to obtain a high energy density, a large electrochemical potential window and high capacitance are required. The capacitance of supercapacitors is determined by the specific surface area of the electrode accessible to the electrolyte ions and porosity of electrode materials. The electrochemical potential window depends on the thermodynamic stability of the electrolyte solution.

Calculation of the maximum specific power (W/kg) can be carried out by the equation,

$$P_{max} = \frac{V^2_{1000}}{4R_{ESR}M} \quad 2.10$$

$$\frac{E_s \cdot 3600}{P_{max}} = 2R_{ESR} \cdot C = 2\tau \quad 2.11$$

where R_{ESR} , τ and C is the equivalent series resistance (ESR), time constant (in s) and capacitance of supercapacitor in F, respectively. The calculation of R_{ESR} can be made through the analysis of the IR drop or voltage variation at the initial stage of the constant current discharge curve,

$$R_{ESR} = \frac{\Delta V}{\Delta I} \quad 2.12$$

where ΔV and ΔI is the IR drop and discharge current change, respectively. In the case of 0 min dwelling time, the current change is:

$$\Delta I = 2I \quad 2.13$$

whereas in the cases of >1 min dwelling time,

$$\Delta I = I \quad 2.14$$

The value of R_{ESR} is contributed from **i)**the electronic resistance of the electrodes **ii)**the contact resistance between current collectors and electrodes and **iii)**the ionic resistance of the electrolyte **iv)**the ionic resistance of the separator and **v)**the ionic resistance of the small pores.

2.2 Applications of Supercapacitors

Supercapacitors store and release energy very quickly and are used in many different applications, some of these applications are described below[2]

2.2.1 Industrial Applications: Currently, supercapacitors are used in uninterruptible power supplies (UPS) to protect hardware such as data centers, computers, telecommunication equipment and other electrical equipment where an unexpected power disruption could cause fatalities, injuries, serious data loss or business disruption. They are also the only power source for low energy applications such as automated

meter reading (AMR) equipment or for event notifications in industrial electronics. Furthermore, they complement a primary energy source like an internal combustion engine, battery or fuel cell, which cannot repeatedly supply quick bursts of power. This combination decreases the cost per cycle, saves on replacement and maintenance costs, allows the battery size to be reduced, and extends battery life.

2.2.2 Transportation

a)Heavy Hybrid Vehicles: Supercapacitors are particularly suitable for city transit buses (Fig 2.3a) with stop-and-go driving; in trash trucks, which can experience as many as a thousand start/stop cycles during a day; and in delivery trucks, which operate on similar drive cycles.

b)Engine Start Modules using supercapacitors shown in Fig 2.3b, can replace the traditional lead acid starter battery and deliver reliable, quick-burst power at ignition—even after loading in hot or cold temperature extremes.

c)Energy Recovery: Supercapacitors can provide a solution to reduce greenhouse gas emissions and energy consumption by capturing and storing energy from regenerative braking which can be used immediately or saved for later use. Long-haul trucks, Fleet vehicles, and other heavy-transportation vehicles such as trams, trains, light rail, and metros all get benefit from the adoption of a hybrid power train approach with the use of supercapacitors. For example, supercapacitors make possible the electric trams in southern Germany Figure 2.3c, to use 30% less energy than their equivalents in other regions. Other examples are industrial cranes and fork lifts.

d)Next Stop, Supercapacitor Buses: Recently, China has been experimenting with new buses that run entirely on carbon-based supercapacitors. Unlike a conventional trolley bus that has to continually touch an overhead power line, supercapacitor buses take big sips of electricity every three to five miles at assigned charging stations. So, while people are getting on and off the bus at bus stops, the supercapacitors can be fully recharged within a couple minutes, Fig 2.3d

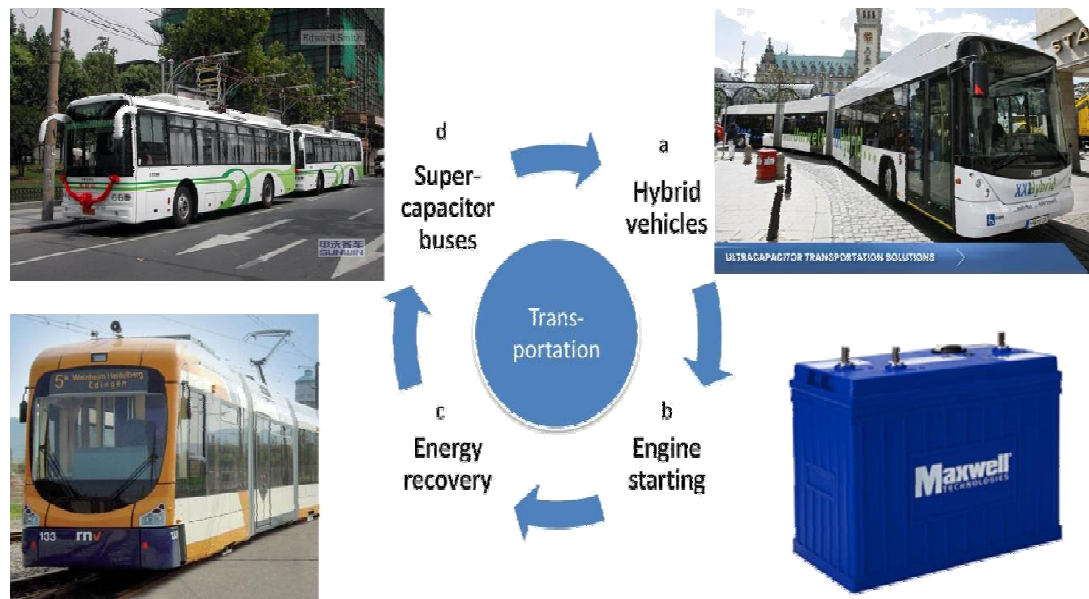


Figure 2.3 Applications of supercapacitors in transportation a) hybrid city-transit bus, b) engine starting module, c) electric trams, Mannheim, Germany and d) supercapacitor buses, Shanghai, China.

2.2.3 Consumer Electronics

a) Mobile Phones: Figure 2.4a shows a SonyEricsson K800 pictured from inside featuring two bulky electrolytic capacitors that precludes a thin form factor of the phone camera. In another example, Fig 2.4b shows two pictures that were taken in a dark room to compare with a standard battery-powered LED flash in a current camera phone and another one modified with a supercapacitor.

b) Power tools: Coleman™ introduced a cordless screwdriver powered by supercapacitors that takes only in 90 seconds for a recharge. This is very advantageous to most conventional cordless screwdrivers using batteries that can take up 3 to 5 hours to recharge, Figure 2.4c

c) Toys: Using a supercapacitor instead of a battery, a toy car can accelerate almost instantly to racing speeds (fig 2.4d). Combined with the ability of supercapacitors to be charged very quickly and recharged 100,000's of times, this application appears to be interesting.

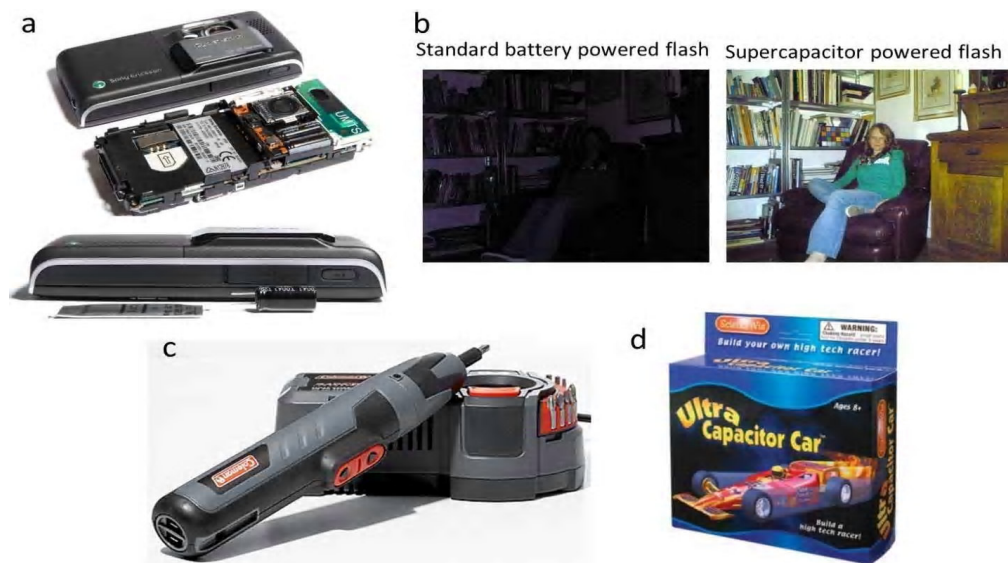


Figure 2.4 Applications of supercapacitors in consumer electronics a)mobile phone device b)camera flash, c)cordless screwdriver, and d)toys.

2.2.4 Energy Harvesting

Because of its rapid charging, a supercapacitor is often combined with the energy harvester to store the energy. The following are a few examples of this application:

a)The World's First Energy-Generating Revolving Door installed at Natuurcafe La Port in the Netherlands is used to generate electricity for a train station coffee shop. The door uses a generator that is operated by the energy applied when people pass through, Fig 2.5a. Supercapacitors store the generated energy and provide a power supply for the ceiling's LED lights.

b)The Forever Flashlight Uses no Batteries or Bulbs. The flashlight is shaken by hand for about 30 seconds to recharge a supercapacitor and it will then provide about 5-7 minutes of light, Fig 2.5b.

c)Wireless Power Modules combine an energy-harvester with a supercapacitor to create a perpetual, battery-free power source. The supercapacitor stores the harvested energy and supply peak transmission power over wireless networks such as the wireless sensors commonly used in security, environmental and condition-monitoring systems (Fig 2.5c).

d)Street lights: Sado City, in Japan's Niigata Prefecture, has street lamps that lights up LEDs at night time with energy generated by solar cells and stored in supercapacitors (Fig 2.5d).



Figure 2.5 Typical applications of supercapacitors for energy harvesting **a)**World's first energy-generating revolving door, Netherlands, **b)**a mechanically powered flashlight, **c)**wireless power modules, and **d)**a stand-alone power source for a street light.

2.2.5 Grid Storage

The variability in wind and solar output creates instability on the grid. This variability also results in poor utilization of these resources by 30-50%. Supercapacitors can help combat these challenges by providing energy storage for firming the output of renewable installations which increases grid stability. As of June 2012, Maxwell Technologies has installed power of >30 GW for the grid market and this use is still growing.

2.2.6 Aircraft

In 2005, Diehl Luftfahrt Elektronik GmbH, a manufacturer of aerospace systems and controls, chose supercapacitors to power emergency actuation systems for doors and evacuation slides in passenger aircraft, including the new Airbus 380 jumbo jet.

2.2.7 Medical

Supercapacitors are used in defibrillators where they can deliver a “lethal” 500 joules of energy providing the burst of power required to shock the heart. Low R_{ESR} supercapacitors are also used in DC motors for pumps, infusion and monitoring devices.

2.2.8 Military

Some of the earliest uses were motor startup for large engines in submarines and tanks. Evans' hybrid supercapacitors based on a ruthenium oxide cathode, shows a frequency response similar to an electrolytic capacitor while at the same time offering an energy content of about a factor of 10 higher than a comparable aluminum electrolytic capacitor of the same size. This makes them perfectly suited for Defense and Aerospace applications requiring high power such as power interruption buffers, filtering and high current pulse generation. Other applications that benefit from the high power of supercapacitors include GPS guided missiles and shells, laser power supplies, Unmanned Aerial Vehicles, radar and high power discharges for naval warfare.

2.3 Supercapacitor's Storage Mechanism

Depending on charge storage mechanism or cell configuration, supercapacitors can be classified into **i)** electrical double-layer capacitors (EDLCs), in which the charge is accumulated by the charge separation at the electrolyte/electrode interface, **ii)** pseudocapacitor, in which the charge is stored by fast Faradaic processes taking place at the electrode/electrolyte interface, which involves surface ion adsorption and insertion and **iii)** hybrid supercapacitor, in which the charge is stored by both the charge separation at the electrode/electrolyte interface and fast Faradaic processes taking place at the electrode/electrolyte interface. The different types of supercapacitor are classified in Fig 2.6 and table 2.1

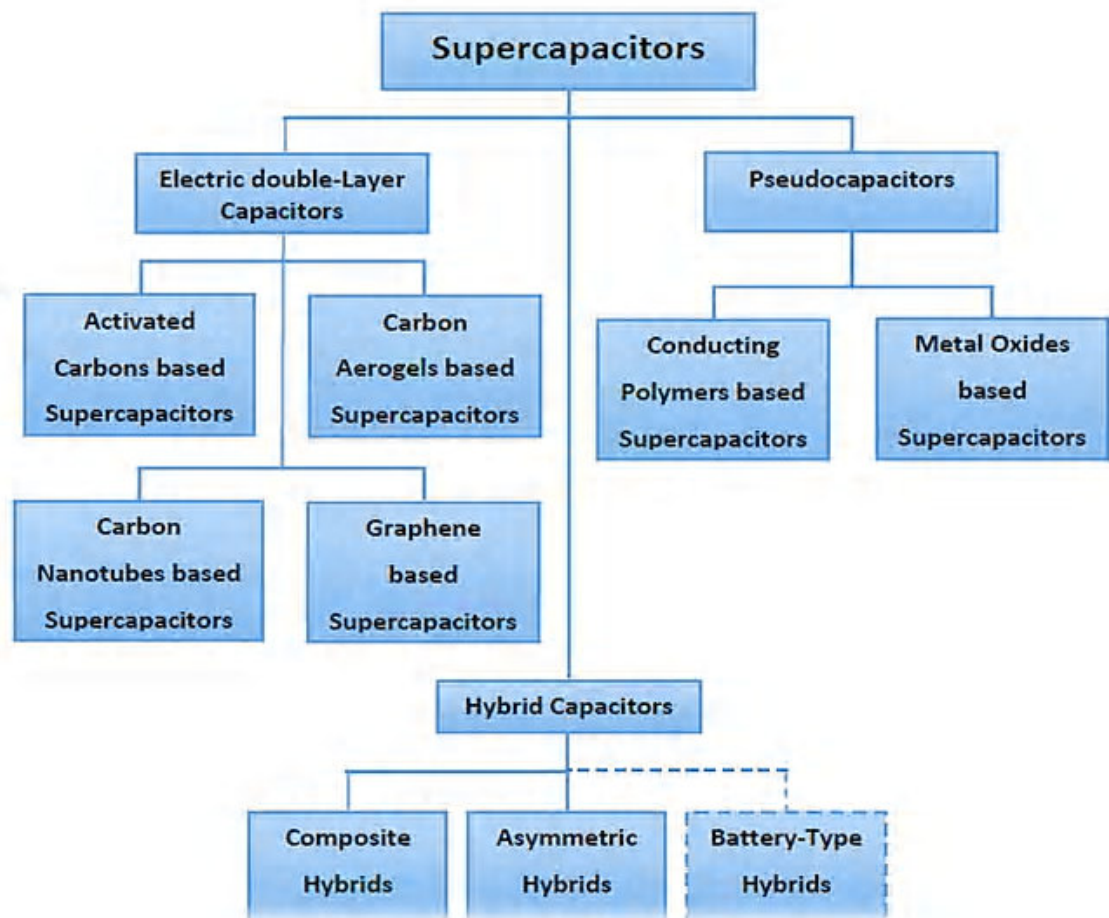


Fig 2.6 Classification of supercapacitors

model, Chapman model and Gouy-Chapman-Stern model are shown in fig 2.7, where Ψ is the potential, Ψ_0 is the electrode potential, d is the double layer thickness (separation between charges), IHP is the inner Helmholtz plane, and OHP is the outer Helmholtz plane in the Stern model.

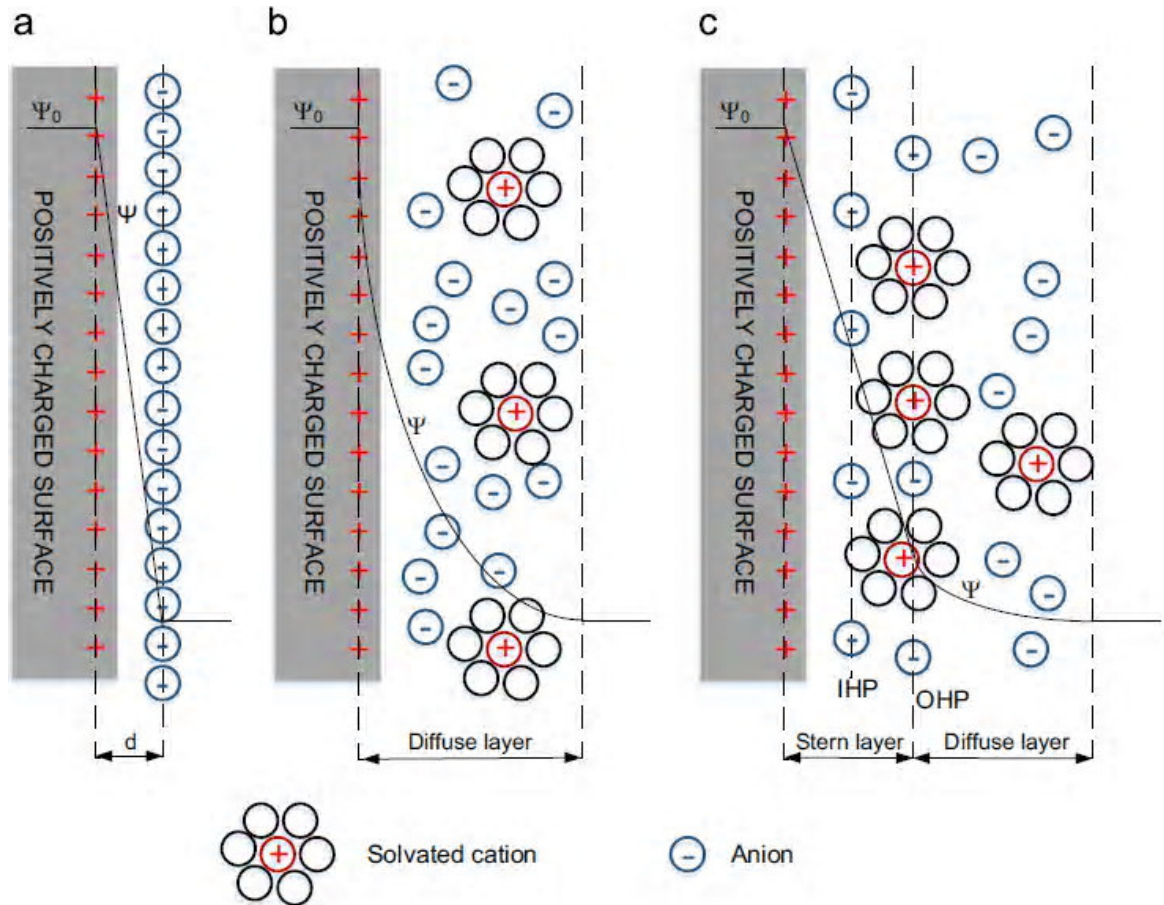


Fig 2.7 EDL models, **a)**Helmholtz model, **b)**Gouy-Chapman model, and **c)**Stern model [7]

Electricity storage and discharge via EDL was first introduced by Becker in 1957 (U.S. Patent

42,800,616) and the supercapacitors are then called electric double layer capacitors (EDLCs).

When a supercapacitor is charged, electron transfer takes place from the positive electrode to the negative electrode through an external circuit whereas cations within the electrolyte accumulate at the negative electrode surface and anions accumulate at the

positive electrode surface forming an EDL that balances for the external charge. During the discharge, electrons are transferred from the negative electrode to the positive electrode through an external circuit, and both kinds of ions in the electrolyte become mixed again until the cell is discharged. Charged and discharged states of EDLC is illustrated in fig 2.8.

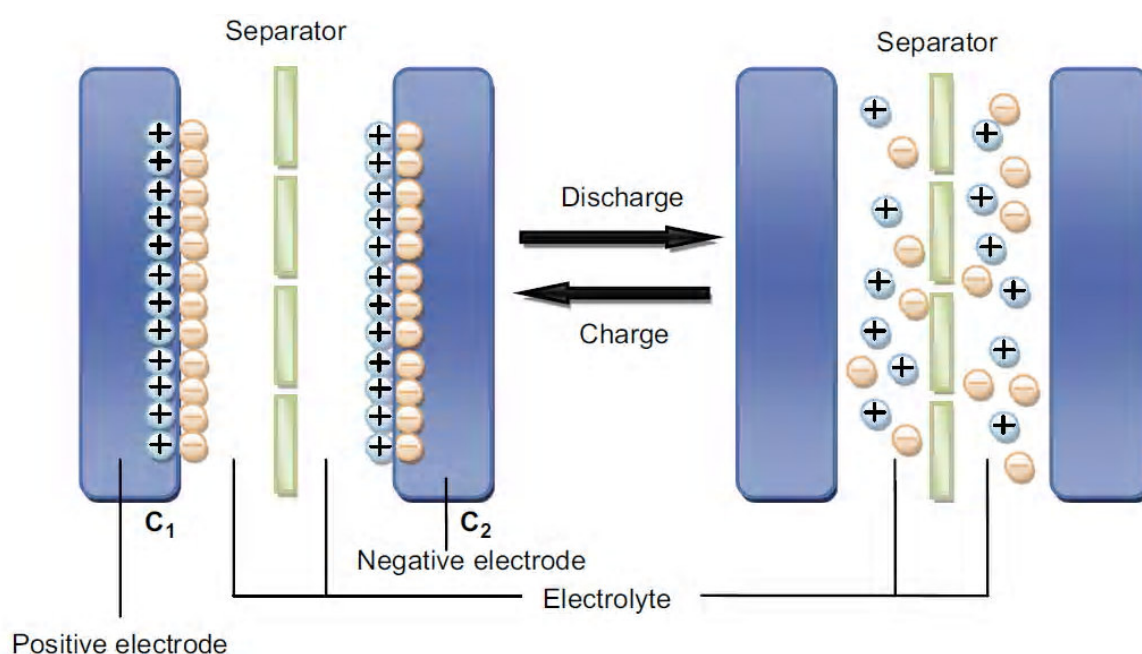


Fig. 2.8 Charged and discharged states of EDLC[8]

EDLCs are based on high specific surface area nanoporous materials as electrode materials, resulting in a huge capacitance compared to electrostatic capacitors. Electrodes for EDLCs usually consist of nanoporous carbon based materials such as graphene, carbon nanotubes, carbon aereogels and activated carbon. The most used electrode materials for commercial EDLCs are activated carbons due to high surface area ($1000\text{-}2500\text{ m}^2/\text{g}$), long cycle life, high conductivity, good rate capability, good cycling stability, relatively low cost, availability and established production technologies. The capacitance (150 F/g^{-1} for carbon) depends on the pore size distribution and active electrode surface area. The energy density of carbon based commercial EDLC supercapacitors with organic electrolyte is about $3\text{-}5\text{ Wh/kg}$, which is much lower than that of electrochemical batteries ($30\text{-}40\text{ Wh/kg}$ for a lead-acid battery and $10\text{-}250\text{ Wh/kg}$ for a lithium ion battery).

Typical cyclic voltammogram (CV) and galvanostatic charge/discharge (GCD) plots of a laboratory type EDLC are given in Fig. 2.9. Rectangular shape of CV is the characteristic of a double layer charge storage mechanism. Assuming the current I is constant, as can be seen from Fig. 2.9a, the capacitance for a given scan rate can be calculated from CV curves according to the equation:

$$C = I/v \quad 2.15$$

where I , v and C is the current in A, the potential scan rate in V/s and the double layer capacitance in F, respectively.

The capacitance can be calculated based on the slopes of the GCD curves according to the equation:

$$C = \frac{It}{(V_f - V_i)} = \frac{It}{\Delta V} \quad 2.16$$

where I , t , V_i and V_f denote the current in A, the charging/discharging time in s, the initial potential in V, and the final potential in V, respectively.

The coulombic efficiencies (CE %) can be calculated from the charge (t_d) and discharge (t_c) times according to the equation;

$$CE \% = \frac{t_d}{t_c} \times 100 \quad 2.17$$

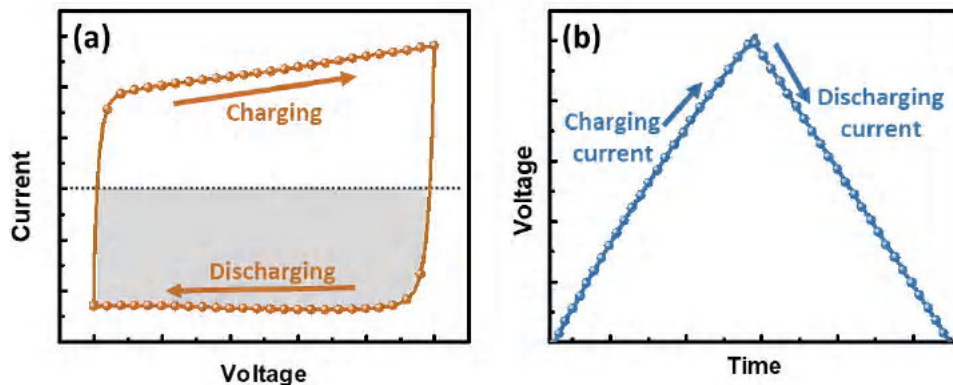


Fig. 2.9 a)cyclic voltammetry and b)galvanostatic charge/discharge plots for EDLC cell [9]

2.3.2 Pseudocapacitors

Pseudocapacitance is based on reversible Faradaic reaction containing charge transfer between the active electrode material and electrolyte. The electrons generated by the redox reaction are transferred across the electrolyte/electrode interface. The mechanism of pseudo capacitors is similar to that of rechargeable batteries except that the latter have much slower charging and discharging rates, as shown in fig 2.10.

Metal oxides/hydroxides or conducting polymers and sometimes functionalized porous carbons combining EDLC and pseudocapacitive charge storage mechanisms are used as electrode materials for pseudocapacitors. Among these materials, transition metal oxides/hydroxides play important role due to their chemical stability, variable valance, high capacitance and high energy density. So far, various metal oxides/hydroxides such as RuO_2 , MnO_2 , Mn_3O_4 , Mn_2O_3 , Fe_3O_4 , Co_3O_4 , NiO , , CuO , SnO_2 , and $\text{Co}(\text{OH})_2$ have been used as electrode materials for supercapacitors. Within these transition metal oxides/hydroxides, RuO_2 was the most widely investigated due to its high conductivity, high specific capacitance and excellent chemical stability. In acidic electrolytes, a fast electron transfer together with an electro-adsorption of protons on the surface of RuO_2 particles occurs, according to the equation, where rutenium oxidation states can change from (I) to (IV):



However, owing to low abundance and high cost of rutenium, there are limitations to its practical applications. Less expensive transition metal oxides/hydroxides have been studied in aqueous electrolytes. Charge storage mechanism for metal oxides/hydroxides such as manganese oxide in aqueous solution is based on surface adsorption of electrolyte cation, $\text{C}^+(\text{Na}^+, \text{K}^+, \text{Li}^+ \text{ etc.})$ together with proton incorporation according to the reaction:



Although metal oxides/hydroxides can have much higher specific capacitance values compared to EDLCs, they have some drawbacks: **i)** redox reactions can lead to swelling and shrinkage of the active materials, resulting in mechanical degradation of electrodes and fading of the electrochemical performance during charge/discharge cycling **ii)** the

conductivity of pseudocapacitive materials except for RuO_2 is very low. The high resistivity of electrode materials increases the sheet resistance and the charge transfer resistance of the electrode and causes a large IR drop at a high current density, leading to the low rate capability and the low power density, and **iii**) the surface area, porosity and pore distribution in metal hydroxide/oxide are difficult to tailor.

To cope with the problem, the metal oxides/hydroxides are combined with conducting polymers and carbon to obtain composite materials, which combines merits and mitigate the shortcomings of both the components. In such composite electrodes, the carbon based materials serve as the physical support of metal oxides/hydroxides and provide the channels for charge transport. The high electronic conductivity of carbon materials supports the rate capability and power density at a large charge/discharge current. Metal oxides/hydroxides contribute to high specific capacitance and high energy density of the composite electrodes. The performance of the composite electrodes depends on their composition, microstructure and physical properties. The electronic conductivity, porosity, pore size distribution, and specific surface area effect the supercapacitor electrode performance.

The charge storage mechanism of n-doped and p-doped conducting polymers is given below:



The conducting polymer (p) such as polyaniline, polypyrrole, and thiophene-based polymers (poly(3,4-ethylenedioxythiophene), PEDOT) is doped with cation (C) or anion (A) to get n-doped or p-doped polymer respectively. The n-doping of polyaniline and polypyrrole needs large negative potential which is not desirable. The use of n-doped polymers for negative electrode is restricted due to the decrease of capacitance in negative potential window. To solve the problem, the conducting polymers are combined with other polymers, carbon, metal oxides and metal hydroxides. An improve performance can be obtained with composite electrodes.

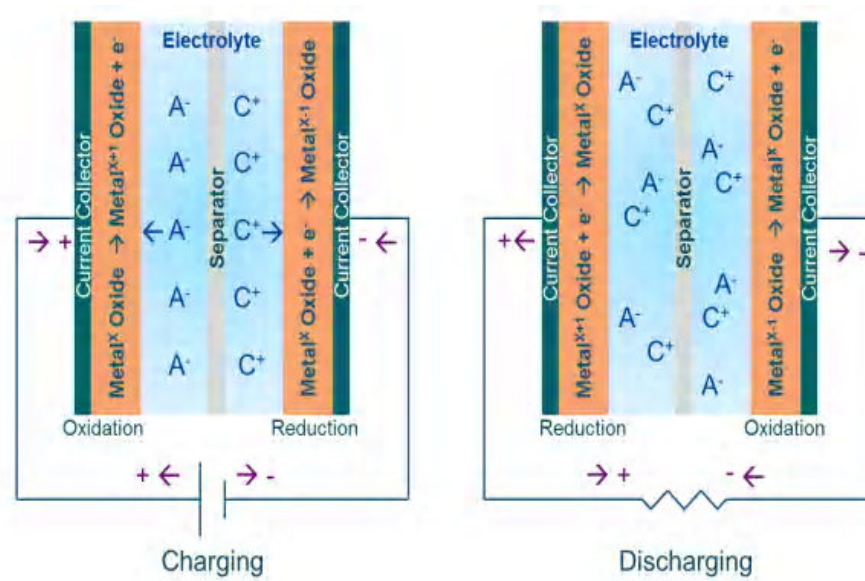


Fig. 2.10 Illustration of the charge storage in pseudocapacitor

In principle, pseudo-capacitance is related to thermodynamics. The theoretical capacitance of metal oxide can be calculated according to the equation:

$$C = \frac{n.F}{M.V} \quad 2.22$$

where n , F , M and V are the number of electrons transferred in the redox reaction, the Faraday constant, the molar mass of the metal oxide and the voltage window, respectively.

Typical cyclic voltammogram and galvanostatic charge/discharge plots of a laboratory type pseudocapacitor are given in Fig. 2.11. Quasi-rectangular shape of CV is the characteristic of a pseudocapacitance mechanism for charge storage. The capacitance for a given scan rate can be calculated from CV as

$$C = \frac{\int_{V_i}^{V_f} I(V) dV}{v(V_f - V_i)} = \frac{\int_0^T I(t) dt}{\Delta V} \quad 2.23$$

where I , V_i , V_f and v denote the current in A, the initial potential in V, the final potential in V, and the potential scan rate in V/s, respectively.

The capacitance can be calculated from GCD as

$$C = \frac{It}{\Delta V} \quad 2.24$$

$$C = \frac{F \int_0^t V(t) dt}{\Delta V^2} \quad 2.25$$

The energy calculated from Eq. 2.24, the highlighted area under the dashed straight lines, is underestimated for charging, but overestimated for discharging. However, the actual energy, the area under the curved solid lines, can be calculated using Eq. 2.25.

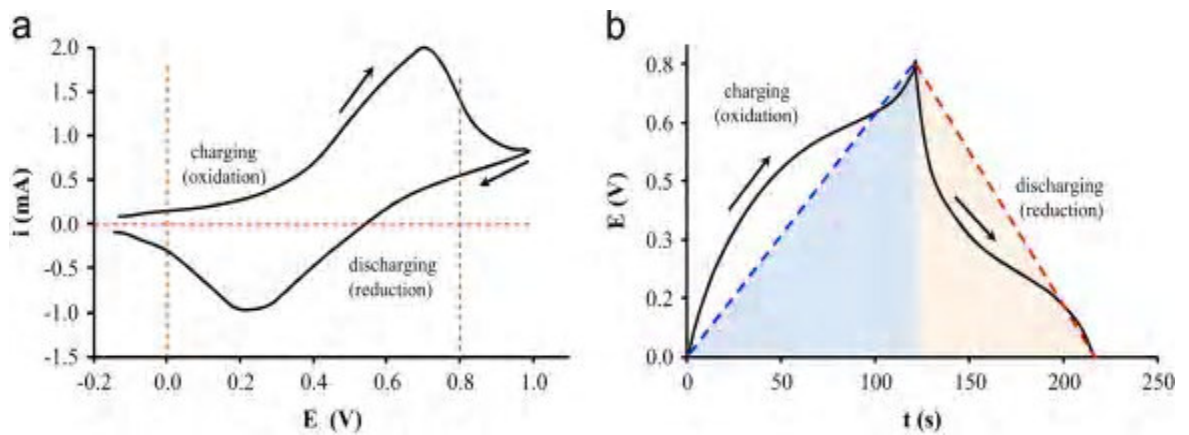


Fig 2.11 a)cyclic voltammetry and b)constant current charge/discharge curves for pseudocapacitors [1]

2.3.3 Hybrid Capacitors

Hybride supercapacitors are constructed by combining a pseudo-capacitive or a battery electrode (energy source) with a capacitive electrode (power source). They combine high capacitance and energy density of the pseudo capacitors or batteries and the higher power density of the EDLC to give better performance. The hybrid supercapacitors can be further classified as symmetric composite, Asymmetric and battery type. This type of supercapacitors uses different kind of electrode materials in one electrode or in the device. The symmetric composite type has two similar electrodes in device but electrodes themselves are composite of different electrode materials. The materials can be composite of metal oxide/hydroxide or conducting polymer with carbon based materials. Assymmetric type supercapacitors use different type electrode materials for the electrodes to expand the operating potential window of the device itself. Metal

oxide/hydroxide or conducting polymer can be used as cathode and carbon as anode for Asymmetric type supercapacitors. Battery type hybrid supercapacitors are made of a battery type electrode and a capacitive carbon electrode. The most widely known battery type hybrid system is the Li-ion capacitor (LIC), which is made of $\text{Li}_4\text{Ti}_5\text{O}_{12}$ nanocrystals or graphite materials as the cathode and activated carbon as the anode. Another example called the “ultrabattery” is the combination of EDLC (activated carbon) and a lead-acid battery. The combination of high energy density of battery materials with long cycle life and short charging/decharging time of supercapacitor materials is thought to be a very promising method.

2.4 Design of Supercapacitors

Supercapacitors are composed of the electrodes, the electrolyte, the current collector, and the separator. Among these, the electrodes are the most important component of supercapacitors. A few important parameters should be taken into account for preparing the electrolyte and electrodes **i)** large electrode surface area to accumulate maximum charges on the electrolyte/electrode interface **ii)** high electrolyte conductivity and **iii)** high corrosion resistance [10].

2.4.1 Electrolytes for Supercapacitors

As indicated by Eqs. (2.8), (2.9) and (2.10), the performance of a supercapacitor not only depends on the electrode materials but also the electrolyte. Electrolyte provides ionic conduction and also determines the electrochemical potential window (the operating voltage) of supercapacitors. Most important properties of electrolytes are the conductivity and the temperature coefficient, which basically determines the R_{ESR} of a supercapacitor. Other properties are a wide voltage window, high electrochemical stability, high ionic concentration, low solvated ionic radius, low volatility, low viscosity, low cost, low toxicity, and availability at high purity. The specific conductivity of a solution can be empirically optimized by means of choosing mixed solvents, modifying thus the solvation of the ions and the viscosity of the solution. The electrolyte concentration has to be high enough to prevent problems of electrolyte depletion (the electrolyte starvation effect) during the charge of the supercapacitor, especially for organic electrolyte. If the electrolyte amount is too small compared to the electrode surface area, the performance of a supercapacitor will be decreased.

Electrolyte concentrations higher than 0.2 M are normally sufficient. The thermodynamic stability of electrolytes determines the electrochemical potential window of supercapacitors. A large electrochemical potential window leads to both high energy and power densities.

Electrolytes currently used in supercapacitors can be classified as **i)** aqueous electrolytes, **ii)** conventional organic electrolytes, and **iii)** ionic liquid (ILs). For symmetric capacitors using aqueous electrolytes, the voltage window is typically limited to 1 V due to the thermodynamic decomposition of water at 1.23 V, whereas cells with organic electrolytes can reach 2.7 V and higher. Nevertheless, the limited voltage window of aqueous electrolytes for symmetric EDLCs has recently been increased to 1.6V using the neutral Na_2SO_4 electrolyte, for the AC-based and the graphene-based supercapacitors. Supercapacitors with aqueous electrolytes have higher capacitance compared to those using organic electrolytes. Aqueous electrolytes commonly used for supercapacitors are H_2SO_4 , KOH, NaOH, Na_2SO_4 , NaClO_4 , LiClO_4 , polyvinyl alcohol (PVA)- H_3PO_4 , H_2SO_4 -PVA and PVA-KOH gel polymer. Organic electrolytes with aprotic solvents such as acetonitrile or propylene carbonate solvents have been widely used in the commercial supercapacitors. Salts commonly used in organic electrolytes are tetraethylammonium tetrafluoroborate (TEABF_4) and triethylmethylammonium tetrafluoroborate (TEMABF_4). However, organic electrolytes suffer from low conductivity, low dielectric constant, high cost, flammability, and toxicity. Organic electrolytes demonstrate nearly 20 times higher specific resistance than aqueous ones, typically a 50 times higher specific resistance. Ionic liquids (ILs) have got much attention due to broad electrochemical potential windows (3.0-3.5V), nonvolatility, and high thermal stability. Recent study showed that CNT-based supercapacitors using 1-ethyl-3-methylimidazolium bis(trifluoromethanesulfonyl)imide ($[\text{EMIm}][\text{NTf}_2]$) as electrolyte provided a specific capacitance of 158 F/g^{-1} and an energy density of 53 Wh/kg with a cell voltage of 3 V[11]. However, their ionic conductivity at room temperature is a few mS.cm^{-1} , so they are mainly used at high temperatures such as in fuel-cell vehicle applications.

2.4.2 Separator

Separator is a membrane which acts as barrier to prevent electronic contact between electrodes but allows the transfer of charged ions. The specific capacitance, internal resistance (ESR), power density and energy density of supercapacitors depend on the choice of the separators. Separators must be **i)**highly porous to give high ionic conductivity **ii)**thin **iii)**mechanically stable to give durability for the supercapacitor **iv)**chemically inert and **v)**preserve wettability to allow ion conduction. The common separator used in research devices are glass filter paper, nylon, polyester, cellulose, nafion, and polymers such as polypropylene membrane with a porosity of 40-60%. In cases of gel electrolyte or semi-solid electrolyte, the use of separator can be excluded[12].

2.4.3 Current Collectors

Current collectors are conductive substrates on which the supercapacitor electrode materials are coated. In principle, any electrolyte inert material with high electronic conductivity can be used as current collector. For commercial supercapacitors, aluminum, copper or stainless steel foil is generally used. In research devices, materials with different structure in dimension from 1D to 3D, such as nickel or gold foil, carbon fabric, stainless steel fiber, and metal foam, have all been used as the current collector. Carbon in the form of a graphene paper or highly conductive nanotube is an attractive material for current collectors since it does not corrode in aqueous electrolytes and is very flexible. The use of carbon nanotube paper for manufacturing flexible supercapacitors is expected to increase as the cost of small-diameter nanotubes for making paper decreases. The thin sheet of nanotubes can potentially serve as an active material and current collector at the same time. Thin-film, wearable and printable supercapacitors could find many applications.

Various treatments on the current collector are used to reduce the contact resistance between the electrode materials and the current collector, including etching, pre-coating, and abrasion, for the contact resistance is considered to be the main contributor to the cell R_{ESR} . Supercapacitor with organic electrolytes use surface modified aluminium foil or grid current collectors.

Current collectors such as ITO coated polyethylene terephthalate (PET, transparent paper) have been employed in testing flexible supercapacitor devices due to their flexibility[13].

2.4.4 Additives

Various additives may be used as the binder for the active material to adhere to the current collector or to improve the conductivity of the electrode active material. For example, polytetrafluoroethylene (PTFE) and highly conductive carbon black are used as the binder and

the conducting materials, respectively for electrode materials. It has been shown that the additives can greatly influence the electrochemical performance and an optimal composition can be found. Some carbon nanostructures, including carbon nanotube, have also been used as additives to improve the performance of supercapacitors[14].

2.5 Performance Evaluation of Supercapacitors

Working voltage V , cell capacitance and equivalent series resistance (ESR), are essential factors to identify power and energy performance of supercapacitors, and they are generally sufficient for commercial supercapacitors where fabrication, cell design and the materials are all assigned. However in order to investigate new materials, more advanced manufacturing processes and new cell design, some other factors become essential. There are many factors that can influence the evaluation of the supercapacitors' performance and a list of key performance metrics, test methods and major influencing factors is presented in fig 2.12. The three essential parameters are emphasized in yellow; the power and energy densities in dark blue; time constant and cycling stability in light orange; all the important factors in light purple; and the related test methods in white. Various instruments or test methods have been developed and used to characterize the electrochemical performance of supercapacitors. Cyclic voltammetric (CV), constant current charge/discharge (CCCD) and electrochemical impedance spectroscopic (EIS) tests are the commonly used ones.

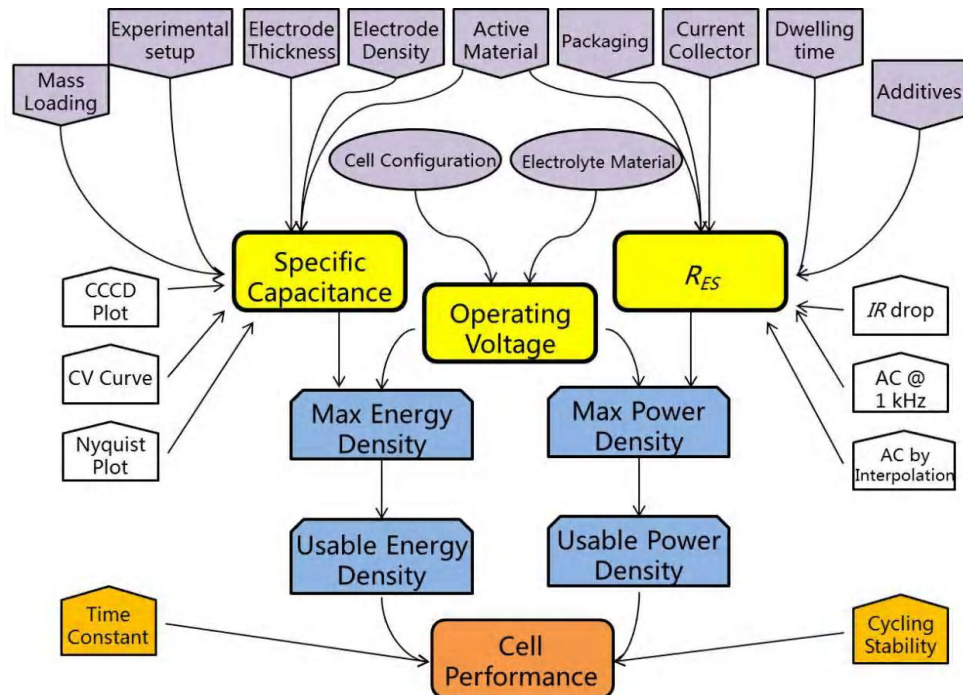


Fig 2.12 Key performance metrics, test methods and major factors for the evaluation of SCs [15]

CHAPTER 3

MATERIALS AND METHOD

3.1 Material Preparation

Nickel nitrate hexahydrate ($\text{Ni}(\text{NO}_3)_2 \cdot 6\text{H}_2\text{O}$), manganese nitrate tetrahydrate ($\text{Mn}(\text{NO}_3)_2 \cdot 4\text{H}_2\text{O}$), cobalt nitrate hexahydrate ($\text{Co}(\text{NO}_3)_2 \cdot 6\text{H}_2\text{O}$), potassium hydroxide (KOH), urea ($(\text{NH}_2)_2\text{CO}$), acetone and anhydrous ethanol were purchased from Sigma-Aldrich (USA). Deionized water was used in washing and synthesis process.

3.1.1 Synthesis of Activated Carbon/Nickel Manganese Hydroxide Carbonates Composites [AC@NiMn(n:m)] and Nickel Manganese Hydroxide Carbonates [NiMn(n:m)]

AC@NiMn(n:m) (n and m, the concentrations of Ni^{2+} and Mn^{2+} respectively with 0, 10, 20 and 30 mM) were synthesized via a hydrothermal process. In a typical procedure, the stoichiometric amounts of $\text{Ni}(\text{NO}_3)_2 \cdot 6\text{H}_2\text{O}$ and $\text{Mn}(\text{NO}_3)_2 \cdot 4\text{H}_2\text{O}$ were dissolved in 70 mL deionized water containing 0.147 g urea (2.45 mmol) and 0.105 g activated carbon to give the n:m values of 0:10, 10:0, 10:10, 10:20, 10:30, 20:10 and 30:10 mM. The suspensions were magnetically stirred for 15 min in air at room temperature and transferred into a Teflon-lined stainless steel autoclave and heated at 140°C for 10 h. Then, the resulting solid products were filtered, washed with deionized water and finally dried at 80°C for 1 h. NiMn(n:m) (the n:m values of 0:10, 10:0, 10:10 mM) were also synthesized under the same reaction conditions using the same procedure given above, but without activated carbon.

The activated carbon (AC) used in this study was prepared from sucrose via a hydrothermal process followed by a chemical activation with KOH. In a typical synthesis, 3M aqueous solution of sucrose was put into a 100 mL capacity Teflon-lined

stainless steel autoclave and heated at 190°C for 8 h. Then, the resulting solid products were filtered, washed with deionized water/alcohol and finally dried under vacuum at 200°C for 12h. For chemical activation, resulting spherical carbon was mixed with KOH in a mass ratio of 1:4, heated at 600°C for 3h in argon atmosphere in a tube furnace, washed with distilled water/0.1M HCl aqueous solution and finally dried at 80°C for 2h in an oven. Stoichiometric amounts of precursor materials used for synthesis of the composites is given in table 3.2

Table 3.1 Stoichiometric amounts of precursor materials for synthesis of AC@NiMn(n:m) and NiMn(n:m) composites

Stoichiometry of precursor for electrode materials	Urea mM	Ni(NO ₃) ₂ .6H ₂ O mM	Mn(NO ₃) ₂ .4H ₂ O mM	Activated carbon g/L
NiMn(1:0)	35	10	---	---
NiMn(0:1)	35	---	10	---
AC@NiMn(1:0)	35	10	---	1.5
AC@NiMn(0:1)	35	---	10	1.5
NiMn (1:1)	35	10	10	---
AC@NiMn (1:1)	35	10	10	1.5
AC@NiMn (1:2)	35	10	20	1.5
AC@NiMn (1:3)	35	10	30	1.5
AC@NiMn (2:1)	35	20	10	1.5
AC@NiMn (3:1)	35	30	10	1.5

3.1.2 Synthesis of Activated Carbon/Cobalt-Manganese Carbonates Hydroxide Hydrates Composites [AC@CoMn (n:m) (CO₃)_x(OH)_y.zH₂O] and Cobalt-Manganese Carbonates Hydroxide Hydrates[CoMn (n:m) (CO₃)_x(OH)_y.zH₂O]

AC@CoMn(n:m) (n and m, concentrations of Co²⁺ and Mn²⁺ with 0, 10, 20 and 30 mM) were synthesized via a hydrothermal method. In a typical procedure, the

stoichiometric amounts of $\text{Co}(\text{NO}_3)_2 \cdot 6\text{H}_2\text{O}$ and $\text{Mn}(\text{NO}_3)_2 \cdot 4\text{H}_2\text{O}$ were dissolved in 70mL deionized water containing 0.147g urea (2.45 mmol) and 0.105 g activated carbon to give the Co:Mn concentration ratios of 0:10, 10:0, 10:10, 10:20, 10:30, 20:10 and 30:10 mM. The suspensions were magnetically stirred for 15 min in air at room temperature and transferred into a Teflon-lined stainless steel autoclave and heated at 140°C for 10 h. Then, the resulting solid products were filtered, washed with deionized water and finally dried at 80°C for 1h. These materials are denoted as AC@CoMn (n:m) (AC, activated carbon; Co, cobalt; and Mn, manganese). CoMn(n:m) (n and m, the Co:Mn concentrations of 0:10, 10:0, and 10:10 mM) were also synthesized under the same reaction conditions using the same procedure given above but without activated carbon. Stoichiometric amounts of starting materials used for synthesis of the composites is given in table 3.2

Table 3.2 Stoichiometric amounts of starting materials for synthesis of AC@CoMn (n:m) $(\text{CO}_3)_x(\text{OH})_y \cdot z\text{H}_2\text{O}$ and CoMn (n:m) $(\text{CO}_3)_x(\text{OH})_y \cdot z\text{H}_2\text{O}$ composites

Stoichiometry of precursor for electrode materials	Urea mM	$\text{Co}(\text{NO}_3)_2 \cdot 6\text{H}_2\text{O}$ mM	$\text{Mn}(\text{NO}_3)_2 \cdot 4\text{H}_2\text{O}$ mM	Activated carbon g/L
CoMn(1:0)	35	10	---	---
CoMn(0:1)	35	---	10	---
AC@CoMn(1:0)	35	10	---	1.0
AC@CoMn(0:1)	35	---	10	1.0
CoMn (1:1)	35	10	10	----
AC@CoMn(1:1)	35	10	10	1.0
AC@CoMn(1:2)	35	10	20	1.0
AC@CoMn(1:3)	35	10	30	1.0
AC@CoMn(2:1)	35	20	10	1.0
AC@CoMn(3:1)	35	30	10	1.0

3.2 Structural Characterization

3.2.1 X-Ray Powder Diffraction

The crystallinity and the phases of the samples were identified by powder X-ray diffraction (XRD) using copper CuK_α radiation ($\lambda=1.5406 \text{ \AA}$) (Bruker AXS D8). The X-ray powder diffraction measurements were made using a Bruker AXS D8 X-ray diffractometer equipped with copper X-ray tube, NaI type scintillation counter detector and graphite monochromator. The diffraction data were collected in 2θ range of 10° - 70° with the step size of 0.02° and a count time of 10 s per step at 40 kV and 40 mA.

3.2.2 Scanning Electron Microscope Measurements

The morphology, particle size and particle size distribution of the samples were investigated using a scanning electron microscope (SEM, LEO 440), operated at an accelerating voltage of 20 kV, equipped with energy dispersive X-ray spectroscopy (EDX). The samples were laid on carbon tape before being measured and covered with Au-Pd alloy under high vacuum. The elemental composition of the samples was determined by EDX.

3.2.3 Conductivity Measurement

The conductivities of the samples were measured at room temperature by linear scanning voltammetry. The powder samples were uniaxially pressed into pellets under a pressure of about 9 tons using a stainless steel die with 13 mm diameter. The prepared pellets were located in a two-electrode Swagelok type cell and the potential versus current values were measured in a potential range of 0-100 mV at a scanning speed of 5 mV.s^{-1} with AMETEK Princeton Applied Research VersaSTAT MC model multi-channel galvanostat/potentiostat. The conductivity is calculated from the slope of current versus potential curve (fig. 3.1).

$$\frac{V}{I} = R, \quad \rho = R \cdot \frac{s}{l} \text{ ve } \chi = \frac{1}{\rho} = \frac{l}{sR}$$

Where V, I, R, ρ , s, l, and χ stand for voltage (mV), current (mA), the resistance (ohm), resistivity (ohm.cm), the surface area of pellet (cm^2), thickness of pellet (cm), and conductivity (S/cm), respectively.

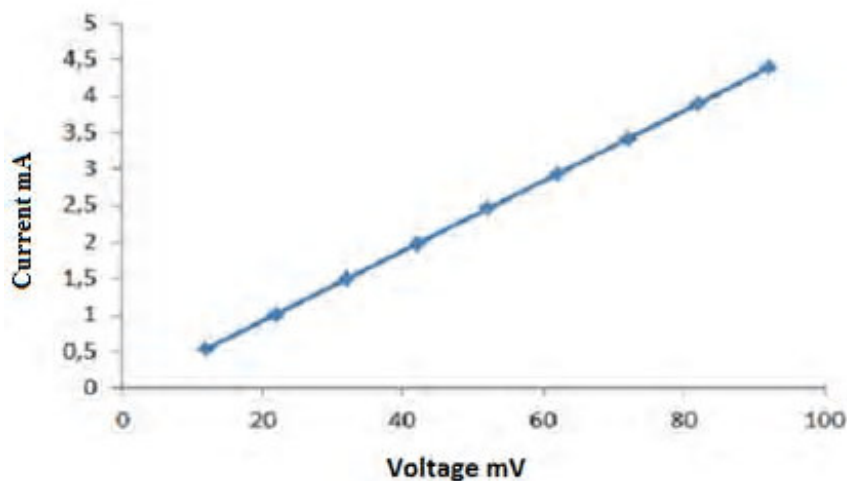


Figure 3.1 Linear scanning voltammetry curve

3.2.4 N₂ Adsorption/Desorption Measurement

Nitrogen adsorption/desorption isotherms of the prepared materials were measured using nitrogen gas adsorption on Micromeritics Corporation TriStar II 3020 V1.03. Before measurements, the samples were degassed at 120 °C for 24 hours. Once degassed, the isotherms were measured at 77 K in a p/p^0 (relative pressure) range of 0.001-1, with P^0 being 760 torr. The specific surface area and the pore size distribution were calculated with the Brunauer-Emmett-Teller (BET) and the density functional theory (DFT), respectively.

3.2.4.1 Adsorption Isotherms

To ease the comparison of adsorption data, the amount adsorbed is drawn against the equilibrium relative pressure (p/p^0) to get adsorption isotherms, where p^0 the saturation pressure of the pure adsorptive at the measurement temperature and p the equilibrium pressure. Adsorption isotherms generally provide some important information such as the adsorption capacity, pore size distribution, surface area, adsorption energy and adsorption type of various solid materials as an adsorbent. The most of adsorption isotherms may be classified into the six types given in figure 3.2. Type I isotherm is obtained with microporous solids having relatively small external surfaces (e.g. molecular sieve zeolites, activated carbons, and certain porous oxides), the uptake being limited by the accessible micropore volume rather than by the internal surface area.

Type II isotherm is obtained with a non-porous or macroporous adsorbent and represents unlimited monolayer-multilayer adsorption. The beginning of the linear middle section of the isotherm (point B), is often used to demonstrate the stage at which monolayer coverage is complete and multilayer adsorption about to start. The type III isotherm is convex to the p/p^0 axis and does not show a point B. This type isotherms is not common; the best known examples are obtained with water vapour adsorption on pure non-porous carbons. The type IV isotherm has a hysteresis loop related to the capillary condensation occurring in mesopores, and the uptake is limited over a range of high p/p^0 . The initial part of the type IV isotherm is ascribed to monolayer-multilayer adsorption since it follows the same path as the corresponding part of a type II isotherm. Type IV isotherms are shown by many mesoporous industrial adsorbents. The type V isotherm is related to the type III isotherm in that the adsorbent—adsorbate interaction is weak, but is acquired with certain porous adsorbents; it is uncommon. The type VI isotherm reflects stepwise multilayer adsorption on a uniform non-porous surface. The step—height now reflects the monolayer capacity for each adsorbed layer and, in the simplest case, remains nearly constant for two or three adsorbed layers. The best examples of type VI isotherms are those found with argon or krypton on graphitised carbon blacks at liquid nitrogen temperature .

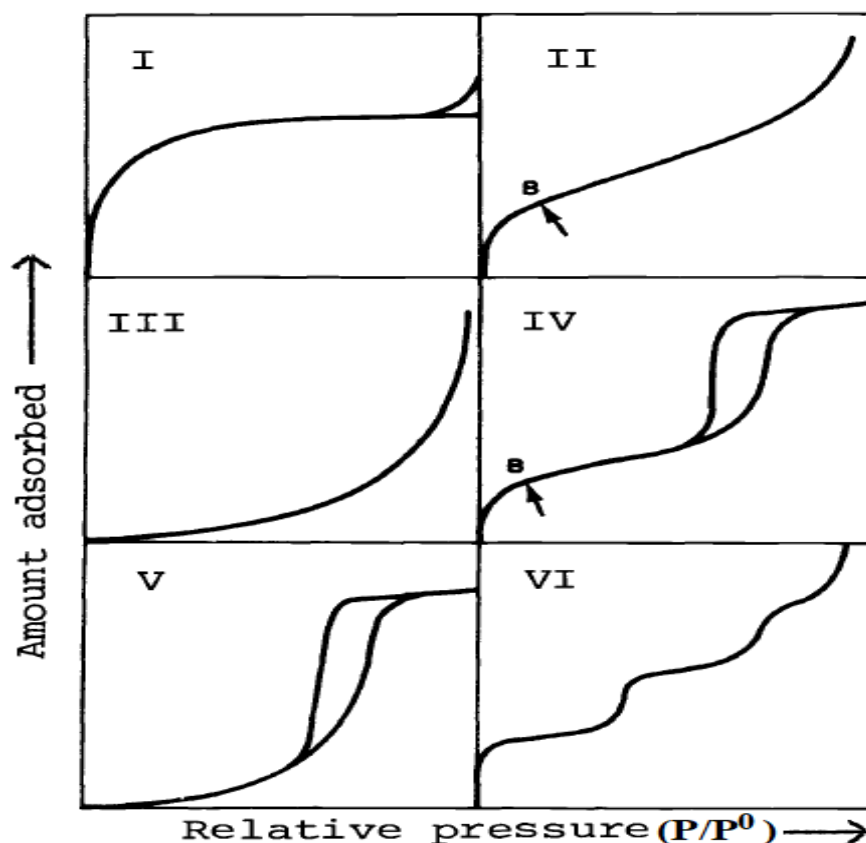


Fig 3.2 The IUPAC classification of adsorption isotherms [16]

3.3 Electrochemical Characterization

The electrochemical properties of the prepared materials were studied using the symmetric and asymmetric supercapacitor (SC) configurations by cyclic voltammetry (CV) and constant current charge/discharge (CCD) on an AMETEK Princeton Applied Research VersaSTAT MC model multi-channel galvanostat/potentiostat. The asymmetric supercapacitors were fabricated using the as prepared materials as the positive electrode, active carbon as the negative electrode, a cellulose paper as the separator and a 6.0M KOH aqueous solution as the electrolyte in a two-electrode Swagelok type cell with the electrode diameter of 13 mm. For the preparation of the electrodes, a slurry mixed with 80 wt. % of the active material, 10 wt.% of Super P conductor and 10 wt. % of polyvinylidene fluoride (PVDF, Fluka) binder in 1-methyl-2-pyrrolidinone (NMP, Merck) was coated on a piece of nickel foam current collector with a diameter of 13 mm, followed by vacuum drying at 120°C for overnight in a vacuum oven and uniaxial pressing between two flat plates at 10t for 5 min. The mass loading of

the positive electrode materials ranged from 9 to 11 mg cm⁻². The mass ratio of the electroactive materials in the positive and negative electrode was determined on the basis of the charge storage balance rule ($q^+ = q^-$) as shown in the following equation:

$$q^+ = q^- = m^+ C_m^+ \Delta V^+ = m^- C_m^- \Delta V^- \quad \frac{m^-}{m^+} = \frac{C_m^+ \Delta V^+}{C_m^- \Delta V^-}$$

where m , C_m , and ΔV are the mass loading of electrode materials, specific capacitance, and potential window of each electrode, respectively. The subscripts “+” and “-” represent the positive and negative electrodes.

Cyclic voltammetry measurements were made at a scan rate of 10 mV/s in different voltage ranges to determine the stable voltage windows of supercapacitors. Based on these curves, an operating voltage window of 0.8V symmetric supercapacitors and 1.2V for Asymmetric supercapacitors were selected. Cyclic voltammograms (CV) were measured at a scan rate of 10 mV s⁻¹ in a potential range of 0.0 to 0.8 V for the symmetric supercapacitors and 0.0 to 1.2V for asymmetric supercapacitors. Constant current charge–discharge measurements (CCD) were carried out in the respective potential windows at different current densities ranging from 0.5 to 15 A g⁻¹. The cycle life stability was studied by using Galvanostatic charge–discharge measurements in the respective potential ranges at a current density of 1A g⁻¹ for 5.000 cycles.

The capacitance, $C(F)$, of the SC devices was calculated from the constant current charge–discharge curves based on the following equation:

$$C = \frac{Q}{\Delta V} = \frac{I \times t}{\Delta V}$$

where Q , I , t and ΔV represent the total charge, discharge current (A), discharge time (s), and potential window (V) during discharge process, respectively.

This capacitance is then normalized by mass (F/g⁻¹) or area (F/cm⁻²) of the electrode to compare the performance accurately to other systems. The specific capacitance, C_m (F/g), and area capacitance, C_s (F/cm⁻²), were calculated using the following equations:

$$C_m = \frac{I \times t}{m \Delta V}$$

$$C_s = \frac{It}{s\Delta V}$$

where m and s represent the total mass of the positive and negative electrode materials (g) and the geometric surface area of one electrode (cm²), respectively.

The Energy density, E (Wh/kg⁻¹), and Power density, P (W/ kg⁻¹), were calculated from the following equations:

$$E = \frac{C_m \Delta V^2}{2 \times 3.6}$$

$$P = \frac{E \times 3600}{t}$$

where C_m, ΔV and t express the specific capacitance (F/g⁻¹), discharge potential window (V) and discharge time (s), respectively.

CHAPTER 4

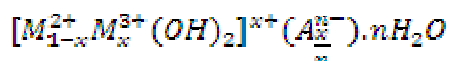
RESULTS AND DISCUSSIONS

4.1 Activated Carbon/Nickel Manganese Hydroxide Carbonates [AC@NiMn(n:m)] and Nickel Manganese Hydroxide Carbonates [NiMn(n:m)] Composites

4.1.1 X-Ray Powder Diffraction

X-ray diffraction pattern (XRD) and the elemental composition detected by energy dispersive X-ray spectroscopy (EDX) for the synthesized composite materials are given in figs 4.1-4.10 and table 4.1, respectively. The phases estimated from the elemental composition and XRD pattern of the composites are given in table 4.1 and figs 4.1-4.10. From table 4.1, it can be seen that the layered double hydroxides (LDH) were obtained with NiMn(1:1), NiMn(2:1) and NiMn(3:1) precursor stoichiometries, while metal oxide, carbonate and hydroxide composites were obtained with the rest of the stoichiometries given in the table.

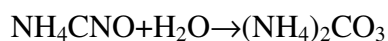
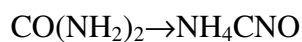
Layered double metal hydroxides are a class of layered ionic compounds that comprise positively charged layers with two kinds of metallic cations and exchangeable hydrated anions placed between layers for charge balance [17]. Cations are octahedrally coordinated by six oxygen atoms of OH group. Each OH group is shared by three octahedral cations. The general formula for LDH is :



where M^{2+} shows divalent cation, (Fe^{2+} , Co^{2+} , Mg^{2+} , etc.), M^{3+} shows trivalent cation (Fe^{3+} , Cr^{3+} , Al^{3+} , etc), and x is the molar ratio, $M^{3+}/(M^{3+}+M^{2+})$.

In the synthesis with urea, carbonate and hydroxide generated by hydrolysis of urea in the presence of M^{2+} and M^{3+} mixture gives rise to formation of layered double metal hydroxide, metal oxides and hydroxides depending on the precursor stoichiometry.

The hydrolysis mechanism of urea is proposed as follows:



The conductivity values of the synthesized composite materials are given table 4.1. As seen from the table, the conductivity of the composites with AC is higher than that of the composites without AC, which is advantage to get high power for supercapacitor.

Table 4.1 Elemental composition, estimated phases, BET surface area and conductivity of the synthesized composite materials

Stoichiometry of precursor for electrode materials	Ni atomic %	Mn atomic %	O atomic %	C atomic %	N Atomic %	Estimated phases for electrode materials	BET (m ² /g)	Conductivity (S.cm ⁻¹)
AC			12.51	87.49		AC	2308.0	0.2
NiMn(1:0)	19.8		60.3	19.9		Ni(OH) ₂ /NiCO ₃	235.4	3.6x10 ⁻⁵
NiMn(0:1)		24.0	55.9	20.1		Mn ₃ O ₄ /MnCO ₃	69.0	4.9x10 ⁻⁵
NiMn(1:1)	24.1	1.6	53.6	11.0	9.7	NiMn(1:1) LDH*	93.0	1.2x10 ⁻⁷
AC@NiMn(1:0)	21.3		29.0	49.8		AC@Ni(OH) ₂ /NiCO ₃	255.0	2.3x10 ⁻⁴
AC@NiMn(0:1)		4.8	29.9	65.4		AC@MnCO ₃	76.5	1.2x10 ⁻³
AC@NiMn(1:1)	2.7	0.3	24.6	72.0		AC@NiMn(1:1) LDH*	267.7	2.0x10 ⁻³
AC@NiMn(1:2)	2.9	1.1	20.0	76.0		AC@NiCO ₃ /MnCO ₃	374.7	7.2x10 ⁻⁵
AC@NiMn(1:3)	5.5	1.8	22.2	70.6		AC@NiCO ₃ /MnCO ₃	339.2	5.3x10 ⁻³
AC@NiMn(2:1)	3.8	0.4	21.8	74.0		AC@NiMn (2:1) LDH*	368.8	2.1x10 ⁻³
AC@NiMn(3:1)	11.4	1.5	45.6	41.5		AC@NiMn (3:1) LDH*	241.5	1.7x10 ⁻³

*Layered double hydroxide

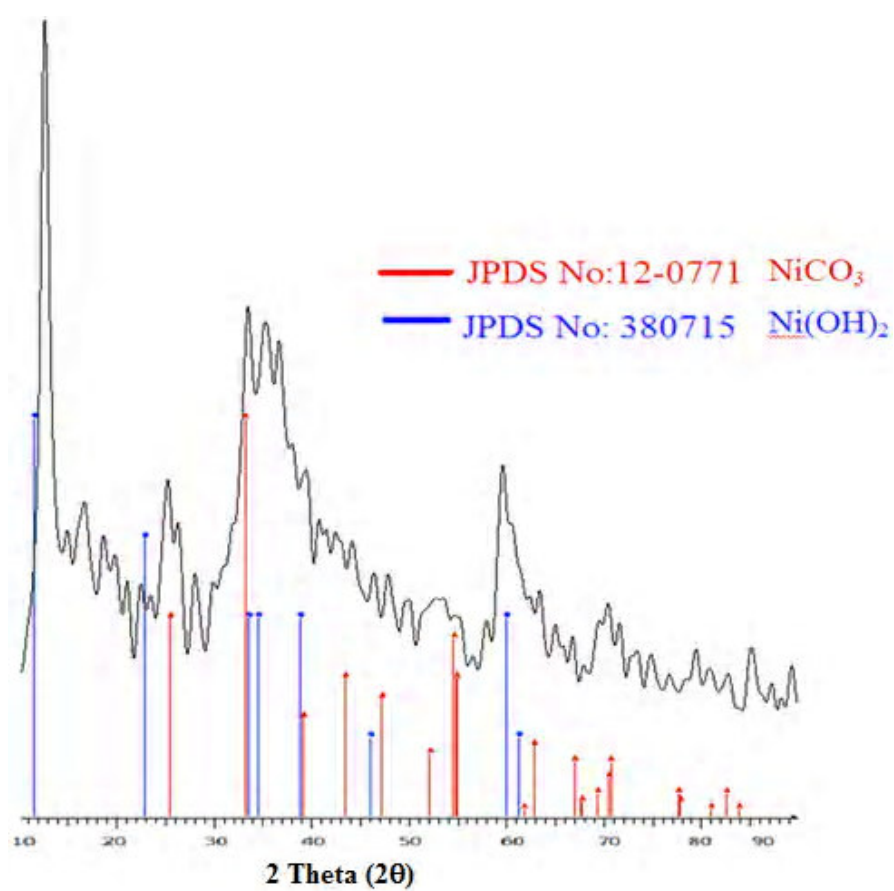


Fig 4.1 XRD pattern for NiMn(1:0) composite

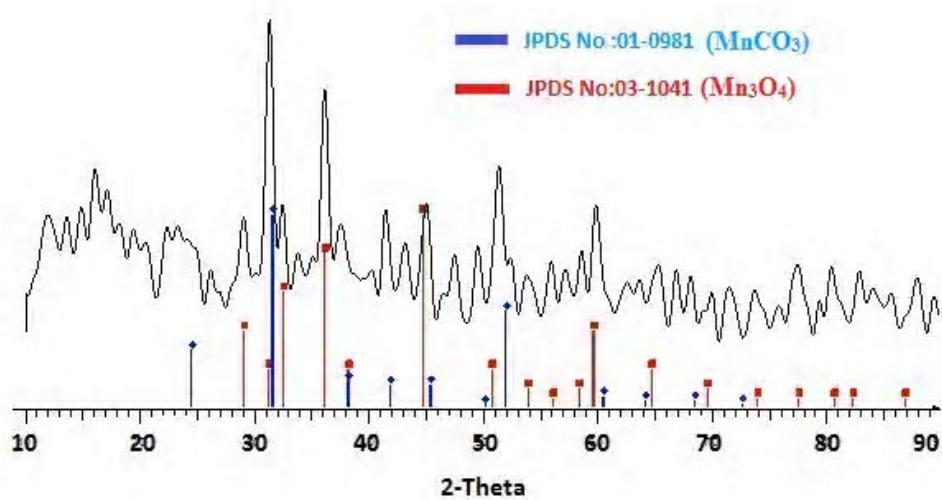


Fig 4.2 XRD pattern for NiMn(0:1) composite

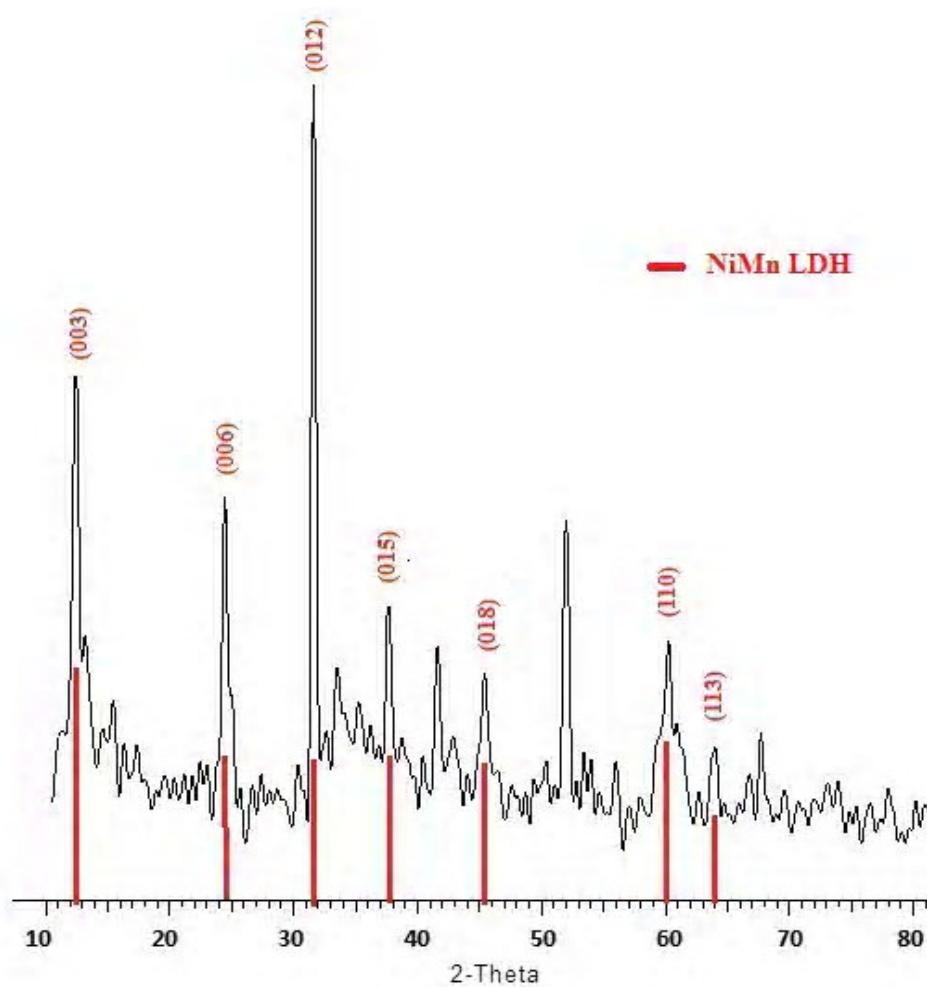


Fig 4.3 XRD pattern for NiMn(1:1) composite

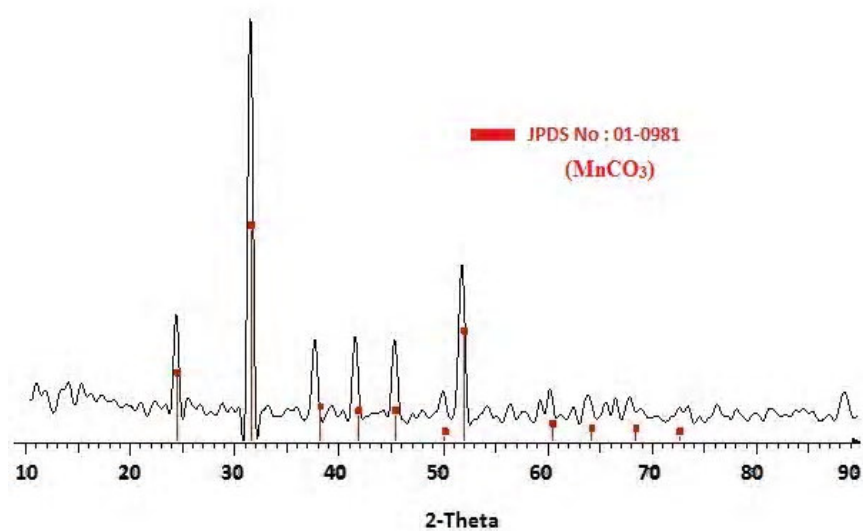


Fig 4.4 XRD pattern for AC@NiMn(0:1) composite

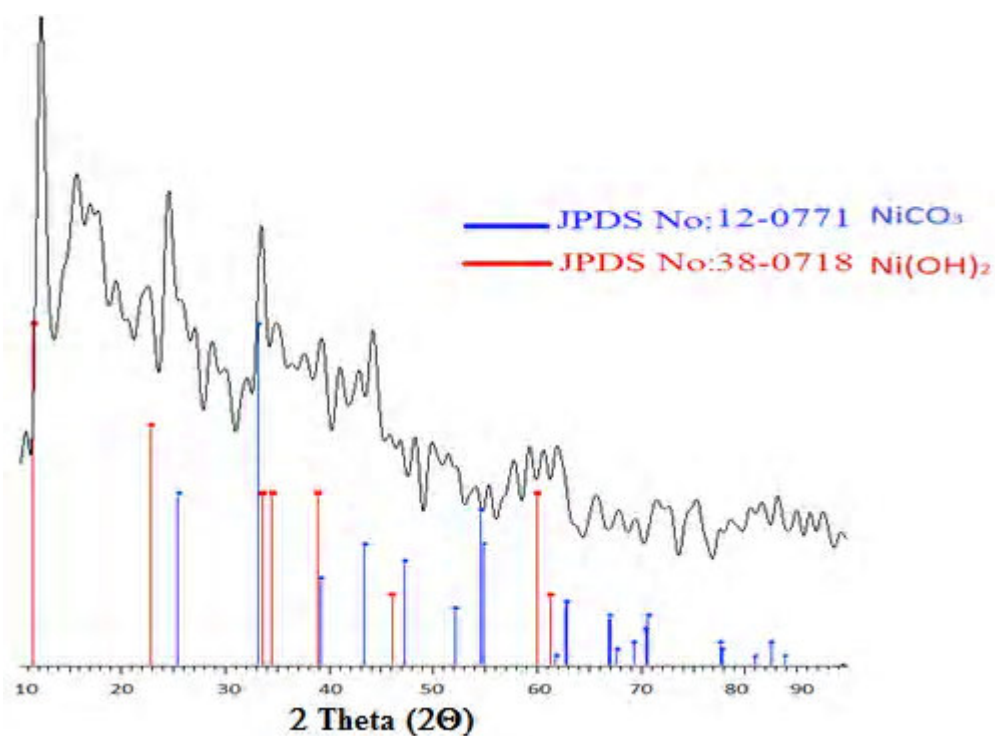


Fig 4.5 XRD pattern for AC@NiMn(1:0) composite

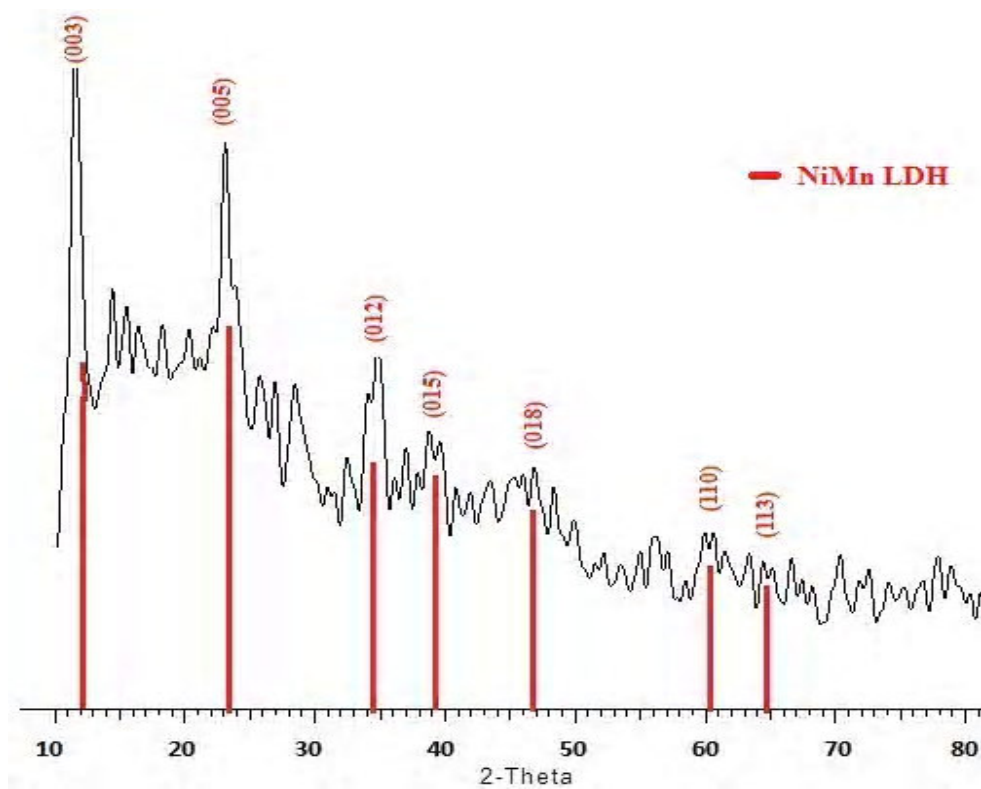


Fig 4.6 XRD pattern for AC@NiMn(1:1) composite

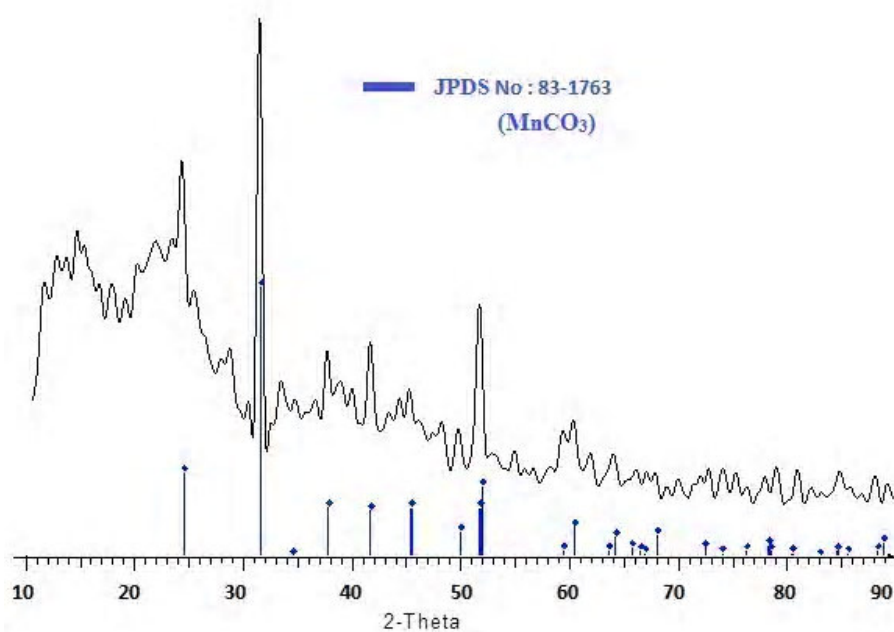


Fig 4.7 XRD pattern for AC@NiMn(1:2) composite

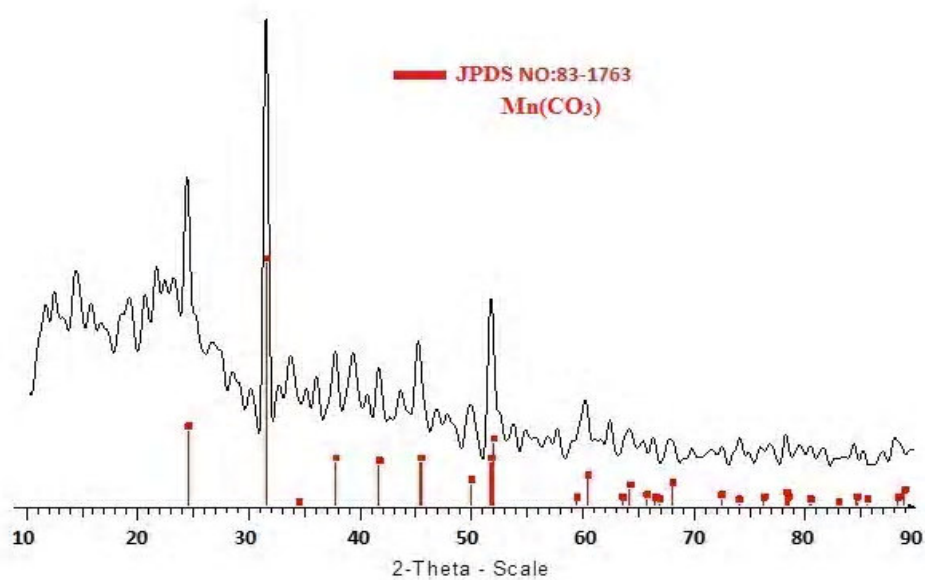


Fig 4.8 XRD pattern for AC@NiMn(1:3) composite

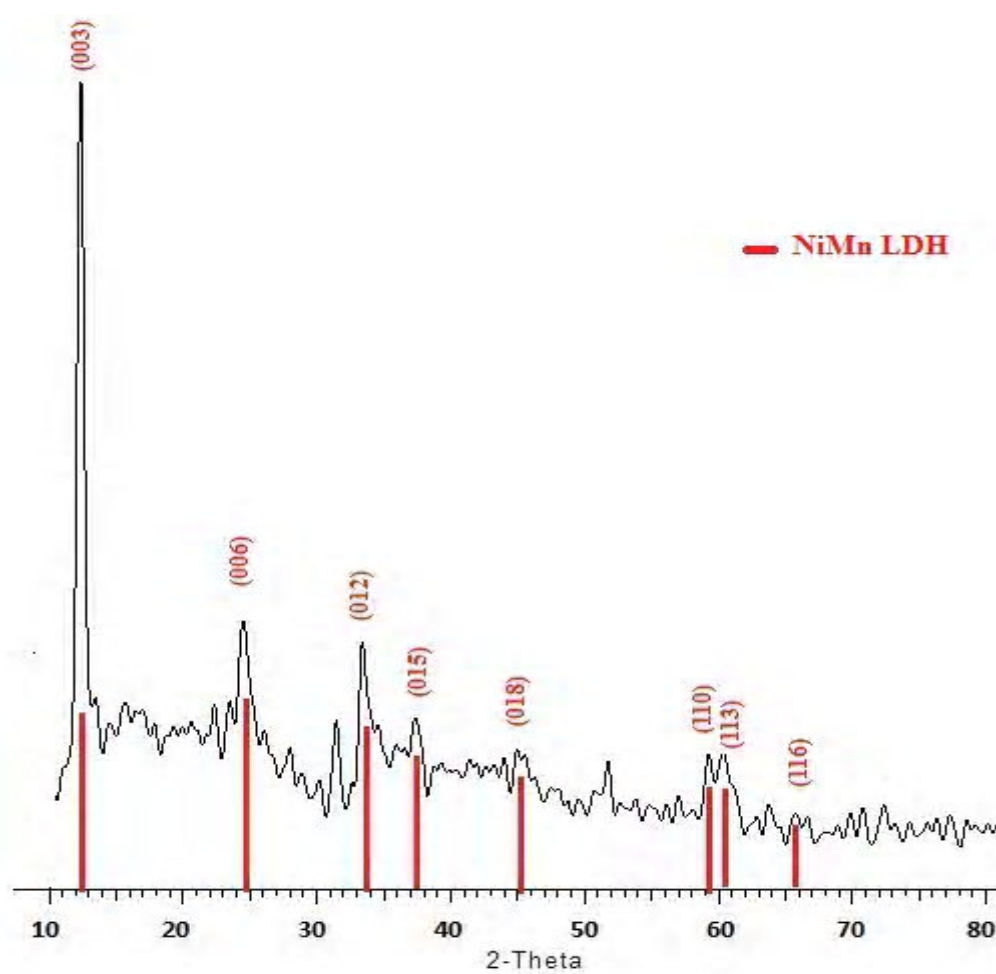


Fig 4.9 XRD pattern for AC@NiMn(2:1) composite

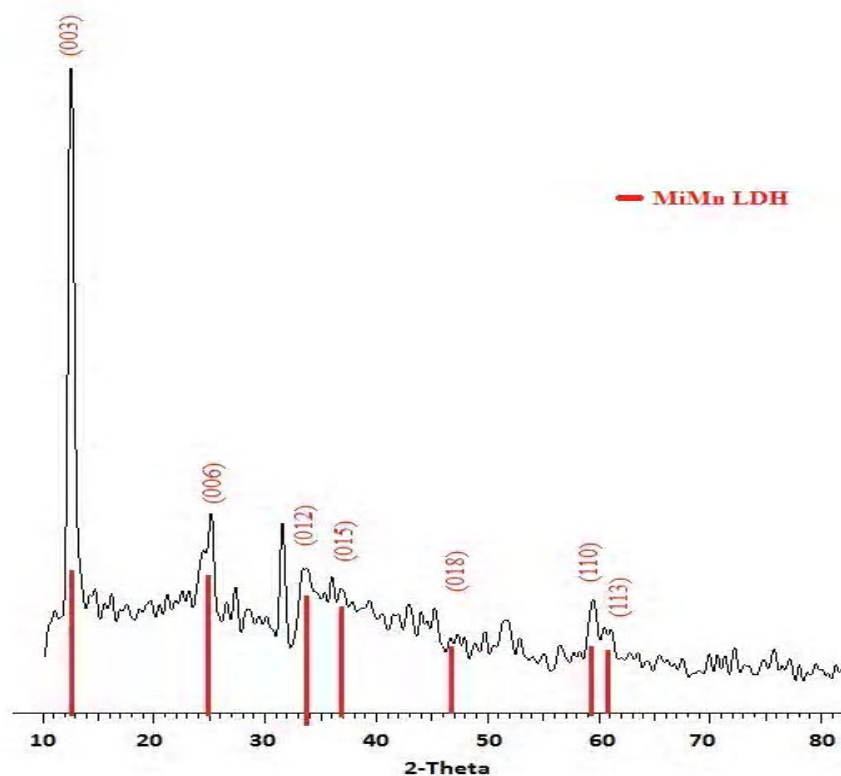


Fig 4.10 XRD pattern for AC@NiMn(3:1) composite

4.1.2 N₂ Adsorption/Desorption Isotherms

Nitrogen sorption isotherms are presented in Figs 4.11 and 4.12 and the specific surface areas calculated using the BET equation are given in table 4.1. From the isotherms, the pore size of activated carbon (AC) convert from microporous to micro- and mesoporous after AC@NiMn(n:m) composites. The surface area decreases from 2308 m²/g for AC to 76-374 m²/g for AC@NiMn(n:m). A decline of the surface area for the composites is thought to be created by blocking the porosity and filling the some pores by NiMn(n:m) particles. AC gives a type-I isotherms, which is typical for microporous solids with small external surface. The isotherms given by NiMn(n:m) and AC@NiMn(n:m) composites are of type-IV, with a hysteresis loop related to capillary condensation occurring in mesopores.

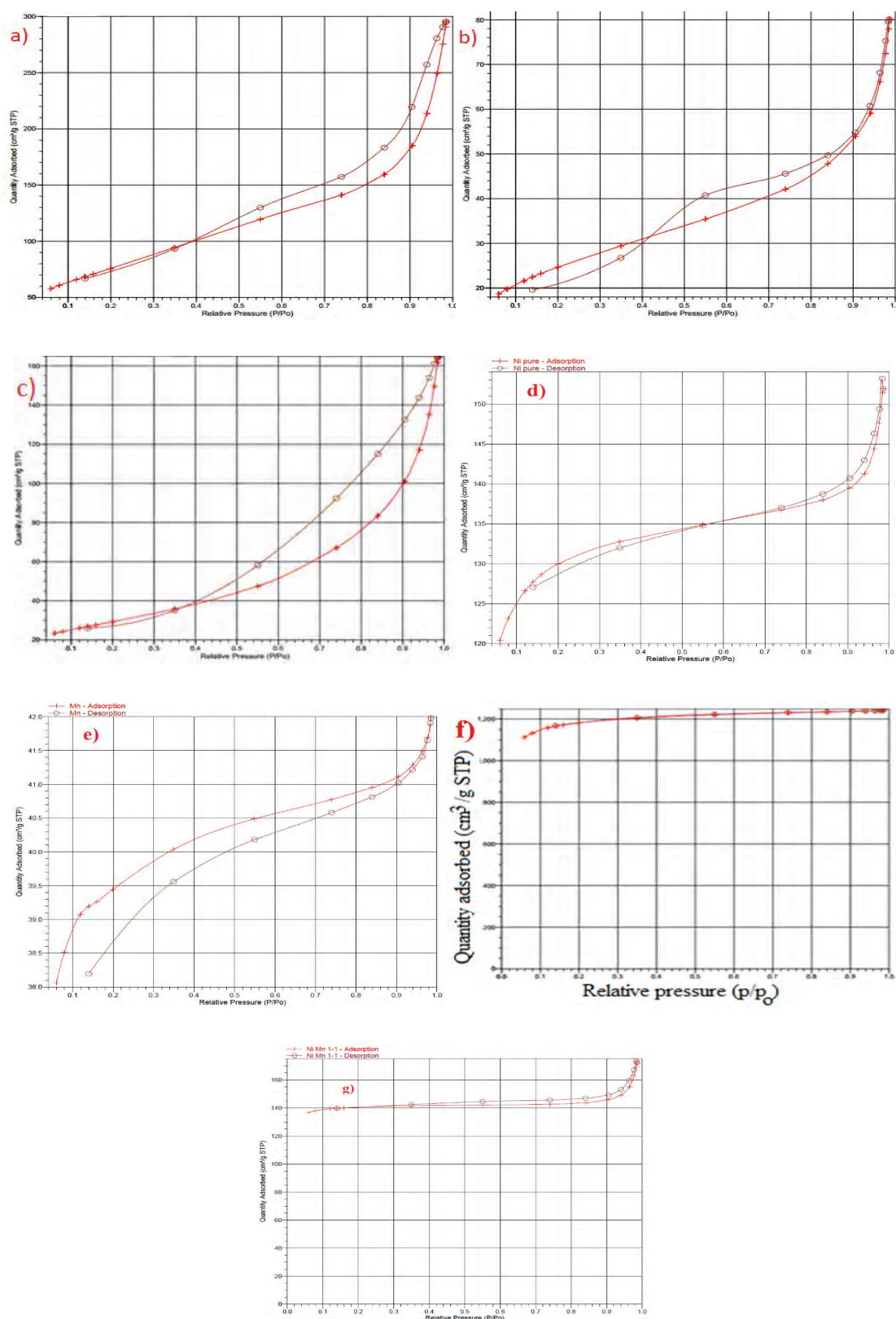


Fig 4.11 Nitrogen adsorption/desorption isotherms of **a)NiMn(1:0)** **b)NiMn(0:1)** **c)NiMn(1:1)** **d)AC@NiMn(1:0)** **e)AC@NiMn(0:1)** **f)AC** and **g)AC@NiMn(1:1)**

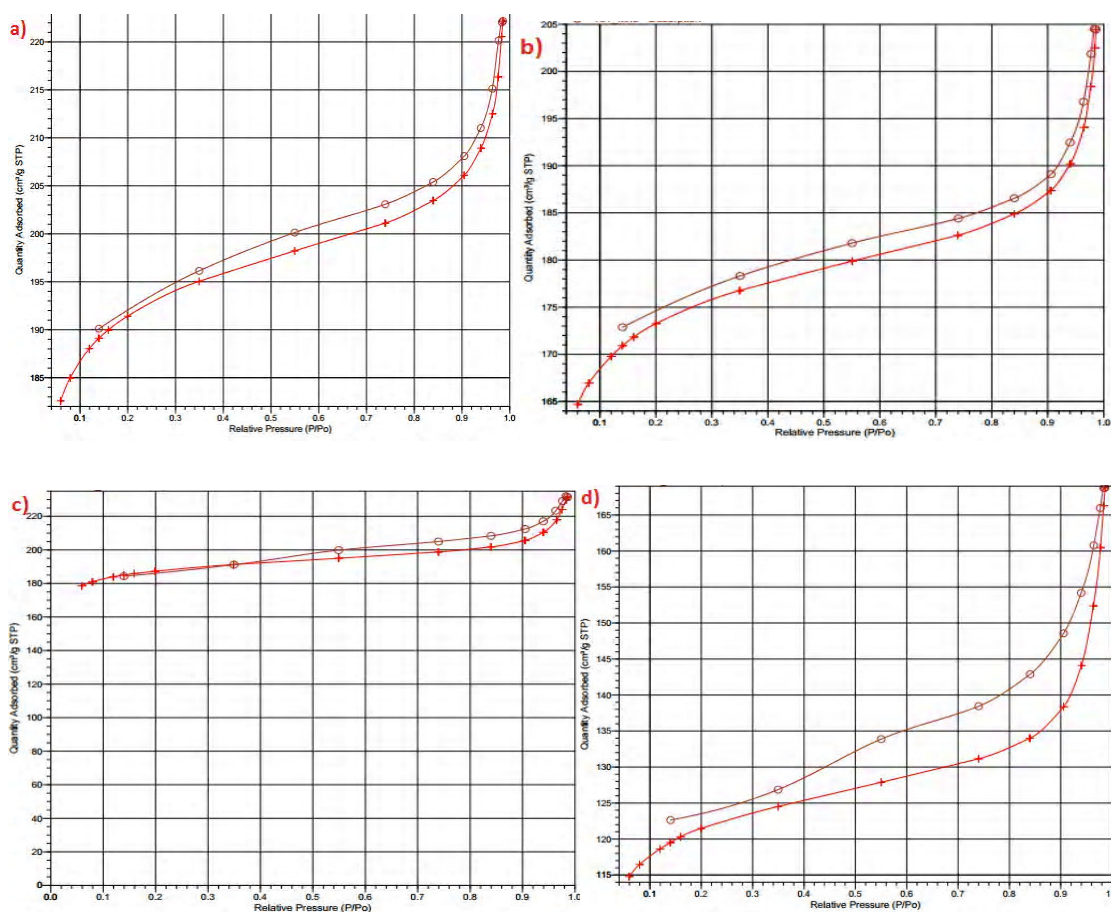


Fig 4.12 Nitrogen adsorption/desorption isotherms of **a)**AC@NiMn(1:2) **b)**AC@ NiMn (1:3) **c)**AC@NiMn (2:1) and **d)**AC@NiMn (3:1) composites

4.1.3 Scanning Electron Microscope (SEM)

The scanning electron microscop (SEM) photographs of the NiMn(n:m) and AC@NiMn(n:m) composites are given in figs 4.13 and 4.14. Fig 4.13a shows the morphology of NiMn(0:1) comprised of nanoparticles. Fig. 4.13b shows that NiMn(1:0) powder is composed of the aggregated secondary particles spherical in shape comprised of primary nanoparticles. As can be seen from fig 4.13 c, NiMn(1:1) is composed of nano- and micro sized particles. Figs 4.13 (d-e) and figs 4.14 (a-d) indicate that AC particles are decorated with NiCO₃/Ni(OH)₂, MnCO₃, NiMn(1:1) LDH, MnCO₃, and NiMn(1:1) LDH particles, respectively. Fig. 4.13f indicates that AC consists of large-sized fragments with sharp edges. Fig 4.14 e shows that MnNi(3:1) particles covers AC particles.

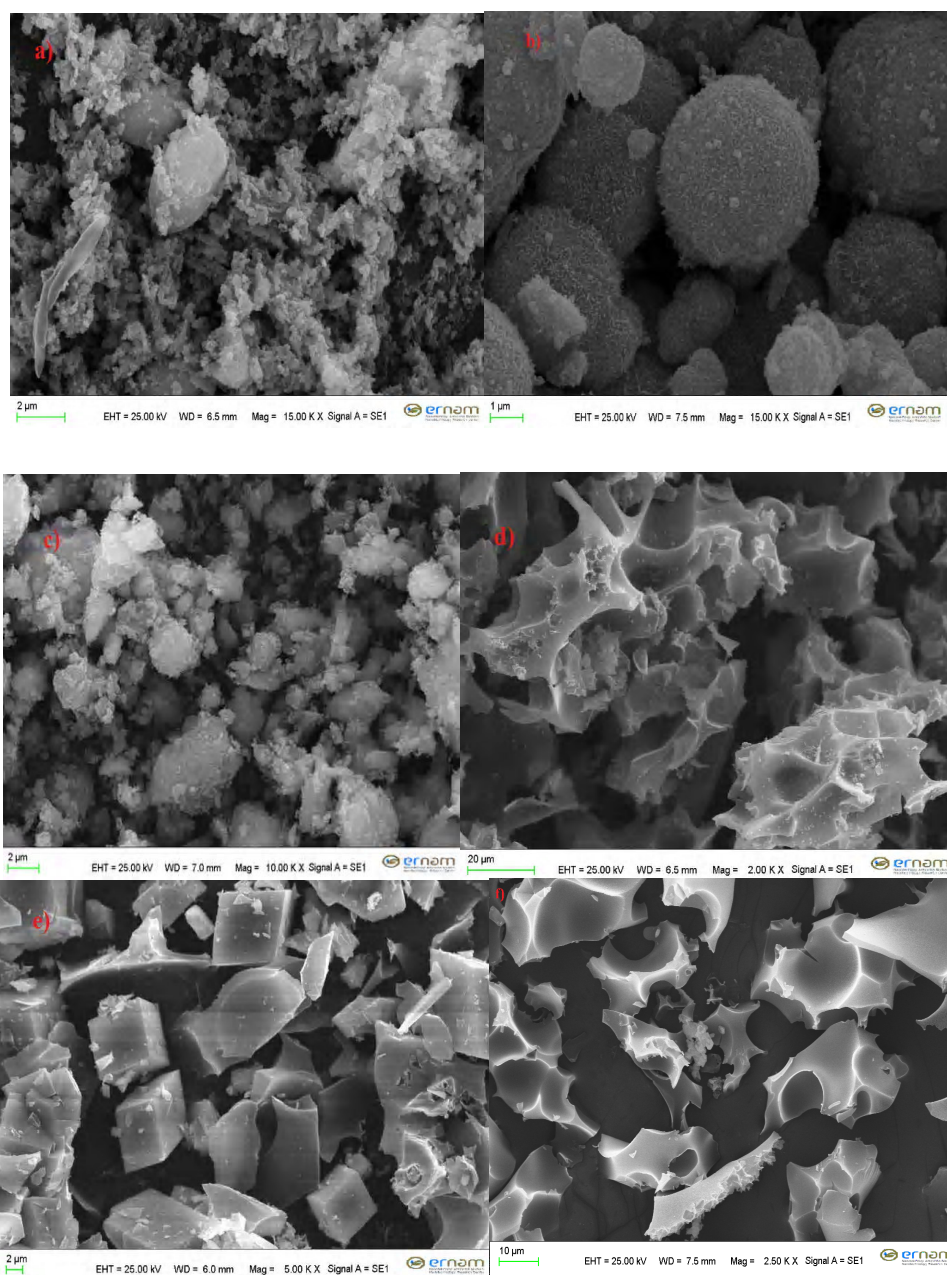


Fig 4.13 SEM images for **a)** NiMn(0:1) **b)** NiMn(1:0) **c)** NiMn(1:1) **d)** AC@NiMn(1:0) **e)** AC@NiMn(0:1) and **f)** AC

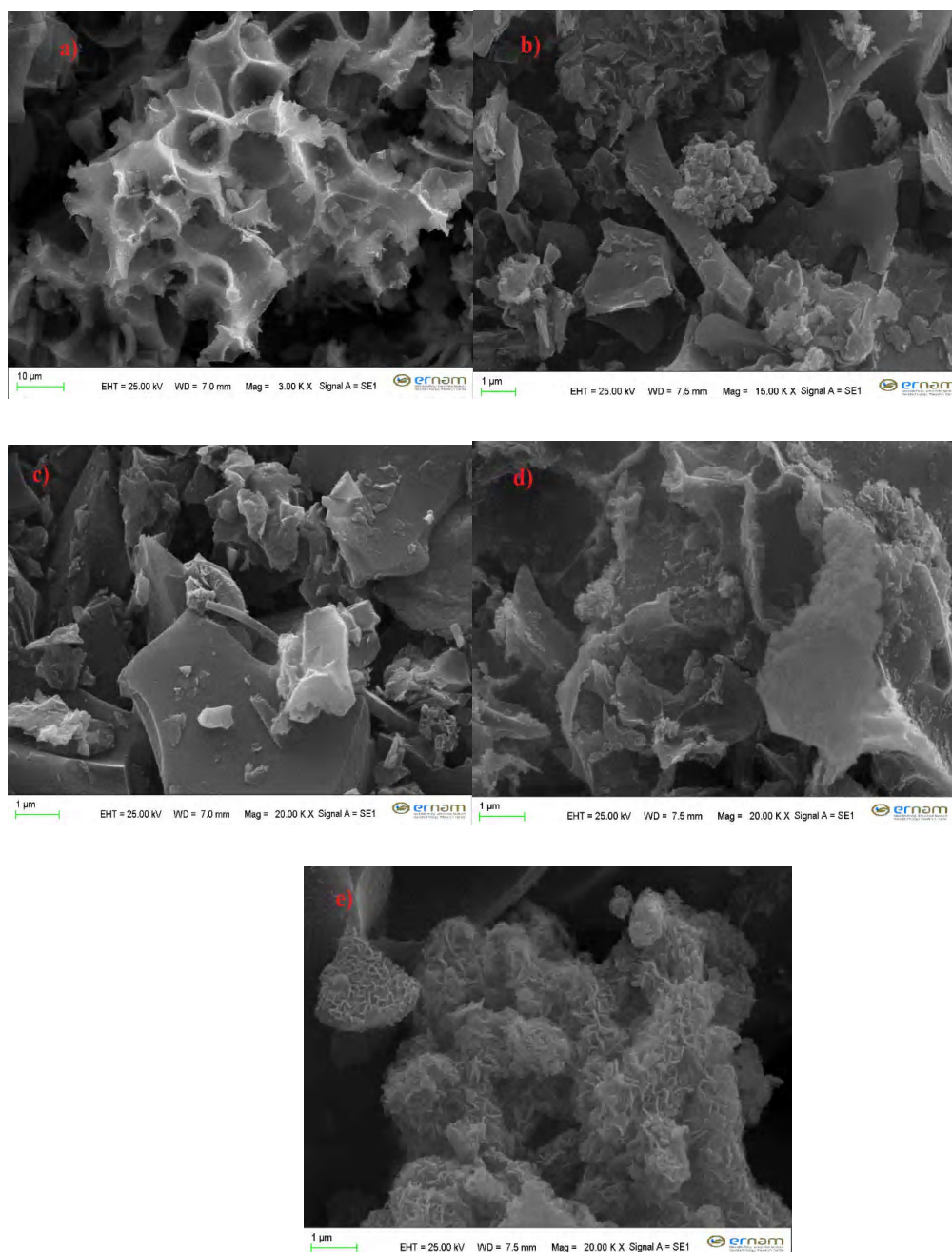


Fig 4.14 SEM images for **a)**AC@NiMn(1:1) **b)**AC@NiMn(1:2) **c)**AC@NiMn(1:3) **d)**AC@NiMn (2:1) and **e)**AC@NiMn (3:1)

4.1.4 Electrochemical Characterization

Cyclic voltammogram (CV), constant current charge/discharge voltage profiles, the capacitance change with current density, galvanostatic charge/discharge voltage profiles after cycling measurements, cycle life and the energy density versus power density values for NiMn(n:m)//NiMn(n:m) and AC@NiMn(n:m)//AC@NiMn(n:m) symmetric capacitors (SC)

and AC//AC@NiMn(1:1) asymmetric supercapacitor (ASC) are given in figs 4.15-4.22. The specific capacitance based on the total mass loading of anode and cathode is given in table 4.2.

As seen from figs 4.15-4.22, CV curves except for that of NiMn(1:1)//NiMn(1:1) capacitor, exhibit almost rectangular shape, indicating a fast charge propagation over the entire voltammetric cycle, which is desired for a supercapacitor. CV curve for NiMn(1:1)//NiMn(1:1) SC (Fig 4.16a) exhibits the distorted rectangular shape, indicating polarization due to low conductivity of NiMn(1:1).

The galvanostatic charge/discharge curves except for that of NiMn(1:1)//NiMn(1:1) are basically symmetric. The NiMn(1:1)//NiMn(1:1) SC shows the asymmetric charge/discharge curves (fig 4.16 b) due to low conductivity of NiMn(1:1) electrode materials. AC@NiMn(1:1)//AC@NiMn(1:1) and AC//AC@NiMn(1:1) demonstrate the higher capacitance at all the current densities compared to others given in table 4.2. NiMn(1:0)//NiMn(1:0) and NiMn(0:1)//NiMn(0:1) show very small capacitance values because of the low conductivity of electrode materials.

All the capacitors except for NiMn(1:1)//NiMn(1:1) and AC@NiMn(0:1)//AC@NiMn(0:1), exhibit high rate capability, as shown in figs 4.15c-4.22c and table 4.2. The specific capacitances of the composites decreased as the increasing current densities, which was attributed to the resistance and insufficient Faradaic redox reactions under higher discharge current densities

Figs 4.15(d-e)-4.22(d-e) display the cycling stability of the devices. it can be seen that 92%-99% of the initial capacitance for all the devices except for AC//AC, was retained after after 5000 cycles, indicating good long term stability. Fig 4.23b compares the cycling stabilities of all the devices among which AC@NiMn(1:1)//AC@NiMn(1:1), AC@NiMn(1:2)//AC@NiMn(1:2), AC@NiMn(1:3)//AC@NiMn(1:3) and AC//AC@NiMn(1:1) show almost no capacitance lost.

The energy (E) and power densities (P) were calculated from the discharge curves and given in figs 4.15(f)-4.22(f). Fig 4.23c compares the energy and power densities for all the devices studied. It is seen that the energy and power densities of AC//AC@NiMn(1:1) ASC is the highest among those of the devices given in fig 4.23c.

Table 4.2 Specific capacitance of the supercapacitors

Cell	Total mass of electrodes (mg)	Capacitance (F/g ⁻¹) at 0.5A/g	Capacitance (F/g ⁻¹) at 1A/g	Capacitance (F/g ⁻¹) at 2A/g	Capacitance (F/g ⁻¹) at 5A/g	Capacitance (F/cm ²) at 1A/g
AC//AC	16	18.12	15	10	6.25	0.24
NiMn(1:0)//NiMn(1:0)		low	low	low	low	low
NiMn(0:1)//NiMn(0:1)		low	low	low	low	low
AC@NiMn(0:1)//AC@NiMn(0:1)	19.44	9.5	8.2	7.0	4.8	0.160
NiMn(1:1) //NiMn(1:1)	17.2	0.36	0.28	0.22	0.18	0.004
AC@NiMn (1:1)//AC@NiMn (1:1)	14.8	35.8	32.7	28.2	20	0.485
AC@NiMn(1:2)//AC@NiMn (1:2)	20.48	19.1	18.1	16.3	15.6	0.371
AC@NiMn(1:3)//AC@NiMn (1:3)	9.6	24.4	23.8	25.0	25.0	0.228
AC@NiMn(2:1)//AC@NiMn (2:1)	13.92	23.7	22.5	22.5	18.5	0.313
AC@NiMn(3:1)//AC@NiMn (3:1)	19.36	36.25	35	32.5	25	0.667
AC//AC@NiMn (1:1)*	18.8	30.4	27.5	25.0	20.8	0.517

* Mass ratio of AC//AC@NiMn(1:1) is 1.97

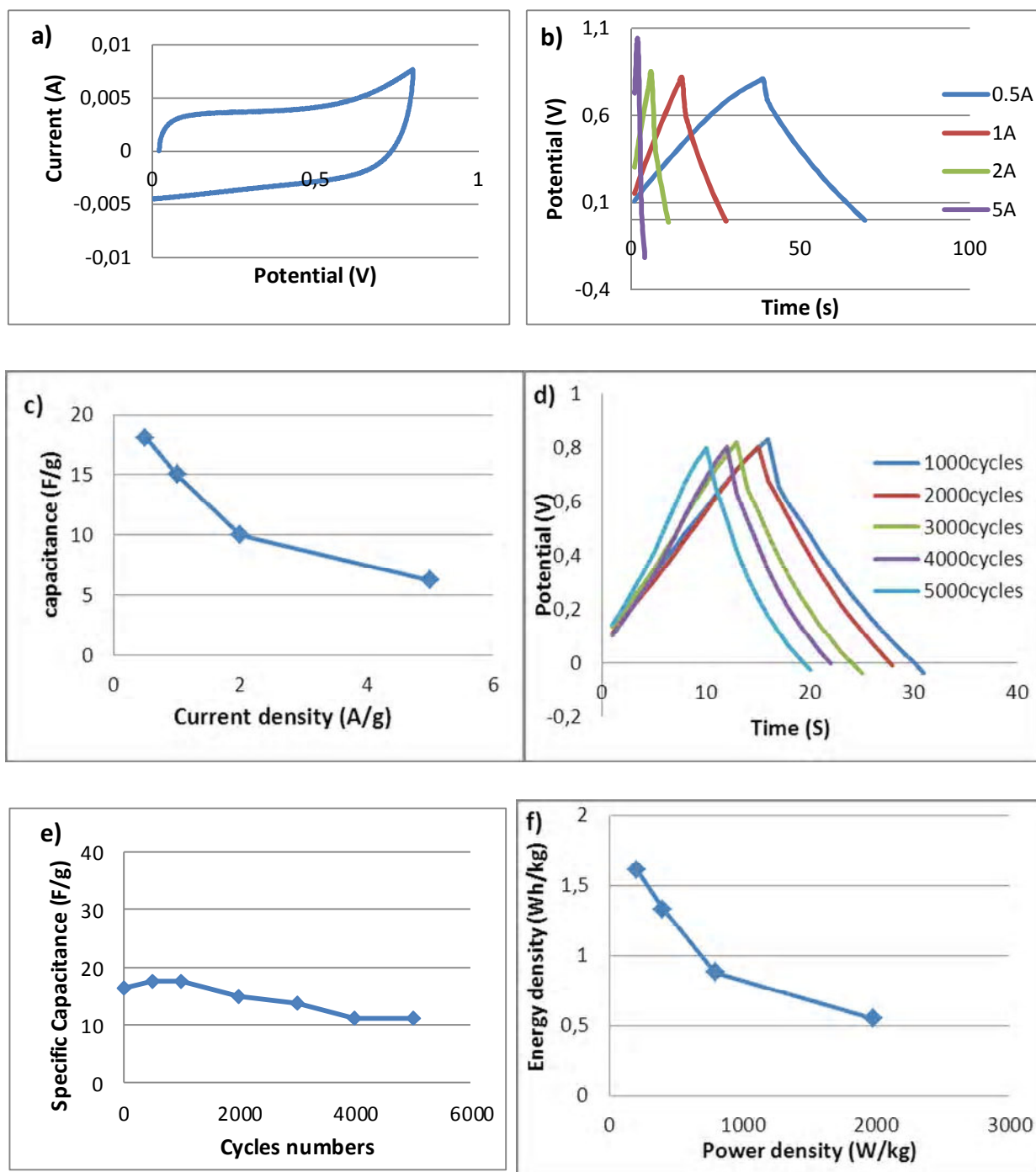


Fig 4.15 Electrochemical performance of AC//AC symmetric capacitor using 6M KOH solution **a)** cyclic voltammogram at 0.01V/s **b)** constant current charge/discharge voltage profiles **c)** effect of the constant current density on the capacitance **d)** galvanostatic charge/discharge curves after cycling measurements **e)** cycle life and **f)** the energy density versus power density values.

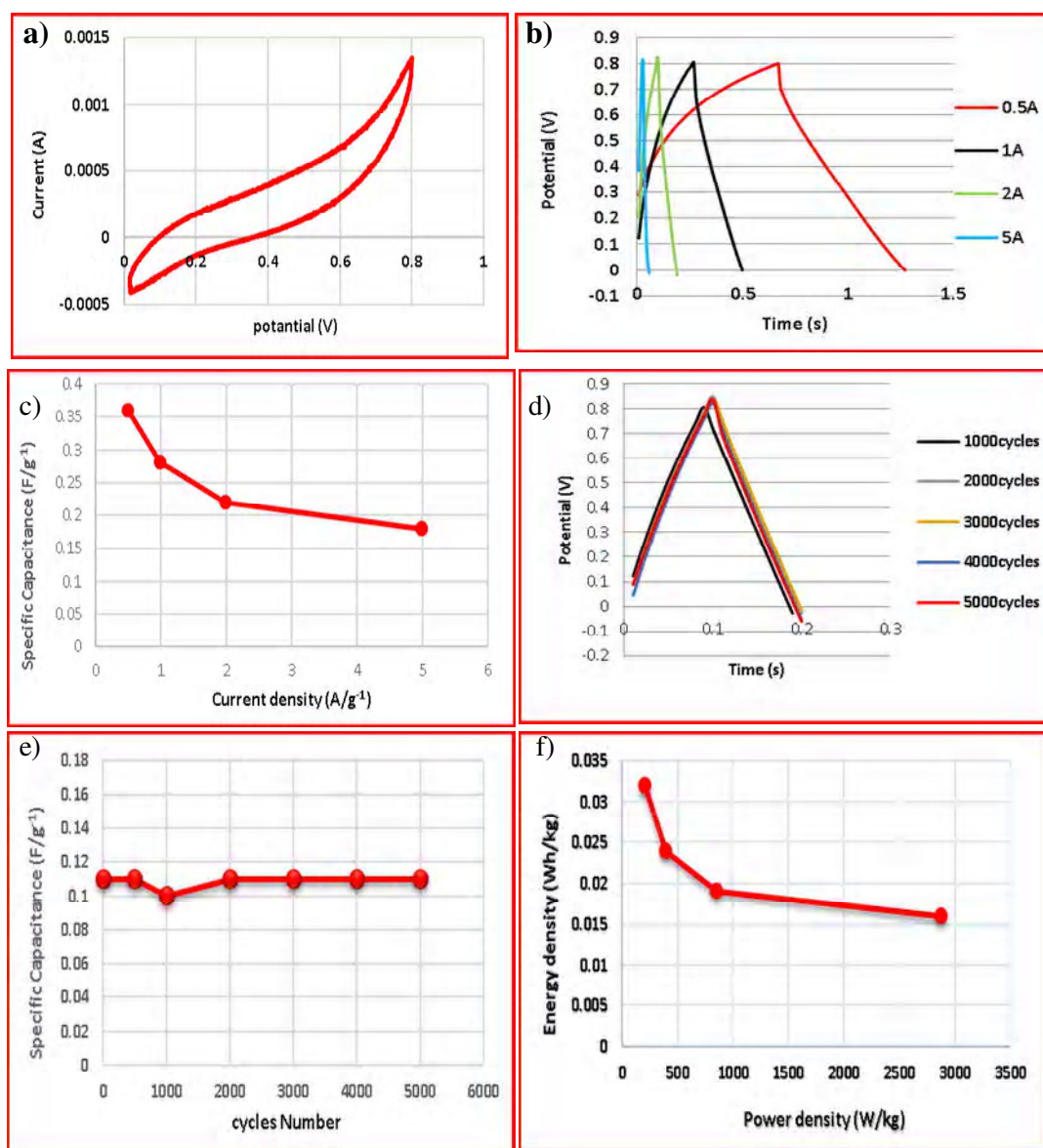


Fig 4.16 Electrochemical performance of NiMn(1:1)//NiMn(1:1) symmetric capacitor using 6M KOH solution **a)** cyclic voltammogram at 0.01V/s **b)** constant current charge/discharge voltage profiles **c)** effect of the constant current density on the capacitance **d)** galvanostatic charge/discharge curves after cycling measurements **e)** cycle life and **f)** the energy density versus power density values.

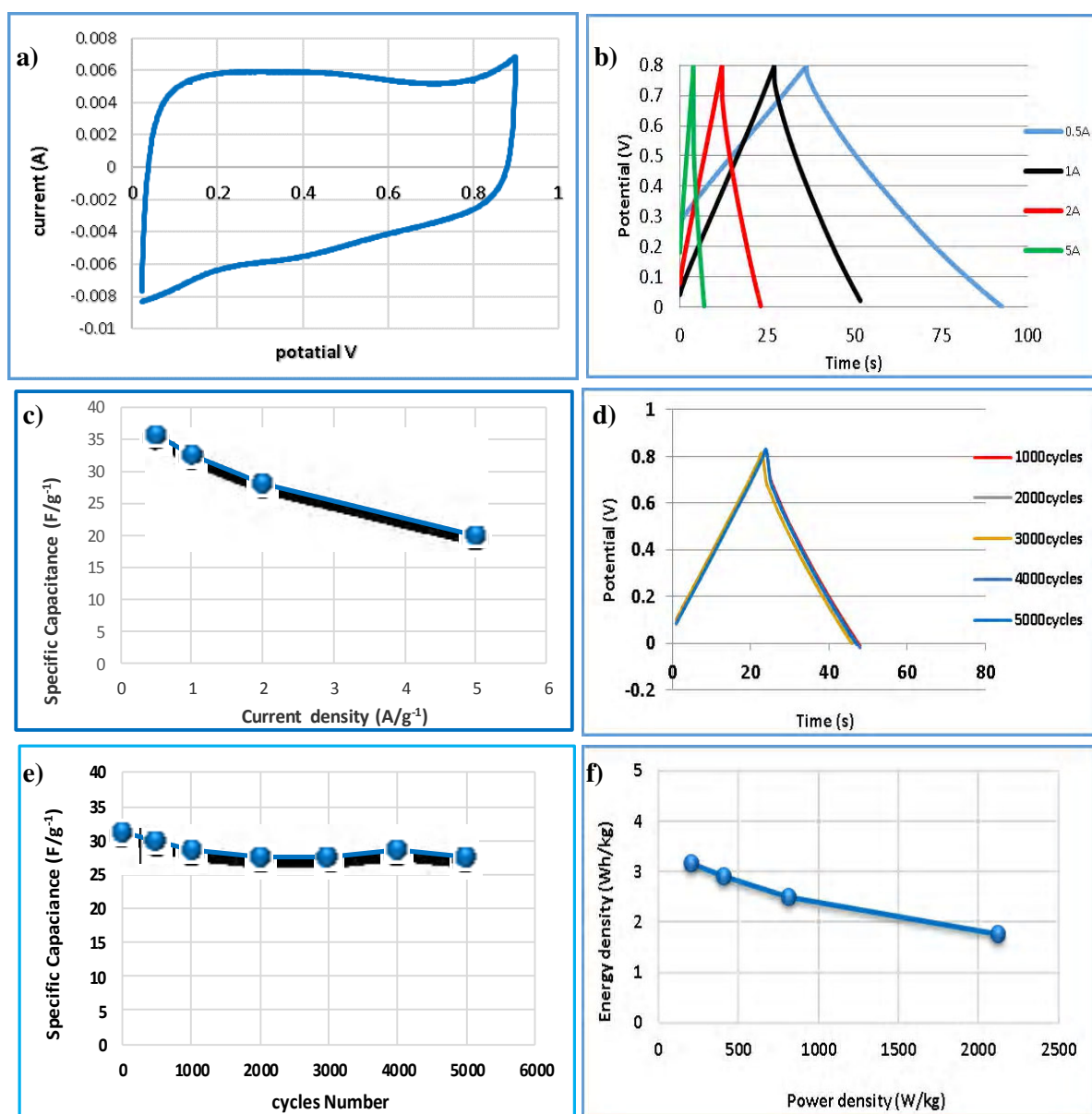


Fig 4.17 Electrochemical performance of AC@NiMn(1:1)//AC@NiMn(1:1) symmetric capacitor using 6M KOH solution **a)** cyclic voltammogram at 0.01V/s **b)** constant current charge/discharge voltage profiles **c)** effect of the constant current density on the capacitance **d)** galvanostatic charge/discharge curves after cycling measurements **e)** cycle life and **f)** the energy density versus power density values.

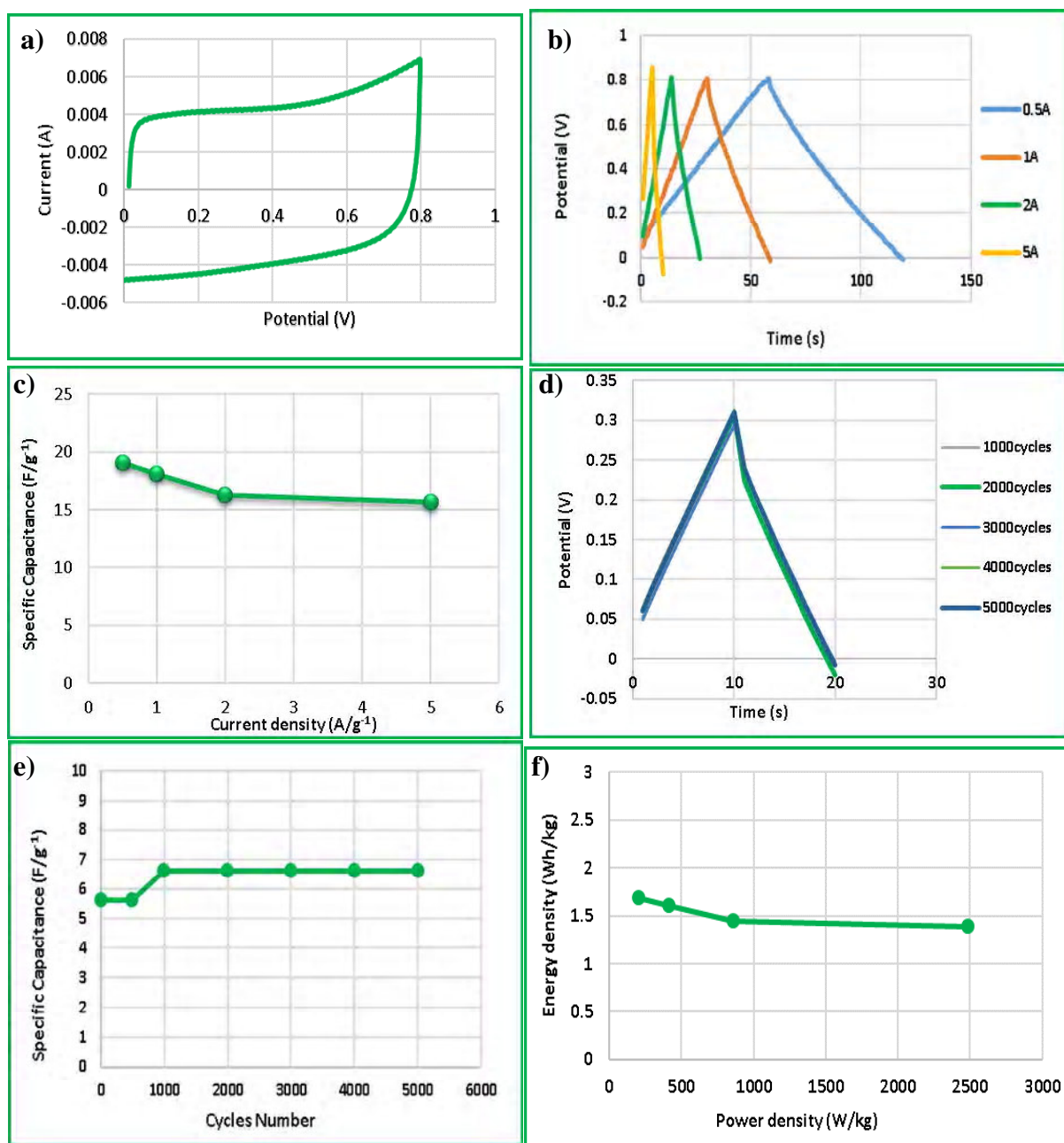


Fig 4.18 Electrochemical performance of AC@NiMn(1:2)//AC@NiMn(1:2) symmetric capacitor using 6M KOH solution **a)**cyclic voltammogram at 0.01V/s **b)** constant current charge/discharge voltage profiles **c)**effect of the constant current density on the capacitance **d)**galvanostatic charge/discharge curves after cycling measurements **e)** cycle life and **f)**the energy density versus power density values

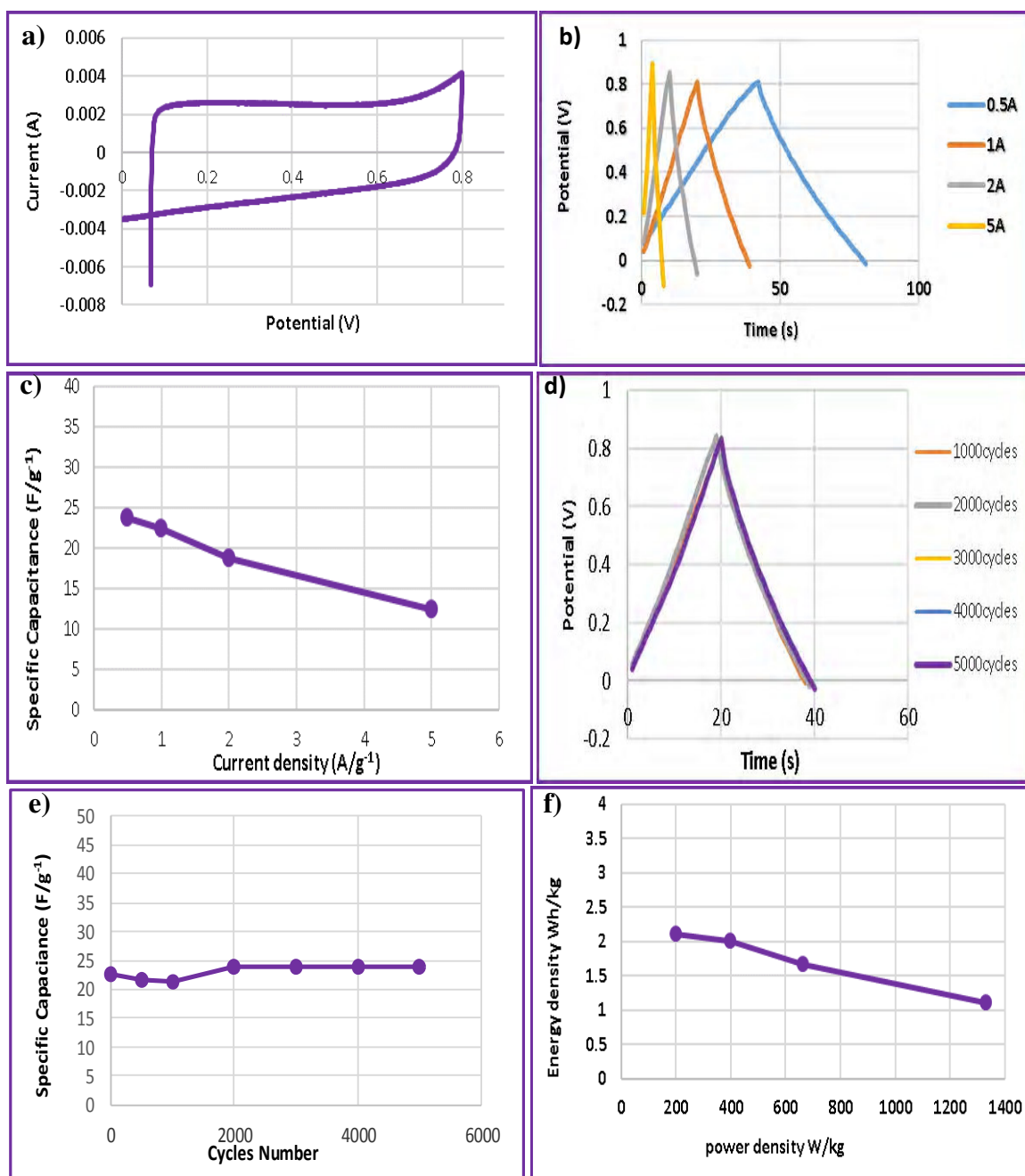


Fig 4.19 Electrochemical performance of AC@NiMn(1:3)//AC@NiMn(1:3) symmetric capacitor using 6M KOH solution **a)** cyclic voltammogram at 0.01V/s **b)** constant current charge/discharge voltage profiles **c)** effect of the constant current density on the capacitance **d)** galvanostatic charge/discharge curves after cycling measurements **e)** cycle life and **f)** the energy density versus power density values

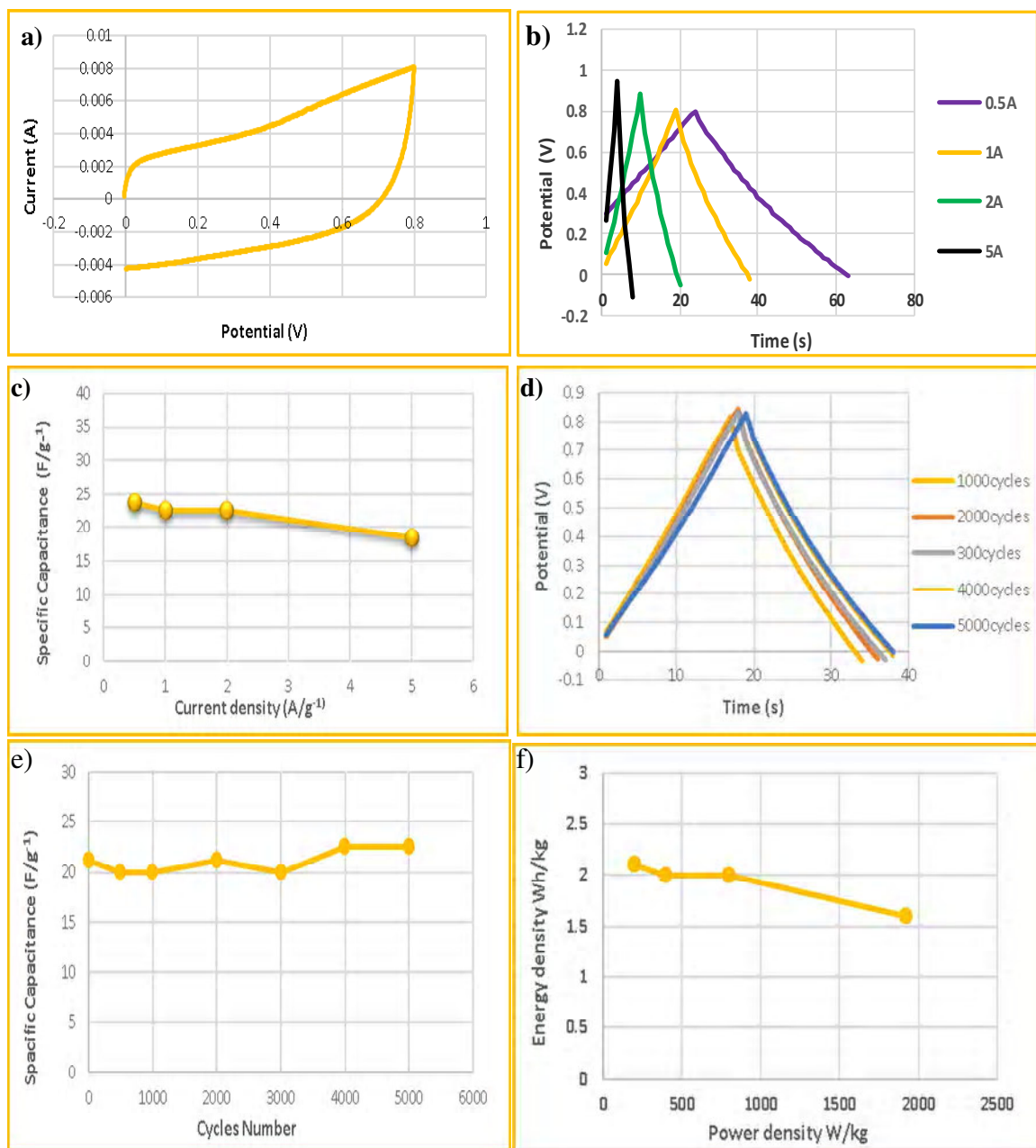


Fig 4.20 Electrochemical performance of AC@NiMn(2:1)//AC@NiMn(2:1) symmetric capacitor using 6M KOH solution **a)** cyclic voltammogram at 0.01 V/s **b)** constant current charge/discharge voltage profiles **c)** effect of the constant current density on the capacitance **d)** galvanostatic charge/discharge curves after cycling measurements **e)** cycle life and **f)** the energy density versus power density values

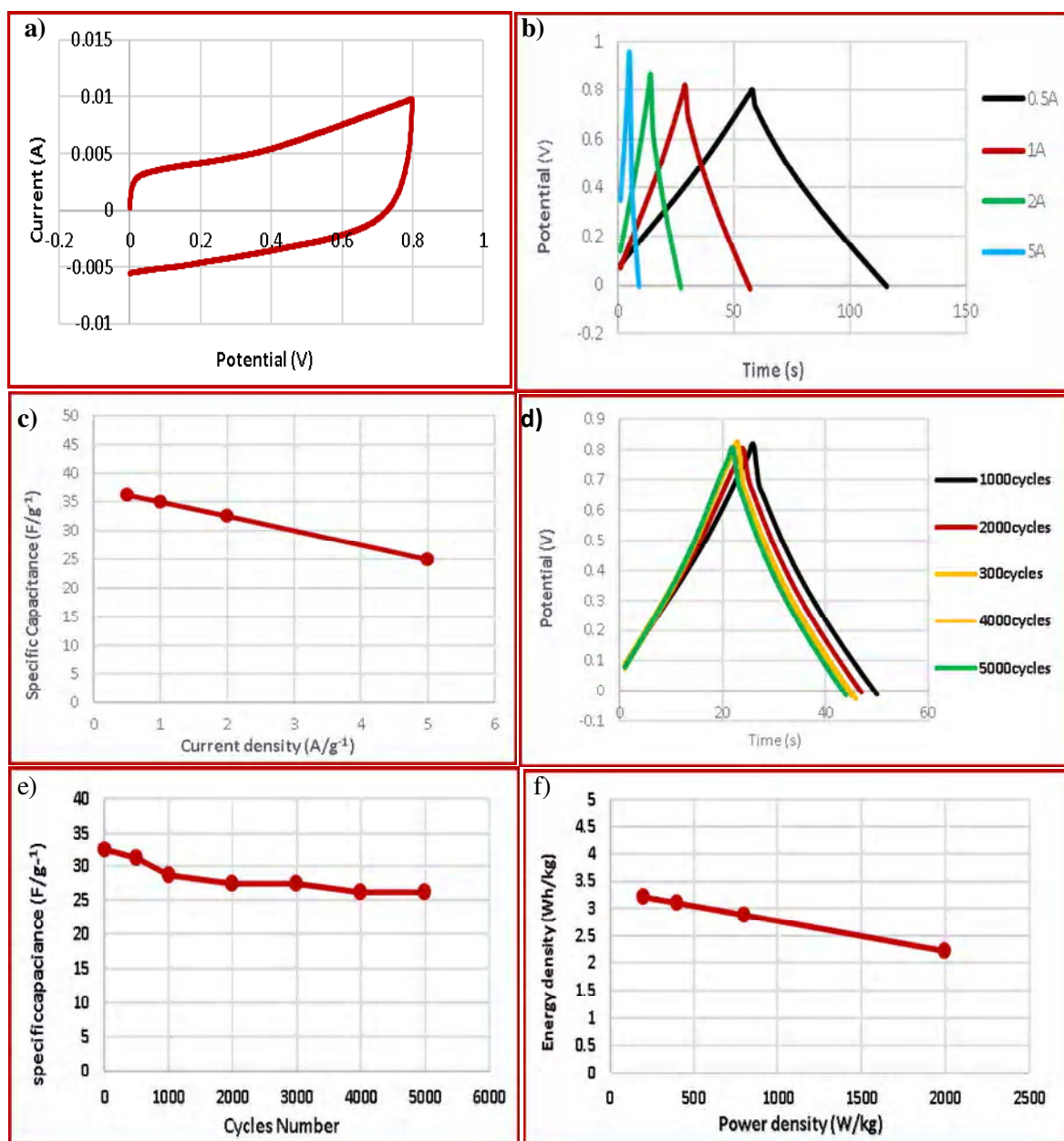


Fig 4.21 Electrochemical performance of AC@NiMn(3:1)//AC@NiMn(3:1) symmetric capacitor using 6M KOH solution **a)** cyclic voltammogram at 0.01V/s **b)** constant current charge/discharge voltage profiles **c)** effect of the constant current density on the capacitance **d)** galvanostatic charge/discharge curves after cycling measurements **e)** cycle life and **f)** the energy density versus power density values.

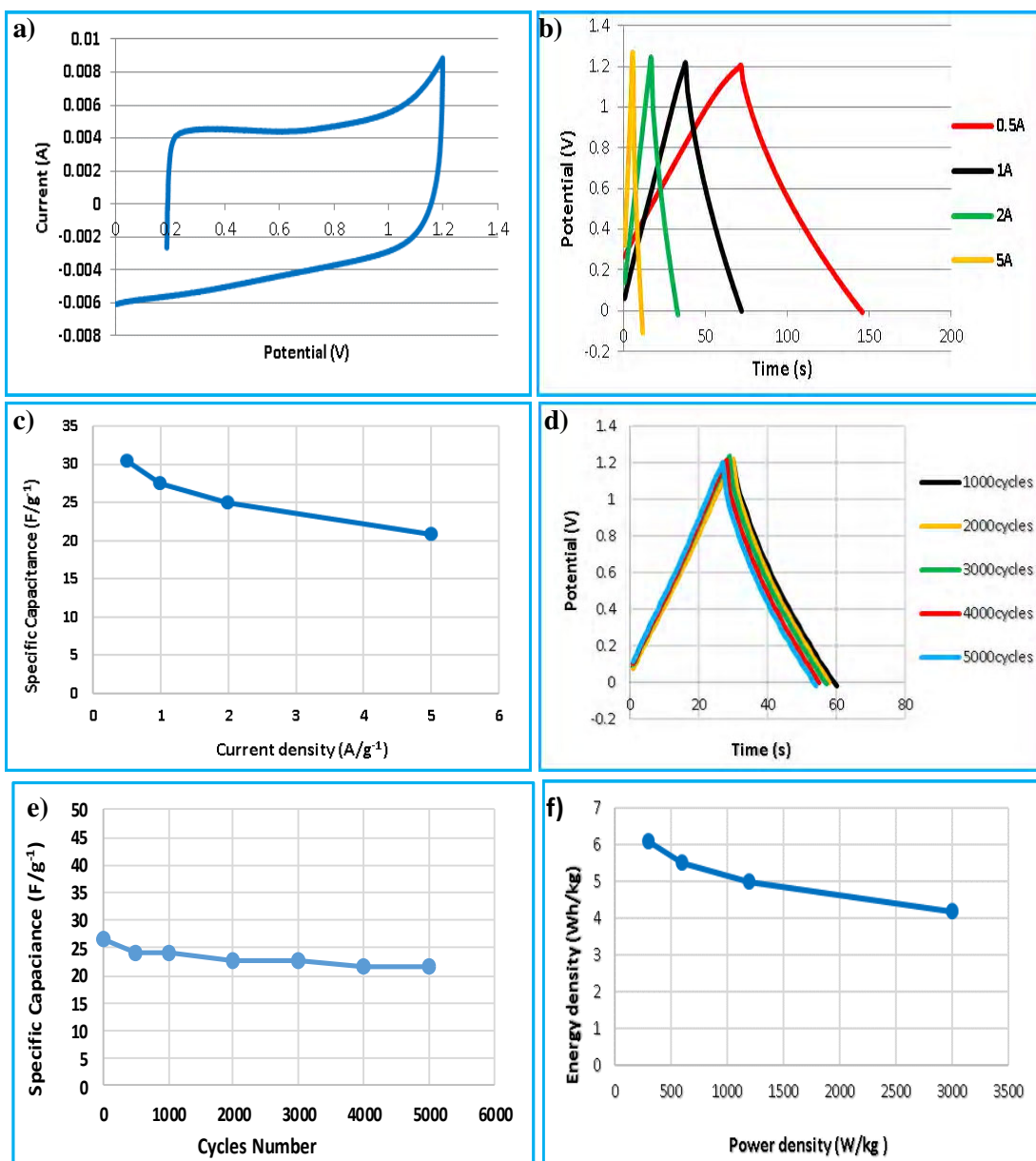
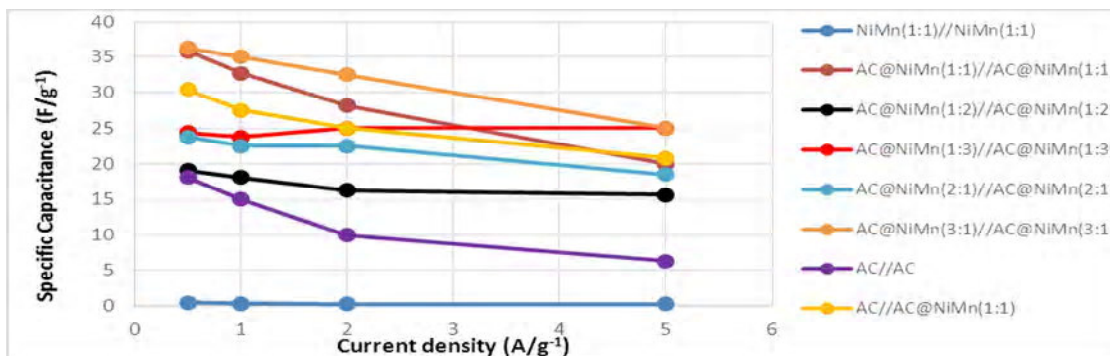
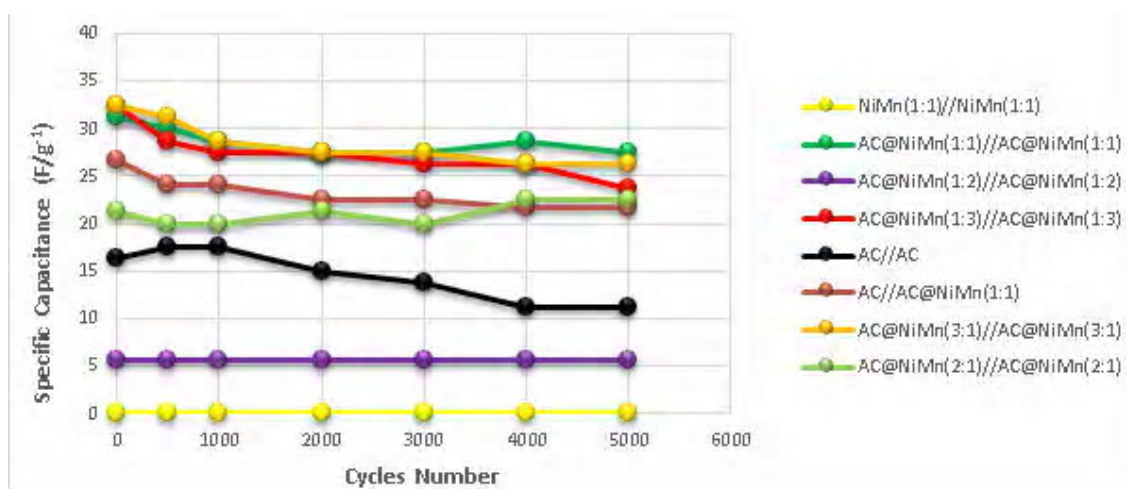


Fig 4.22 Electrochemical performance of AC//AC@NiMn(1:1) asymmetric capacitor using 6M KOH solution **a)** cyclic voltammogram at 0.01V/s **b)** constant current charge/discharge voltage profiles **c)** effect of the constant current density on the capacitance **d)** galvanostatic charge/discharge curves after cycling measurements **e)** cycle life and **f)** the energy density versus power density values.

a)



b)



c)

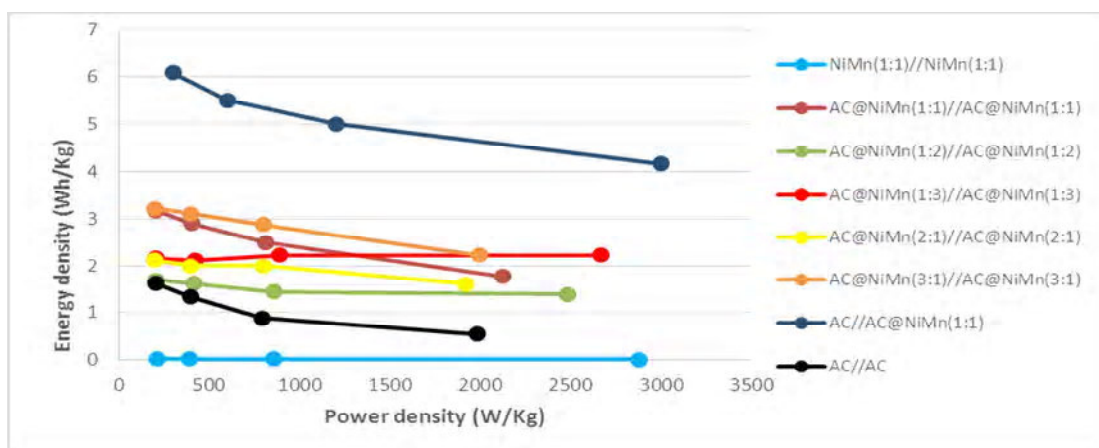


Fig 4.23 Comparison of electrochemical peformans of the symmetric and Asymmetric capacitors using 6M KOH solution **a)**effect of the current density on the capacitance **b)**cycle life **c)**the energy density versus power density.

4.2 Activated Carbon/Cobalt-Manganese Carbonates Hydroxide Hydrates Composites [AC@CoMn (n:m) (CO₃)_x(OH)_y.zH₂O] and Cobalt-Manganese Carbonates Hydroxide Hydrates[CoMn (n:m) (CO₃)_x(OH)_y.zH₂O]

4.2.1 X-Ray Powder Diffraction (XRD)

X-ray diffraction pattern (XRD) and the elemental composition assessed by energy dispersive X-ray spectroscopy (EDX) for the synthesized composite materials are given in figs 4.24-4.33 and table 4.3, respectively. The phases estimated from the elemental composition and XRD pattern of the composites are given in table 4.3 and figs 4.24-4.33. From the table 4.3, it can be seen that metal oxide, carbonate and hydroxide composites were obtained from the precursors. The AC@CoMn (3:1) composite demonstrates a featureless diffraction pattern, indicating the amorphous nature of the sample (fig 4.33).

The conductivity values of the synthesized composite materials are shown in table 4.3. As seen from the table, the conductivity of the composites with AC is bigger than that of ones without AC, which is advantage to get high power for supercapacitor.

Table 4.3 Elemental composition, estimated phases, BET surface area and conductivity of the synthesized composite materials

Stoichiometry of precursor for electrode materials	Co atomic %	Mn atomic %	C atomic %	O atomic %	Estimated phases for electrode materials	BET (m ² /g)	Conductivity (S.cm ⁻¹)
CoMn(1:0)	24.1	---	19.7	56.2	Co(CO ₃) _{0.5} (OH) _{0.11} H ₂ O	118.3	3.1x10 ⁻⁵
CoMn(0:1)	---	24.0	20.1	55.9	MnCO ₃ /Mn ₃ O ₄	69.0	4.8x10 ⁻⁵
CoMn(1:1)	17.0	6.5	23.1	53.3	MnCO ₃ /CoCO ₃ /CoOCO ₂	4.8	7.6x10 ⁻⁵
AC@ CoMn(1:0)	21.7	---	41.0	36.4	Co(CO ₃) _{0.5} (OH) _{0.11} H ₂ O	15.0	3.2x10 ⁻⁴
AC@ CoMn(0:1)	---	4.8	65.4	29.9	MnCO ₃	76.5	1.2x10 ⁻³
AC@ CoMn(1:1)	2.7	1.1	72.6	23.2	AC@MnCO ₃ /CoCO ₃ /CoOCO ₂	302.3	1.0x10 ⁻³
AC @CoMn(1:2)	1.48	0.4	82.9	15.2	AC@CoCO ₃ /MnCO ₃	374.5	9.2x10 ⁻⁴
AC@ CoMn(1:3)	1.7	1.1	73.0	23.6	AC@CoCO ₃ /MnCO ₃	182.1	5.7x10 ⁻³
AC@CoMn(2:1)	7.3	1.6	62.9	28.2	AC@CoCO ₃ /MnCO ₃	77.7	1.1x10 ⁻³
AC@ CoMn(3:1)	12.0	1.8	54.8	30.8		202.1	3.8x10 ⁻³

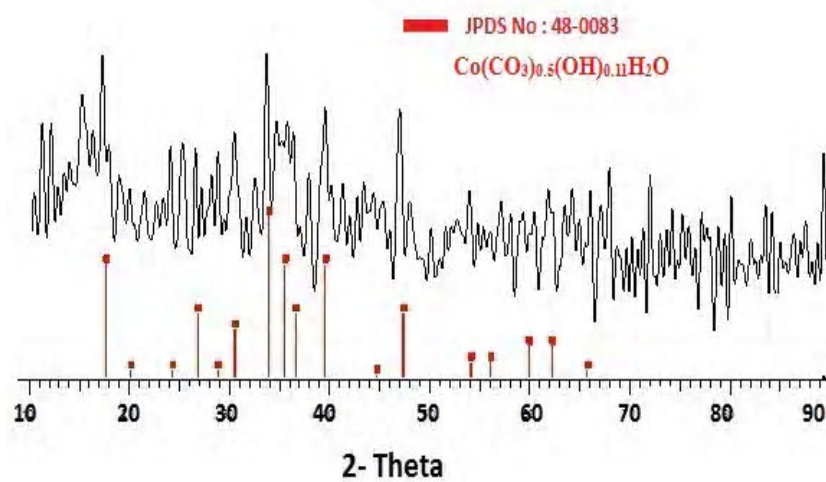


Fig 4.24 XRD pattern for CoMn(1:0)

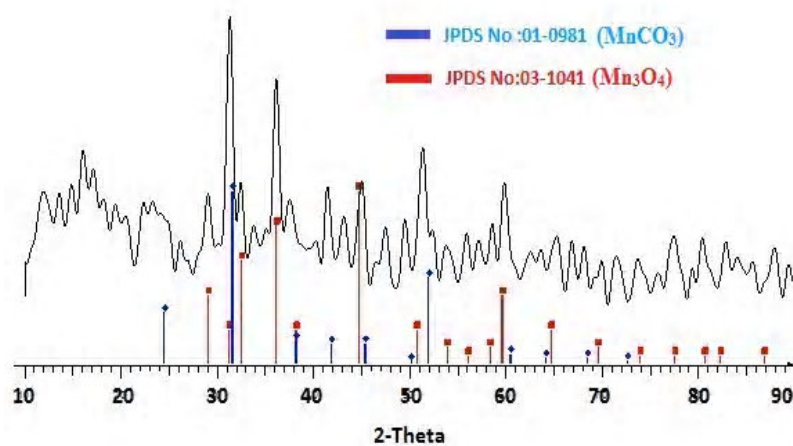


Fig 4.25 XRD pattern for CoMn(0:1)

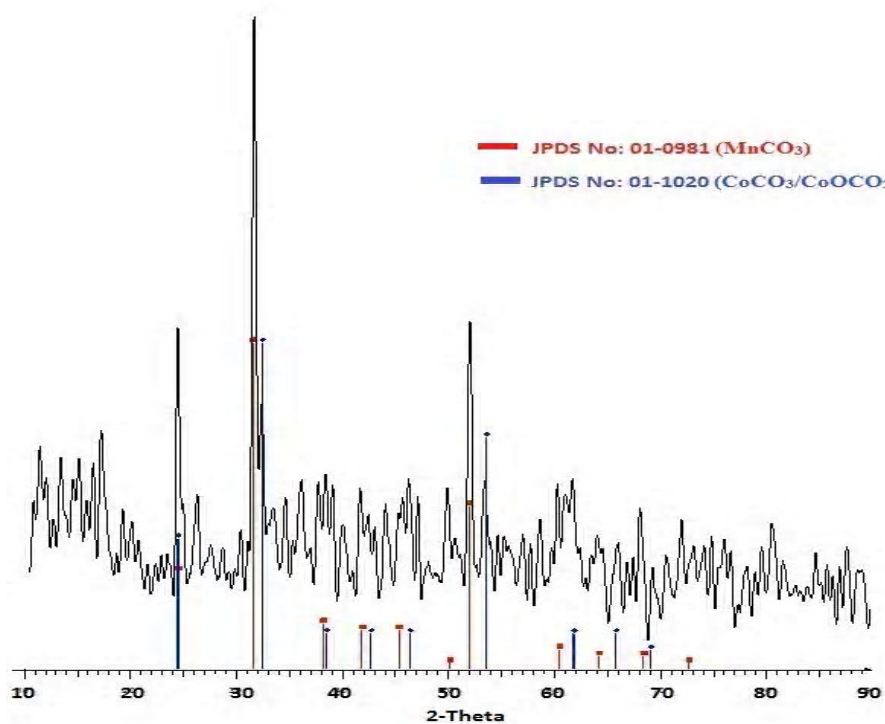


Fig 4.26 XRD pattern for CoMn (1:1)

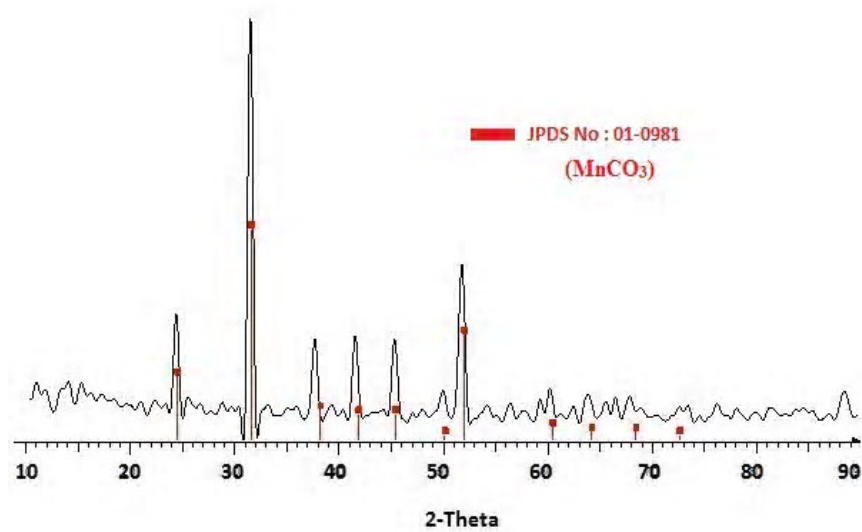


Fig 4.27 XRD patterns for AC@CoMn(0:1)

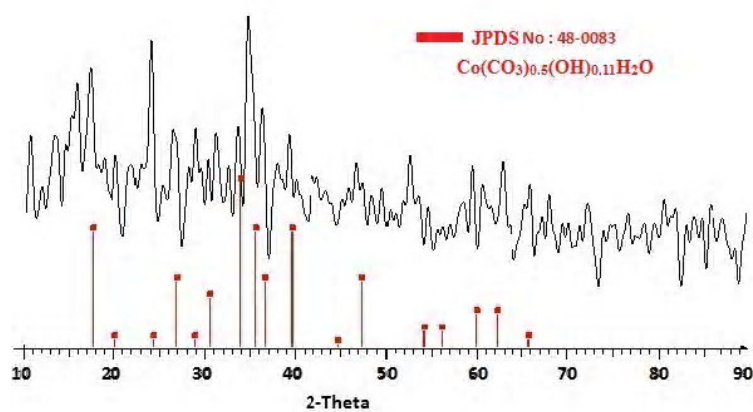


Fig 4.28 XRD patterns for AC@CoMn(1:0)

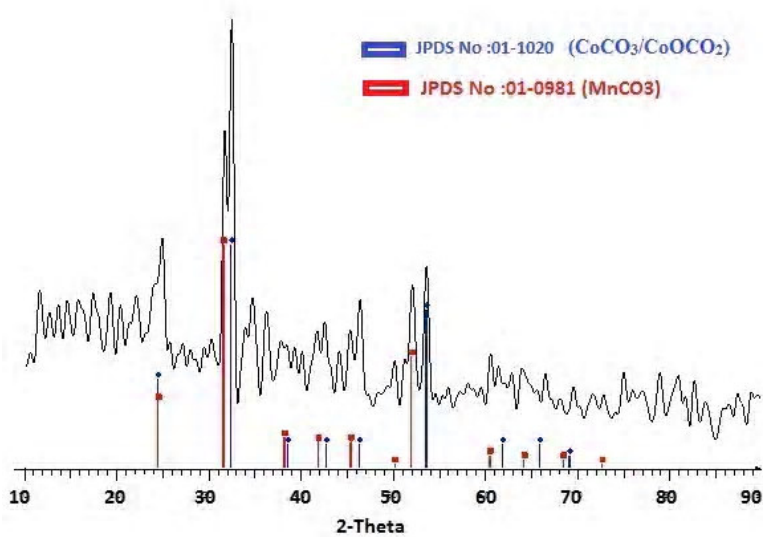


Fig 4.29 XRD patterns for AC@CoMn (1:1)

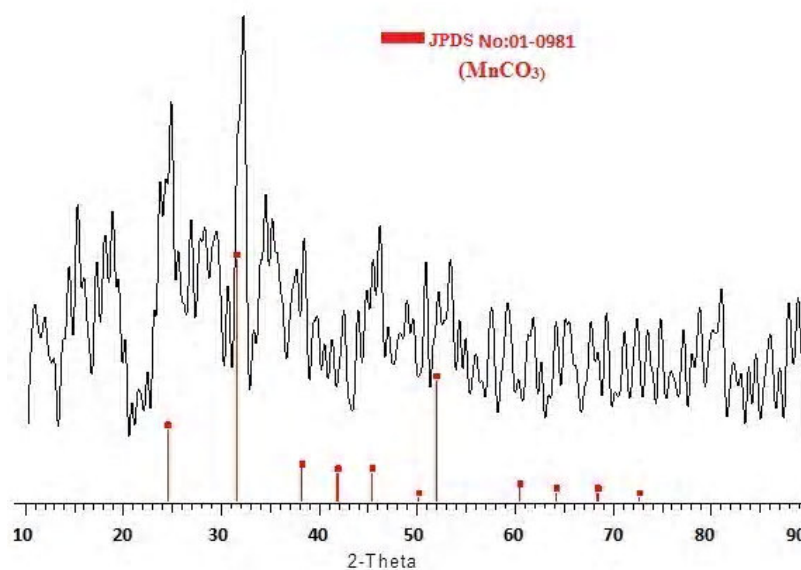


Fig 4.30 XRD pattern for AC@CoMn (1:2)

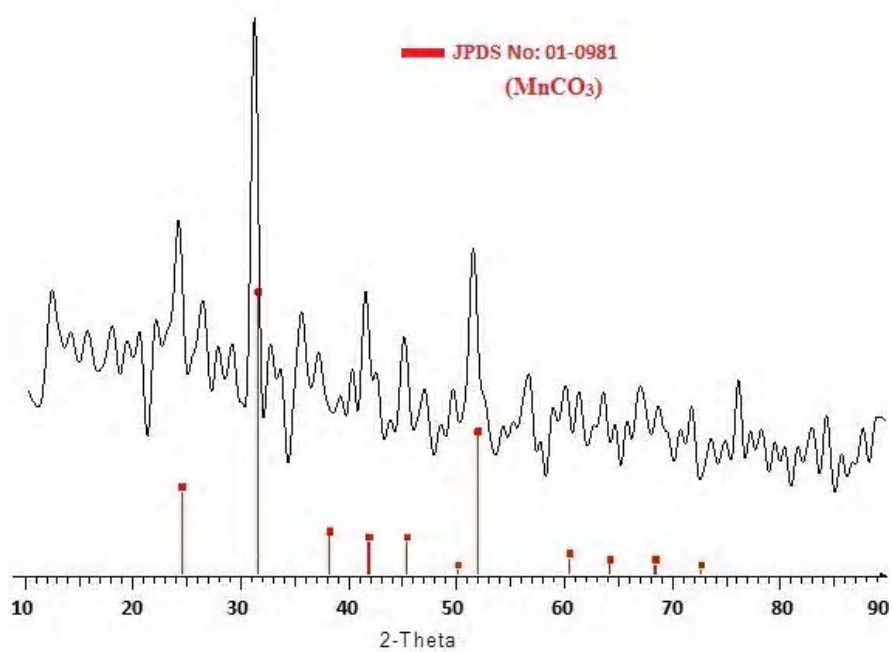


Figure 4.31 XRD pattern for AC@CoMn (1:3)

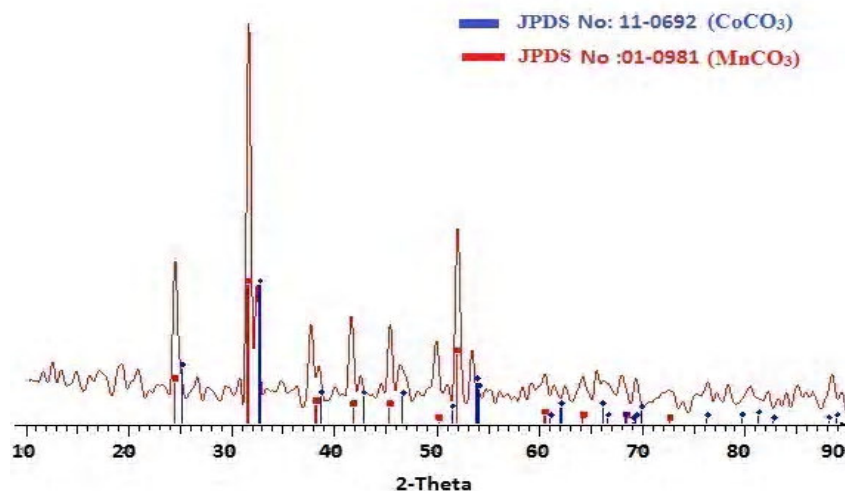


Figure 4.32 XRD pattern for AC@CoMn (2:1)

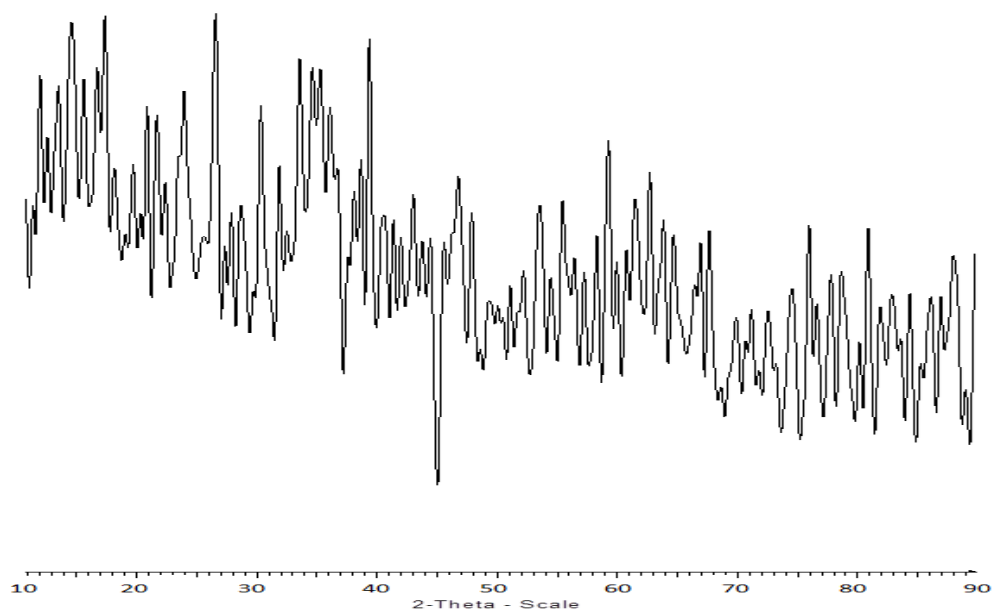


Fig 4.33 XRD pattern for AC@CoMn (3:1)

4.2.2 N_2 Adsorption/Desorption Isotherms

Nitrogen sorption isotherms are presented in Figs 4.34 and 4.35 and the specific surface areas calculated using the BET equation are given in table 4.3. From the isotherms, the pore size of activated carbon (AC) converts from microporous to micro- and mesoporous after AC@CoMn(n:m) composites. The surface area reduces from 2308 m^2/g for AC to 15-374 m^2/g for AC@CoMn(n:m) composites. A decline of the BET

surface area for the composites is thought to be created by blocking the porosity and filling the some pores by CoMn(n:m) particles. AC gives a type-I isotherms, which is distinctive for microporous solids with small external surface. The isotherms given by CoMn(n:m) and AC@ CoMn(n:m) composites are of type-IV, with a hysteresis loop related to capillary condensation occurring in mesopores

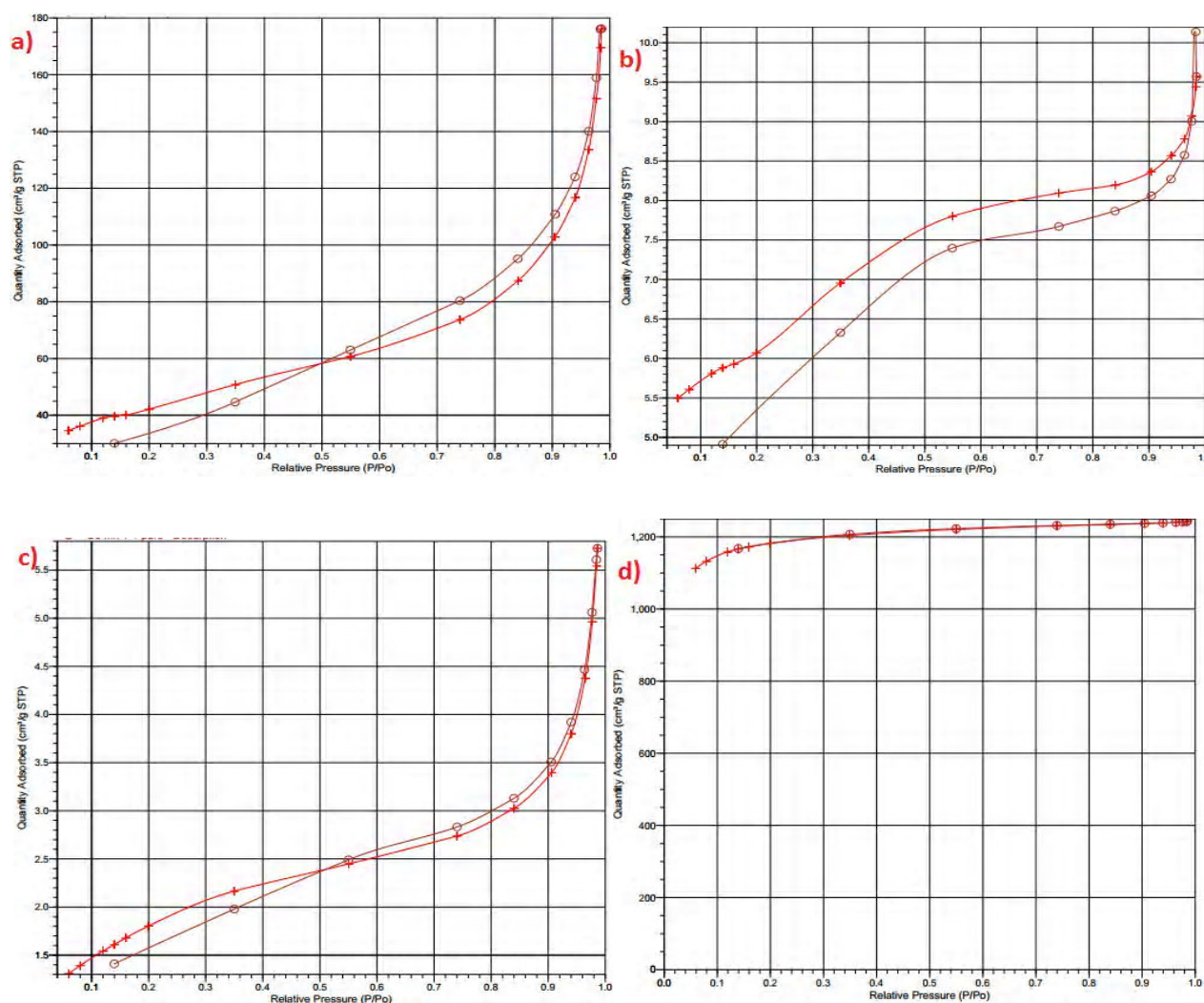


Fig 4.34 Nitrogen adsorption/desorption isotherms of **a)CoMn(1:0)** **b)AC@CoMn(1:0)** **c)CoMn(1:1)** and **d)AC**

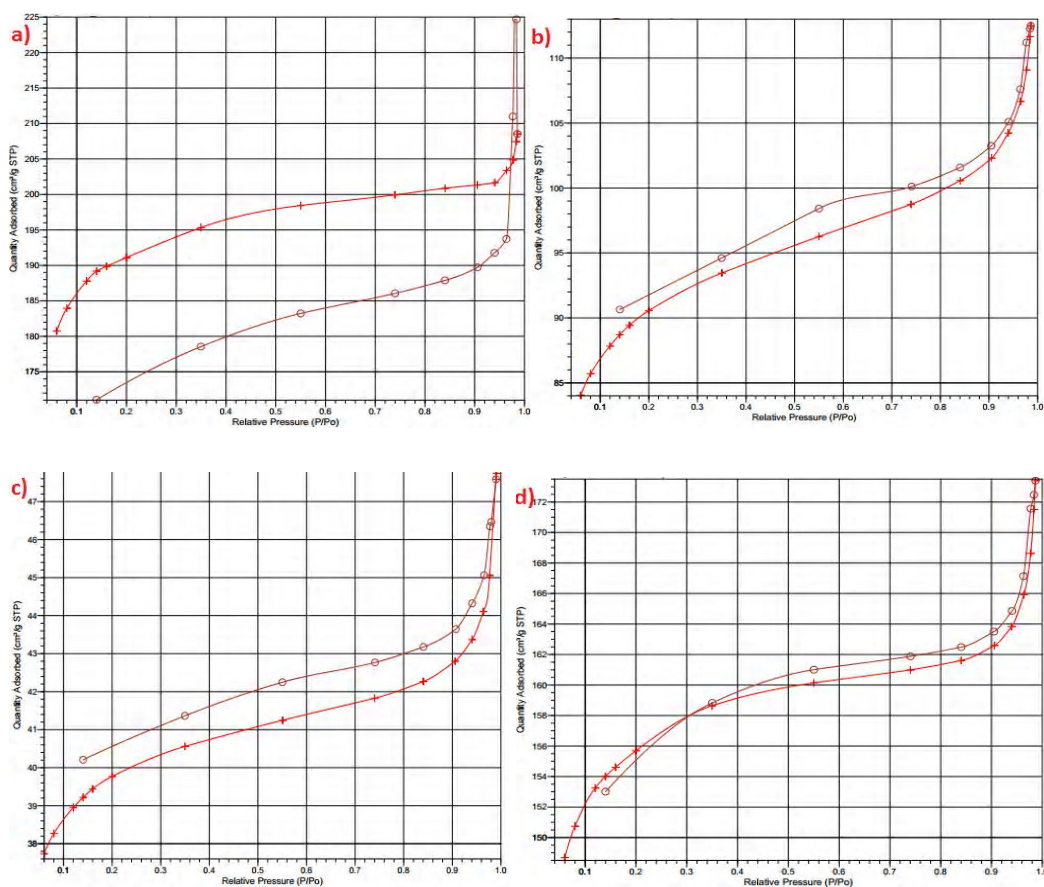


Fig 4.35 Nitrogen adsorption/desorption isotherms of **a)**AC@CoMn (1:2) **b)**AC@CoMn (1:3) **c)**AC@CoMn (2:1) and **d)** AC@CoMn(1:1) composites

4.2.3 Scanning Electron Microscope (SEM)

The scanning electron microscope photographs for the CoMn(n:m) and AC@CoMn(n:m) composites are given in figs 4.36 and 4.37. Fig 4.36a shows the morphology of Co(0:1) consisted of nanoneedles. As can be seen from fig 4.36b, CoMn(1:1) is composed of nano- and micro sized particles. Fig 4.36 (c-d) and fig 4.37 (a-d) indicate that AC particles are decorated with CoCO_3 , Mn_3O_4 , and MnCO_3 particles.

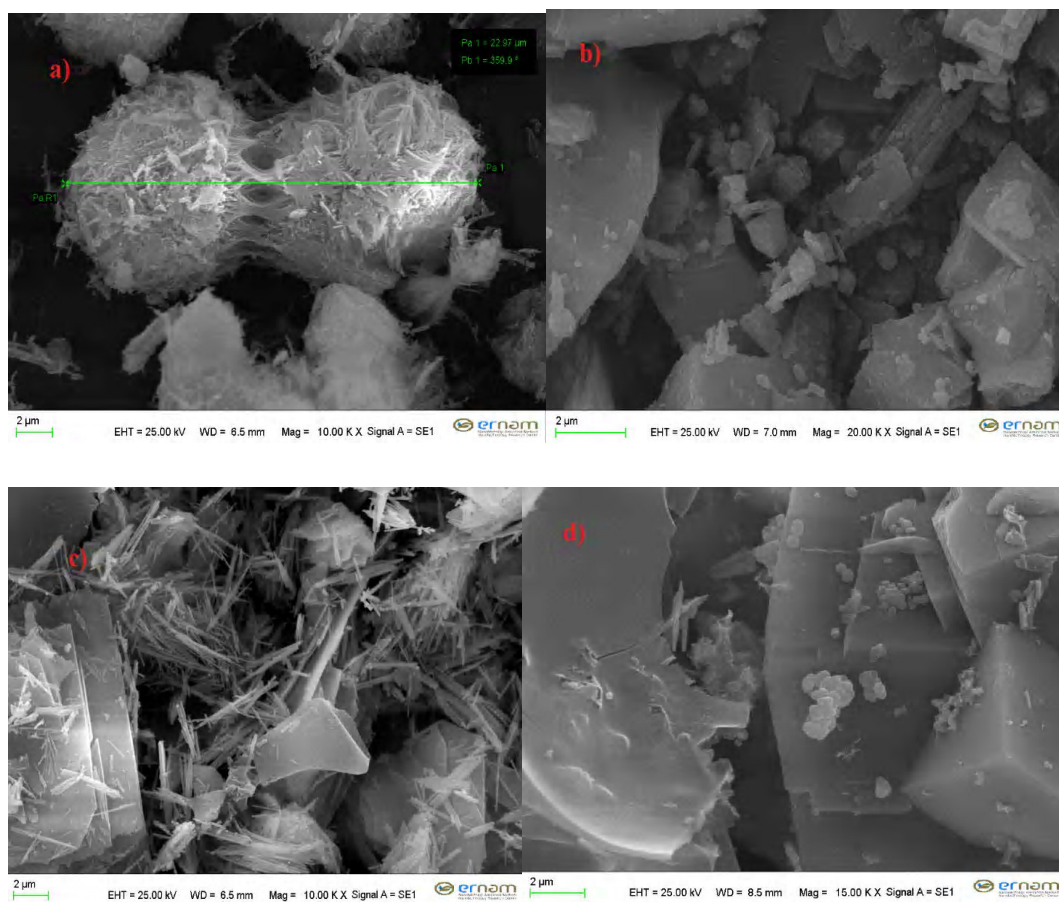


Fig 4.36 SEM images of **a)CoMn(1:0)** **b)CoMn(1:1)** **c)AC@CoMn(1:0)** and **d) AC@CoMn(1:1)**

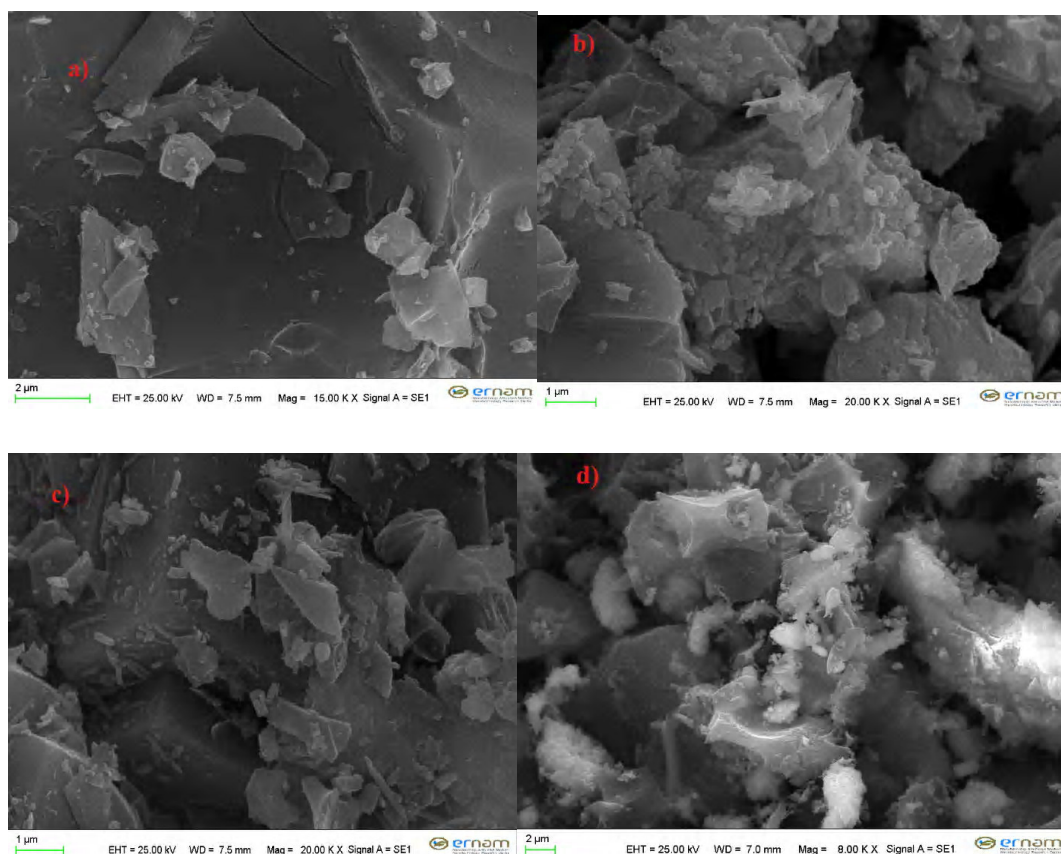


Fig 4.37 SEM image of **a)**AC@CoMn(1:2) **b)**AC@CoMn(1:3) **c)**AC@CoMn(2:1) and **d)**AC@CoMn(3:1)

4.2.4 Electrochemical Characterization

Cyclic voltammogram (CV), constant current charge/discharge voltage profiles, the capacitance change with current density, galvanostatic charge/discharge curves after cycling measurements, cycle life and the energy density versus power density values for CoMn(n:m)//CoMn(n:m) and AC@CoMn(n:m)//AC@CoMn(n:m) SC and AC//AC@CoMn(1:1) ASC are given in figs 4.38-4.43. The specific discharge capacitance based on the total mass of anode and cathode is given in table 4.4.

As seen from figs 4.38-4.43, CV curves except for that of CoMn(1:1)//CoMn(1:1) SC, exhibit almost rectangular shape, indicating a fast charge propagation over the entire voltammetric cycle, which is desired for a supercapacitor. CV curve for CoMn(1:1)//CoMn(1:1) SC (Fig 4.38a) exhibits the distorted rectangular shape, indicating polarization due to low conductivity of CoMn(1:1).

All the galvanostatic charge/discharge curves are basically symmetric. AC@CoMn(1:1)//AC@CoMn(1:1) and AC@CoMn(2:1)//AC@CoMn(2:1) demonstrate the higher capacitance at all the current densities compared to others given in table 4.4. CoMn(1:0)//CoMn(1:0), CoMn(0:1)//CoMn(0:1), CoMn(1:1)//CoMn(1:1),

AC@CoMn(1:0)//AC@CoMn(1:0) and AC@CoMn(0:1)//AC@CoMn(0:1) show very small capacitance values because of the low conductivity and low BET surface area of electrode materials.

All the capacitors except for AC@CoMn(1:3)//AC@CoMn(1:3), exhibit high rate capability, as shown in figs 4.38c-4.43c and table 4.4. The specific capacitances of the composites decreased as the increasing current densities, which was attributed to the resistance and insufficient Faradaic redox reactions under higher discharge current densities.

Figs 4.38(d-e)-4.43(d-e) display the cycling stability of the devices and fig 4.44b compares the cycling stabilities of all the devices. It can be seen that 99% of the initial capacitance for all the devices except for AC//AC, was retained after after 5000 cycles, indicating long cycling stability.

The energy (E) and power densities (P) were calculated from constant current charge/discharge voltage profiles and given in figs 4.38(f)-4.43(f). Fig 4.44c compares the energy and power densities for all the devices studied. It is seen that the energy and power densities of AC//AC@CoMn(1:1) ASC is the highest among those of the devices given in fig 44c.

Table 4.4 Specific capacitance of the supercapacitors

Cell	Total mass of electrodes (mg)	Capacitance (F/g ⁻¹) at 0.5A	Capacitance (F/g ⁻¹) at 1A	Capacitance (F/g ⁻¹) at 2A	Capacitance (F/g ⁻¹) at 5A	Capacitance (F/cm ²) at 1A/g ⁻¹
CoMn(1:0)//CoMn(1:0)		low	low	low	low	low
CoMn(0:1)//CoMn(0:1)		low	low	low	low	low
AC//AC	16	18.12	15	10	6.25	0.24
CoMn(1:1)//CoMn(1:1)	19.76	0.06	0.06	0.08	0.12	0.001
AC@CoMn(1:0)//AC@CoMn(1:0)	13.68	7.8	7.5	6.8	5.1	0.103
AC@CoMn(0:1)//AC@CoMn(0:1)	19.44	9.5	8.2	7.0	4.8	0.160
AC@CoMn(1:1)//AC@CoMn(1:1)	16.80	37.5	35.5	33.8	28.1	0.596
AC@CoMn(1:2)//AC@CoMn(1:2)	15.04	40.6	38.7	32.5	25	0.582
AC@CoMn(1:3)//AC@CoMn(1:3)	13.60	29.7	25.6	22.5	15.6	0.348
AC@CoMn(2:1)//AC@CoMn(2:1)	20.96	18.1	17	15	12	0.356
AC//AC@CoMn(1:1)*	18.5	26.3	25.0	21.7	20.8	0.462

* Mass ratio of AC/AC@CoMn(1:1) is 2.06

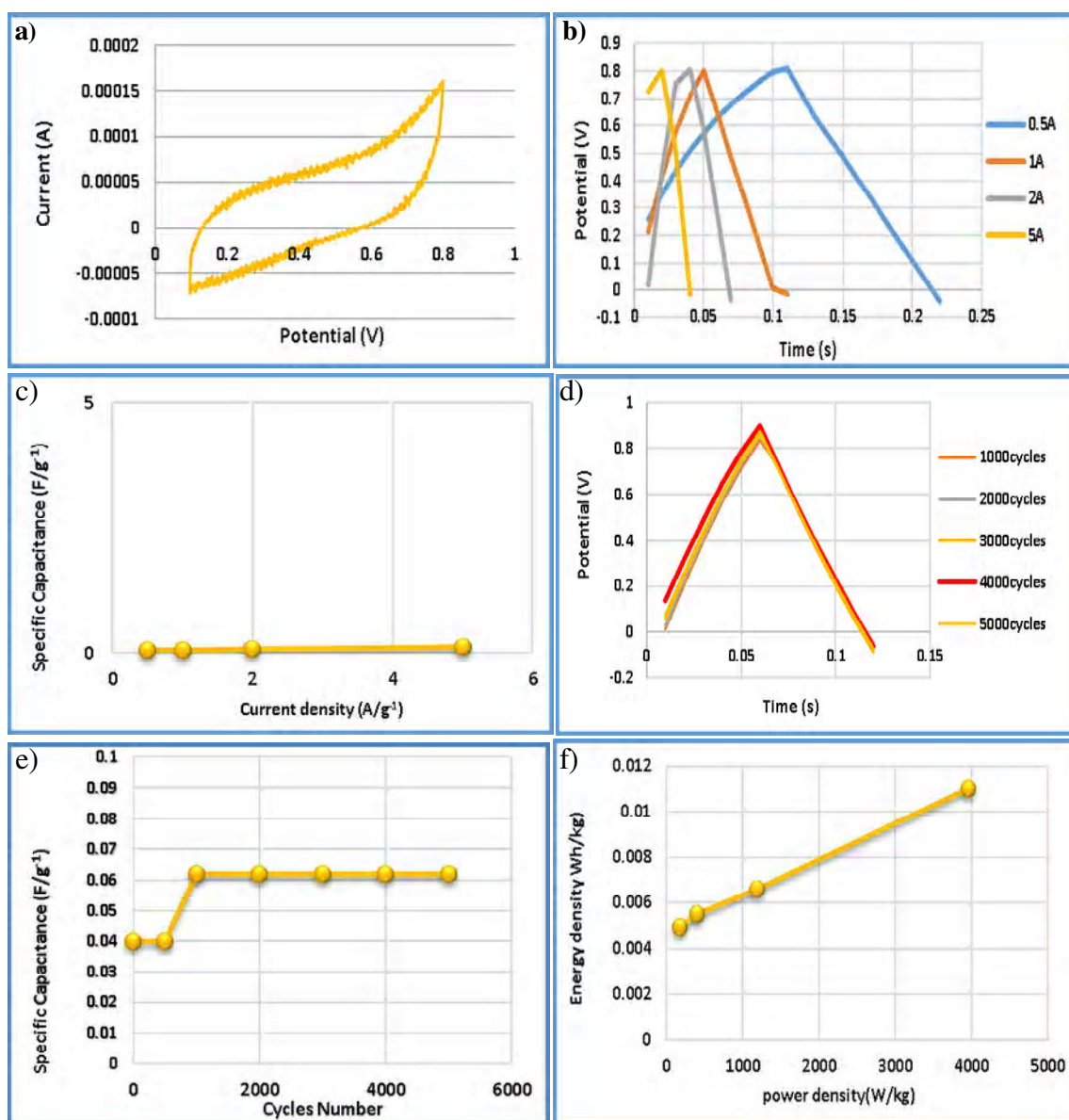


Fig 4.38 Electrochemical performance of CoMn(1:1)//CoMn(1:1) symmetric capacitor using 6M KOH solution **a)** cyclic voltammogram at 0.01 V/s **b)** constant current charge/discharge curves **c)** effect of the constant current density on the capacitance **d)** galvanostatic charge/discharge curves after cycling measurements **e)** cycle life and **f)** the energy density versus power density values.

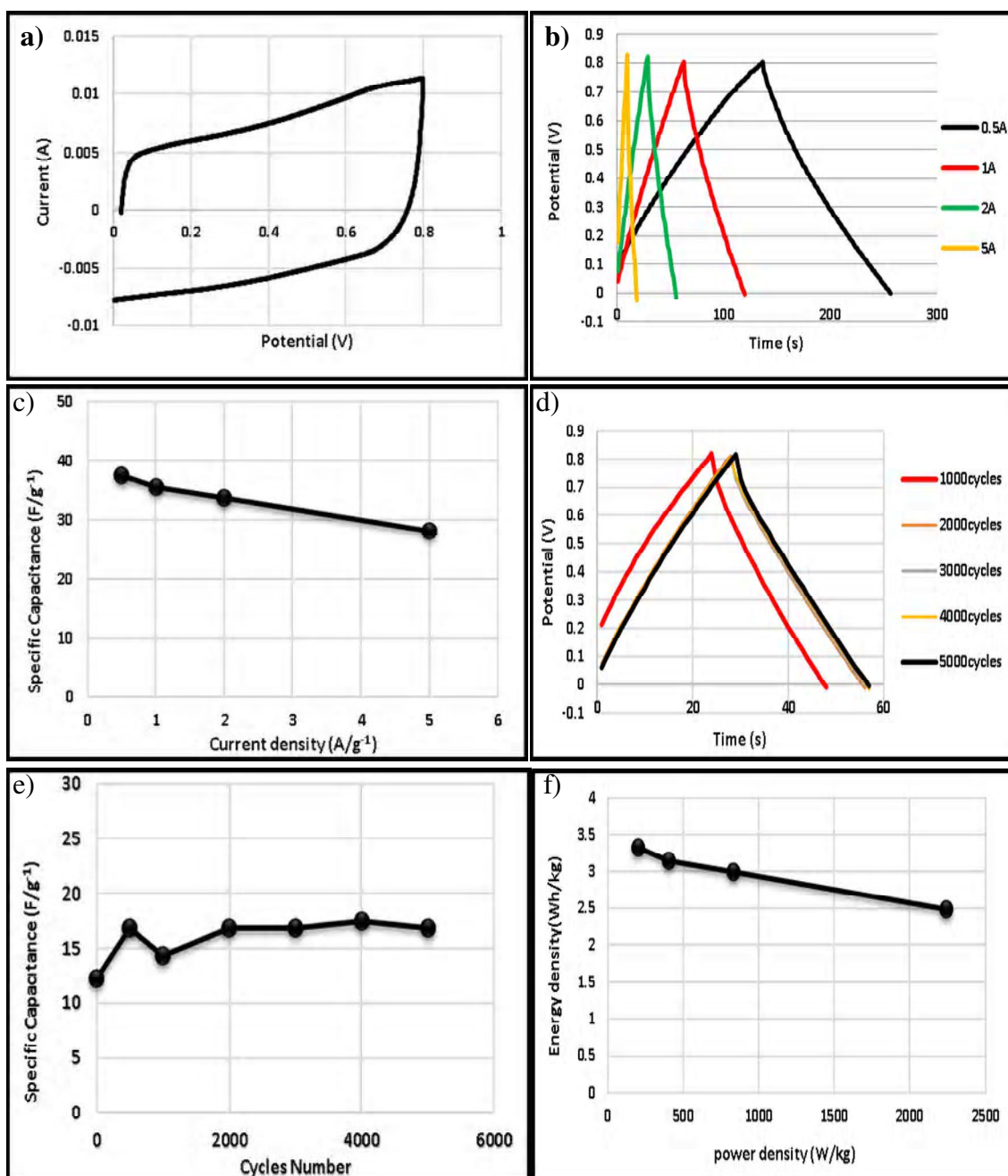


Fig 4.39 Electrochemical performance of AC@CoMn(1:1)//AC@CoMn(1:1) symmetric capacitor using 6M KOH solution **a)** cyclic voltammogram at 0.01V/s **b)** constant current charge/discharge curves **c)** effect of the constant current density on the capacitance **d)** galvanostatic charge/discharge curves after cycling measurements **e)** cycle life and **f)** the energy density versus power density values

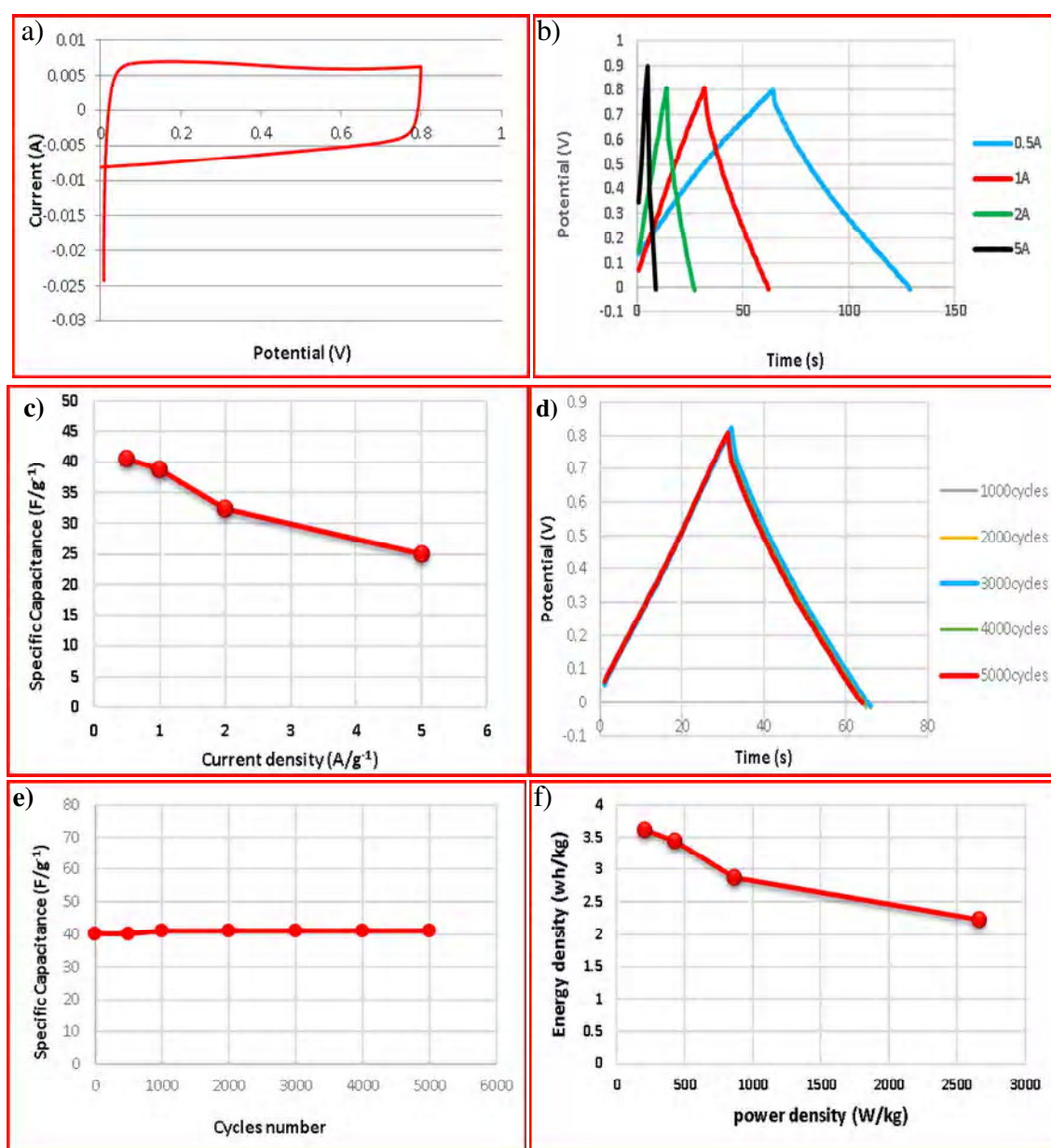


Fig 4.40 Electrochemical performance of AC@CoMn(1:2)//AC@CoMn(1:2) symmetric capacitor using 6M KOH solution **a)** cyclic voltammogram at 0.01V/s **b)** constant current charge/discharge curves **c)** effect of the constant current density on the capacitance **d)** galvanostatic charge/discharge curves after cycling measurements **e)** cycle life and **f)** the energy density versus power density values

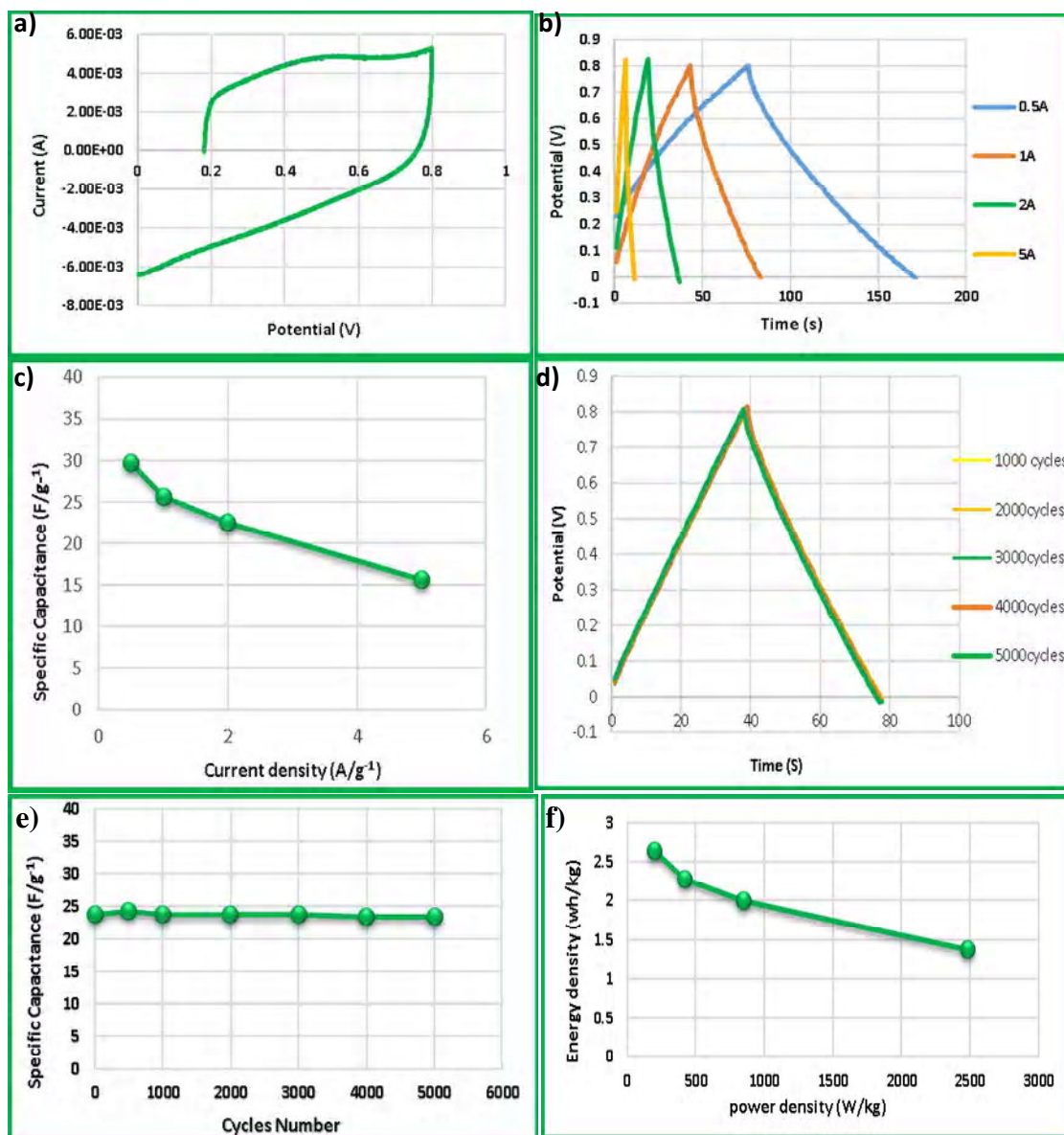


Fig 4.41 Electrochemical performance of AC@CoMn(1:3)//AC@CoMn(1:3) symmetric capacitor using 6M KOH solution **a)** cyclic voltammogram at 0.01V/s **b)** constant current charge/discharge curves **c)** effect of the constant current density on the capacitance **d)** galvanostatic charge/discharge curves after cycling measurements **e)** cycle life and **f)** the energy density versus power density values

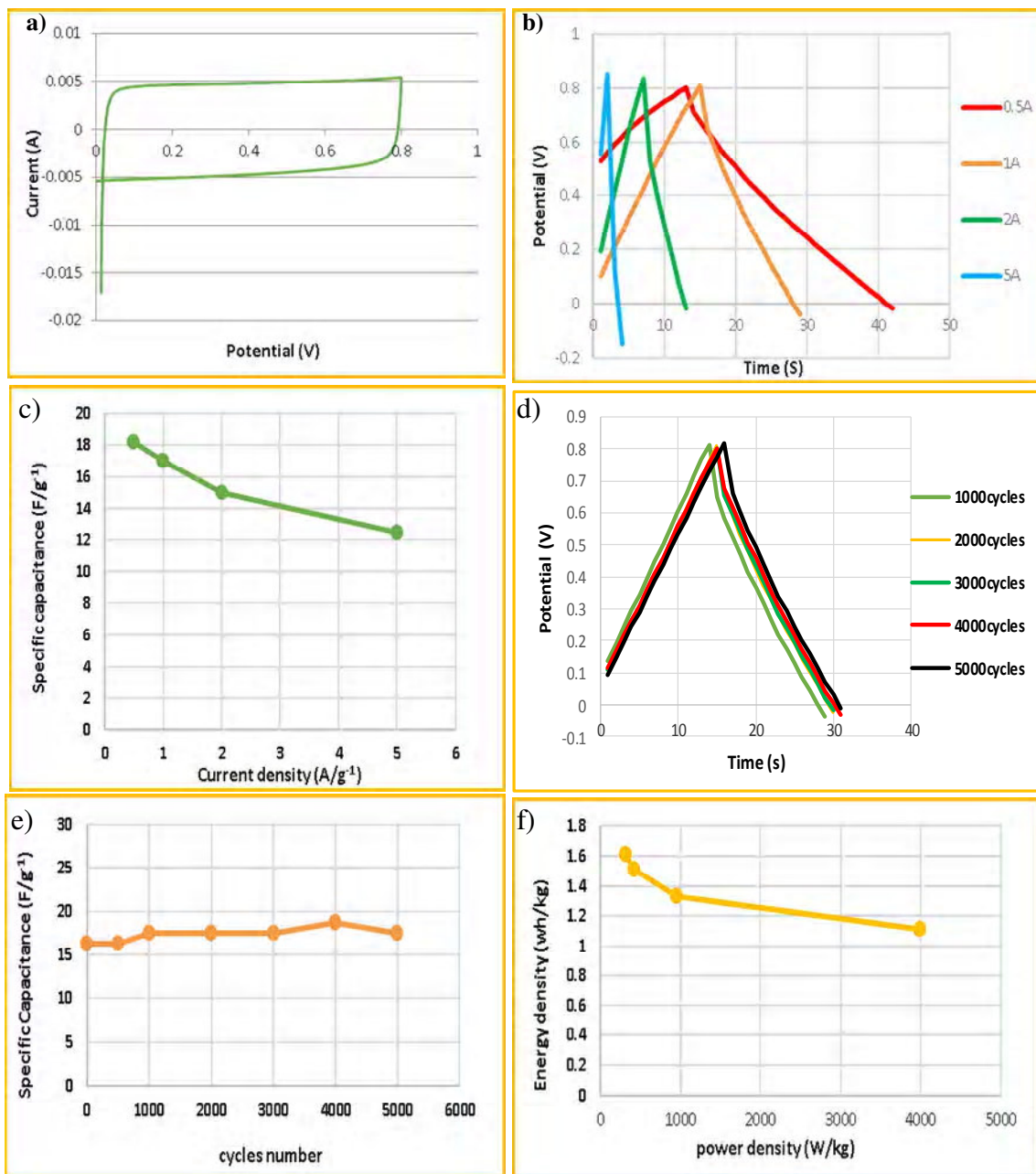


Fig 4.42 Electrochemical performance of AC@CoMn(2:1)//AC@CoMn(2:1) symmetric capacitor using 6M KOH solution **a)** cyclic voltammogram at 0.01V/s **b)** constant current charge/discharge curves **c)** effect of the constant current density on the capacitance **d)** galvanostatic charge/discharge curves after cycling measurements **e)** cycle life and **f)** the energy density versus power density values

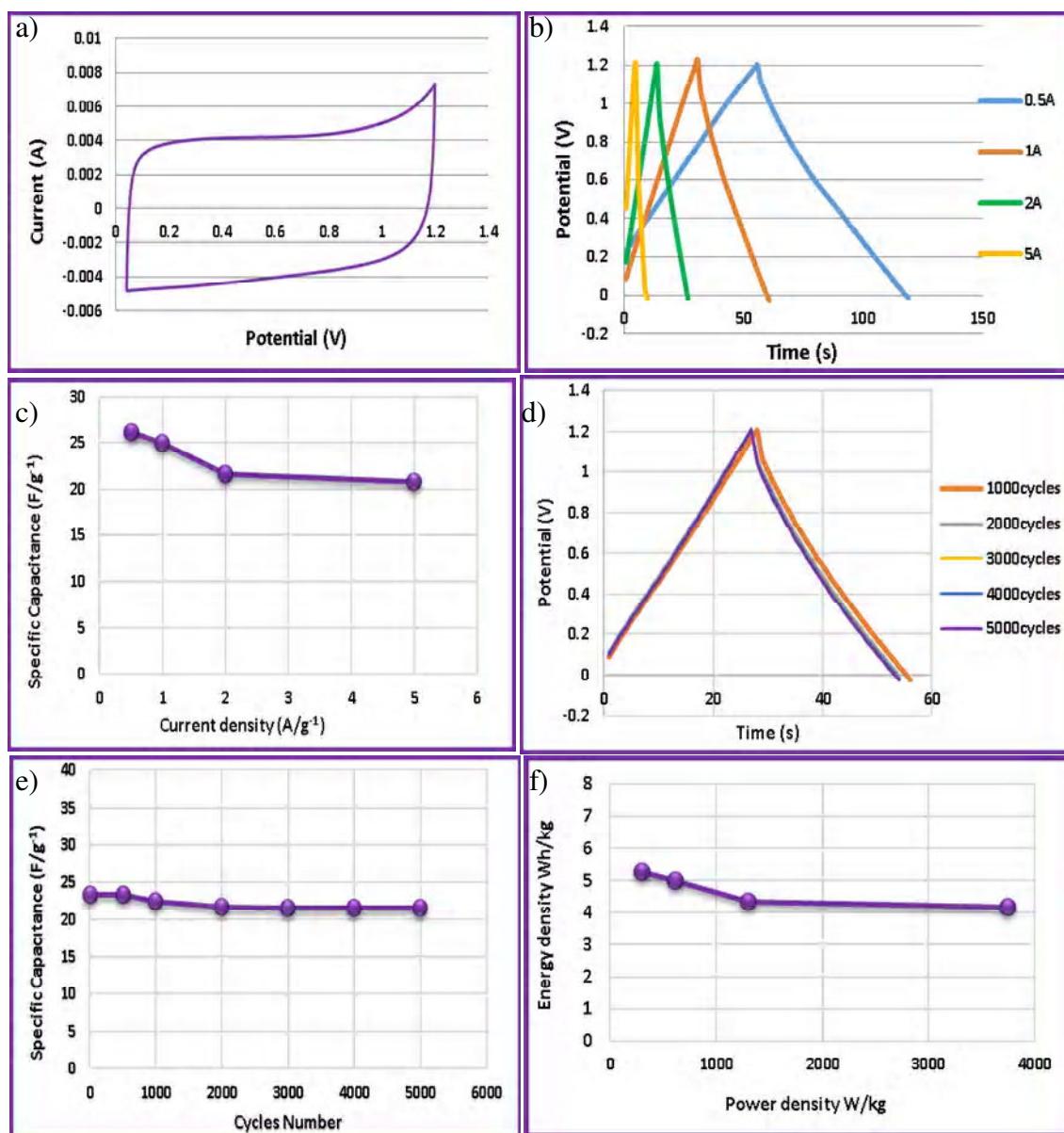


Fig 4.43 Electrochemical performance of AC//AC@CoMn(1:1) asymmetric capacitor using 6M KOH solution **a)**cyclic voltammogram at 0.01V/s **b)**constant current charge/discharge curves **c)**effect of the constant current density on the capacitance **d)**galvanostatic charge/discharge curves after cycling measurements **e)**cycle life and **f)**the energy density versus power density values.

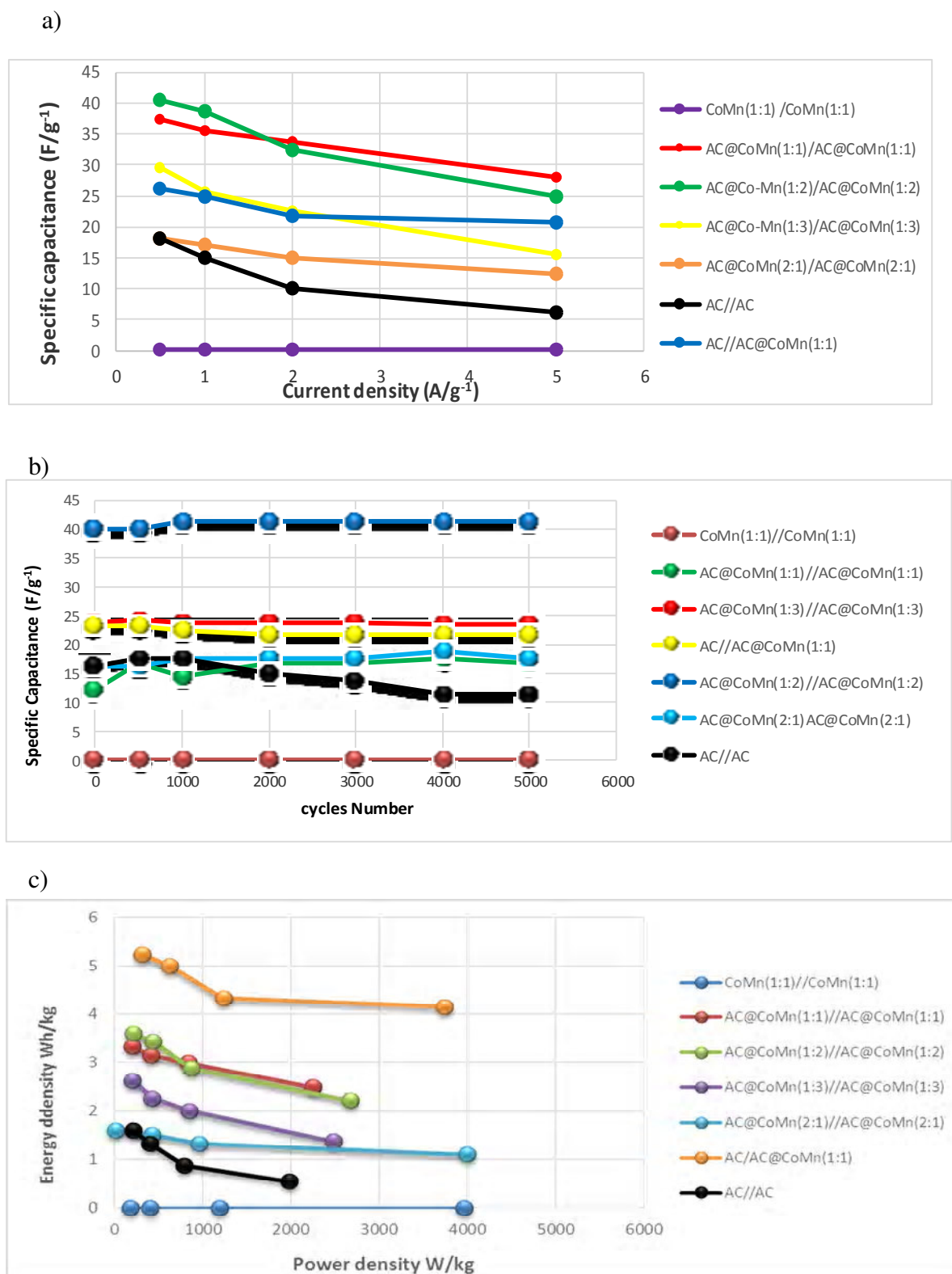


Fig 4.44 Comparison of electrochemical peformans of the symmetric and Asymmetric capacitors using 6M KOH solution a)effect of the constant current density on the capacitance b)cycle life c)the energy density versus power density.

CHAPTER 5

CONCLUSIONS

In this work, NiMn LDH, Co_3O_4 , Mn_3O_4 , CoCO_3 , MnCO_3 , $\text{Co}(\text{OH})_2$ and $\text{Ni}(\text{OH})_2$ particles were successfully grown on the surface of activated carbon particles by a hydrothermal method. In these composites, NiMn LDH, Co_3O_4 , Mn_3O_4 , CoCO_3 , MnCO_3 , $\text{Co}(\text{OH})_2$ and $\text{Ni}(\text{OH})_2$ play the role of electrochemically active species and activated carbon serves as electron conductor. AC//AC@NiMn(1:1) and AC//AC@CoMn(1:1) ASC exhibit high energy and power densities, good rate capability and excellent cycling stability, which can be attributed to the synergetic effects between the conductivity of the activated carbon and the redox properties of the metal oxide/hydroxide/carbonate. The AC@//AC@NiMn(1:1) ASC with 1.2 V voltage window delivers a high energy density of 5.5 W h kg^{-1} at a power density of 1000 W kg^{-1} and excellent cycling stability with 96% retention of initial capacitance after 5000 cycles. The AC//AC@CoMn(1:1) ASC with 1.2 V voltage window delivers a high energy density of 4.9 W h kg^{-1} at a power density of 1000 W kg^{-1} and excellent cycling stability with 97% retention of initial capacitance after 5000 cycles.

AC//AC@NiMn(1:1) ASC demonstrate a specific capacitance of 21.9 F/g^{-1} at 5 A/g^{-1} , indicating 72% retention of the capacitance at 0.5 A/g^{-1} . AC//AC@CoMn(1:1) ASC demonstrate a specific capacitance of 20.8 F/g at 5 A/g , showing 79% retention of the capacitance at 0.5 A/g^{-1} .

This work provides a facile hydrothermal method to synthesize metal oxide/hydroxide/carbonate@AC composite electrode materials for high-performance supercapacitors. Metal oxide/hydroxide/carbonate@AC composite electrode materials were found to be promising electrode materials for the supercapacitor working at high current density.

REFERENCES

1. George Z. Chen, “Understanding supercapacitors based on nano-hybrid materials with interfacial conjugation”, **Progress in Natural Science: Materials International** 2013;23(3):245–255
2. Maher El-Kady, Graphene Supercapacitors: Charging Up the Future, **Ph D. Thesis, University Of California**, 2013
3. Mingjia Zhi, Chengcheng Xiang, Jiangtian Li, Ming Li and Nianqiang Wu, “Nanostructured carbon–metal oxide composite electrodes for supercapacitors: a review”, **Nanoscale**, 2013, 5, 72–88
4. H. von Helmholtz, Ann. Phys., 165 (1853) 211-233
5. A.J. Bard, L.R. Faulkner, Electrochemical Methods: Fundamentals and Applications, 2nd ed., **Wiley, New York**, 2000.
6. H. Wang, L. Pilon, The Journal of Physical Chemistry C, 115 (2011) 16711-16719
7. Ander González, Eider Goikolea, Jon Andoni Barrena, Roman Mysyk, “Review on supercapacitors: Technologies and materials” **Renewable and Sustainable Energy Reviews** 58 (2016) 1189–1206
8. Xin Li, Bingqing Wei, Supercapacitors based on nanostructured carbon, **Nano Energy**. 2 (2013) 159-173]
9. Katherine L. Van Aken, “**Relationship between Carbon Electrode Materials and Electrolytes in Capacitive Energy Storage**”, Drexel University, PhD Thesis, 2017
10. Mohamad K. Khawaja, Synthesis and Fabrication of Graphene/Conducting Polymer/Metal Oxide Nanocomposite, **Materials for Supercapacitor Applications**, Th D Thesis, University of South Florida, 2015
11. B. Kim, H. Chung, and W. Kim, “High-performance supercapacitors based on vertically aligned carbon nanotubes and nonaqueous electrolytes”, **Nanotechnology** 23, 155401 (2012)

12. Sanliang Zhang, **Synthesis and Characterization of Carbon Nanostructures for Supercapacitors, Ph D Thesis, University Of California, 2016**
13. Patrice Simon and Yury Gogotsi, Materials for electrochemical capacitors, **nature materials**, 7, 2008, pp 845-854
14. Sanliang Zhang, **Synthesis and Characterization of Carbon Nanostructures for Supercapacitors, Ph D Thesis, University Of California, 2016**
15. Sanliang Zhang and Ning Pan, “Supercapacitors Performance Evaluation, **Adv. Energy Mater.** 2015, 5, 1401401
16. K. S. W. SING, Pure & Appl.Chem. Vol.54, No.11, pp.2201—2218, 1982.
17. Agnieszka Malak-Polaczyk, Cathie Vix-Guterl, and Elzbieta Frackowiak, “Carbon/Layered Double Hydroxide (LDH) Composites for Supercapacitor Application”, **Energy Fuels** 2010, 24, 3346–3351

CURRICULUM VITAE

Name and Surname: MUSTAFA RAQEEB MOHAMMED

Nationality: Iraqi

Birth date and Place: 29 October 1986. Baghdad

Marital status: Married

Cell Phone: Turkey +905511485598

Iraq +9647708490279

E-Mail: mustafaraqeeb@outlook.com

mustafaalmarsumy@yahoo.com

Correspondence Address: Talas /KAYSERİ

EDUCATION

Degree	Institution	Date of graduation
M.Sc.	Erciyes University	2018
License	AL-Mustansiriya University	2008
High School	Salah al-Din al-Ayoubi	2004

Mother tongue

- Arabic

Foreign language

- English

- Turkish